FINAL REPORT

GPS Based Positioning System for Geophysical Surveys in Foliage Areas

ESTCP Project MR-201311

SEPTEMBER 2020

David Hodo
Integrated Solutions for Systems (IS4S)

Richard Grabowski
Rick Grabowski
Bob Selfridge
USAESCH

REPORT DOCUMENTATION PAGE

Form Approved
OMB No. 0704-0188

1. REPORT DATE *(DD-MM-YYYY)*
30/09/2020

2. REPORT TYPE
ESTCP Final Report

3. DATES COVERED *(From - To)*
4/30/2013 - 10/30/2018

4. TITLE AND SUBTITLE
GPS Based Positioning System for Geophysical Surveys in Foliage Areas

5a. CONTRACT NUMBER
13-C-0053

5b. GRANT NUMBER

5c. PROGRAM ELEMENT NUMBER

6. AUTHOR(S)

David Hodo
Integrated Solutions for Systems

Richard Grabowski
Rick Grabowski
Bob Selfridge
USAESCH

5d. PROJECT NUMBER
MR-201311

5e. TASK NUMBER

5f. WORK UNIT NUMBER

7. PERFORMING ORGANIZATION NAME(S) AND ADDRESS(ES)
Integrated Solutions for Systems

8. PERFORMING ORGANIZATION REPORT NUMBER
MR-201311

9. SPONSORING/MONITORING AGENCY NAME(S) AND ADDRESS(ES)
Environmental Security Technology Certification Program
4800 Mark Center Drive, Suite 16F16
Alexandria, VA 22350-3605

10. SPONSOR/MONITOR'S ACRONYM(S)
ESTCP

11. SPONSOR/MONITOR'S REPORT NUMBER(S)
MR-201311

12. DISTRIBUTION/AVAILABILITY STATEMENT
DISTRIBUTION STATEMENT A. Approved for public release: distribution unlimited.

13. SUPPLEMENTARY NOTES

14. ABSTRACT

Geophysical mapping is a key step in the process of remediating sites contaminated with unexploded ordnance (UXO). In order to accurately locate UXO, accurate measurements of the positions of the geophysical sensors are needed. The need for accurate, real-time pose (position and attitude) estimates has increased in recent years as more advanced sensors are developed that are capable of not only detecting anomalies, but also discriminating items of interest from cultural debris. The goal of this work was to improve the accuracy and availability of position measurements for geophysical surveys in heavy foliage environments by developing a Global Positioning System (GPS) software defined receiver (SDR) using vector tracking techniques combined with complementary sensors.

15. SUBJECT TERMS
GPS Based Positioning System, Geophysical Surveys, Foliage Areas

16. SECURITY CLASSIFICATION OF: a. REPORT	b. ABSTRACT	c. THIS PAGE	17. LIMITATION OF ABSTRACT	18. NUMBER OF PAGES	19a. NAME OF RESPONSIBLE PERSON
UNCLASS	UNCLASS	UNCLASS	UNCLASS	98	David Hodo
					19b. TELEPHONE NUMBER *(Include area code)* 256-975-2237

FINAL REPORT

Project: MR-201311

TABLE OF CONTENTS

Page

TABLE OF CONTENTS (Continued)

Page

LIST OF FIGURES

Page

LIST OF FIGURES

LIST OF FIGURES

Page

LIST OF TABLES

Page

ACRONYMS AND ABBREVIATIONS

AMBA	Advanced Microcontroller Bus Architecture
ASIC	Application Specific Integrated Circuit
AXI	Advanced eXtensible Interface
C/N0	Carrier to Noise Density Ratio
CEHNC	Corps of Engineers – Huntsville Center
CSAC	Chip-scale Atomic Clock
EKF	Extended Kalman Filter
FLL	Frequency Locked Loop
FPGA	Field-Programmable Gate Array
GPP	General Purpose Processor
GPS	Global Positioning System
HDL	Hardware Description Language
IC	Integrated Circuit
IF	Intermediate Frequency
IMU	Inertial Measurement Unit
INS	Inertial Navigation System
NCO	Numerically Controlled Oscillator
PL	Programmable Logic
PLL	Phase Locked Loop
PPS	Pulse Per Second
PS	Processor System
PVT	Position, Velocity, and Time
RF	Radio Frequency
RSA	Redstone Arsenal
RTK	Real-time Kinematic
SDR	Software Defined Receiver
SWAP-C	Size, Weight, Power, and Cost
TCXO	Temperature Compensated Crystal Oscillator
TOA	Time of Arrival
USAESCH	US Army Engineering and Support Center, Huntsville
UXO	Unexploded Ordnance
VT	Vector Tracking

ACKNOWLEDGEMENTS

We would like to thank ESTCP for providing guidance and funding for this effort. We would also like to thank the Army Corp of Engineers Huntsville Center for their support on the effort and in particular their support in obtaining and preparing a demonstration site and providing truth data.

ABSTRACT

INTRODUCTION AND OBJECTIVES

Geophysical mapping is a key step in the process of remediating sites contaminated with unexploded ordnance (UXO). In order to accurately locate UXO, accurate measurements of the positions of the geophysical sensors are needed. The need for accurate, real-time pose (position and attitude) estimates has increased in recent years as more advanced sensors are developed that are capable of not only detecting anomalies, but also discriminating items of interest from cultural debris. The goal of this work was to improve the accuracy and availability of position measurements for geophysical surveys in heavy foliage environments by developing a Global Positioning System (GPS) software defined receiver (SDR) using vector tracking techniques combined with complementary sensors.

TECHNOLOGY DESCRIPTION

A GPS software defined receiver (SDR) has been developed that is capable of providing a position solution in degraded GPS environments such as under heavy foliage by making use of vector tracking techniques. The GPS position can be optionally blended with the output of a commercial IMU to provide attitude measurements and allow brief periods of dead-reckoning during complete GPS outages. A chip scale atomic clock (CSAC) is also optionally used as a stable frequency reference to further improve the receiver's ability to operate with a limited number of satellites. The SDR based design allows the receiver algorithms to be defined completely in software, allowing an easy upgrade path as more advanced algorithms are developed. This design also drastically reduces development cost when compared to a traditional application-specific integrated circuit (ASIC).

PERFORMANCE AND COST ASSESSMENT

A demonstration was performed at Redstone Arsenal in Huntsville, AL to analyze the performance of the system. The developed receiver was compared to a commercially available receiver typically used in geophysical surveys and the position availability and accuracy were compared. The demonstration showed significantly improved position availability and accuracy in dense foliage environments when compared to the commercial receiver. The developed receiver was comparable to the commercial receiver in open sky environments providing similar position availability with slightly reduced accuracy

IMPLEMENTATION ISSUES

The primary issue to be considered when choosing to implement the demonstrated system is the presence of foliage or other GPS challenges on the site. Significant improvement in position availability and survey time were demonstrated for moderate to dense foliage. No significant improvement was seen in open sky environments.

SELECTED PUBLICATIONS

Keyser, B., Hodo, D., Martin, S., Bevly, D., "Implementation Details of Real-Time SoC-Based Vector Tracking Receiver. Proceedings of the 27th International Technical Meeting of the Satellite Division of the Institute of Navigation (ION GNSS+ 2014).

Martin, S.M. "Improved GPS Carrier Phase Tracking in Difficult Environments Using A Vector Tracking Approach." Presented to Southern California Chapter of the Institute of Navigation. Torrance, CA, December 2014.

EXECUTIVE SUMMARY

INTRODUCTION

Geophysical mapping is a key step in the process of remediating sites contaminated with unexploded ordnance (UXO). In order to accurately locate UXO, accurate measurements of the positions of the geophysical sensors are needed. The need for accurate, real-time pose (position and attitude) estimates has increased in recent years as more advanced sensors are developed that are capable of not only detecting anomalies, but also discriminating items of interest from cultural debris. A combination of a global positioning system (GPS) receiver and an inertial navigation system (INS) is a common method of determining the pose of these sensors.

Currently, in areas where there are strong or frequent attenuations or blockages of the GPS signal alternative methods of positioning such as laser or RF based ranging systems or odometry are used. Ranging based systems such as robotic total stations that are traditionally used in surveying applications or more developmental RF based ranging systems are capable of providing very accurate position measurements in GPS denied areas. They often, however, require line of sight to the receiver and are cumbersome and time consuming to set up. Systems such as total stations are also generally considerably more expensive than a GPS receiver. Odometry solutions, based on wheel encoders or inertial measurement units (IMUs), have error characteristics that grow over time and require prohibitively expensive sensors to provide accurate positions for periods longer than a few minutes.

In this effort, a system has been developed that improves the accuracy and availability of position measurements for geophysical surveys by providing a GPS/INS system capable of providing positions in environments where standard GPS receivers provide a poor solution or fail to provide a solution at all. A GPS software defined receiver (SDR) has been developed that is capable of providing a position solution in degraded GPS environments such as under heavy foliage by making use of vector tracking techniques. The GPS position can be optionally blended with the output of a commercial IMU to provide attitude measurements and allow brief periods of dead-reckoning during complete GPS outages. A chip scale atomic clock (CSAC) is also optionally used as a stable frequency reference to further improve the receiver's ability to operate with a limited number of satellites. The SDR based design allows the receiver algorithms to be defined completely in software, allowing an easy upgrade path as more advanced algorithms are developed. This design also drastically reduces development cost when compared to a traditional application-specific integrated circuit (ASIC).

OBJECTIVES

The objective of the demonstrations performed was to validate the performance of the developed GPS receiver under controlled conditions and compare its performance to GPS/INS systems currently used for geophysical surveys. Additionally, surveyed ground truth points and a ranging based positioning system (e.g., robotic total station) were used to provide truth measurements allowing the absolute performance of the system to be determined in addition to comparing it to a traditional GPS receiver.

The primary performance objective for the system demonstration is to improve the availability of position measurements for geophysical surveys when compared to currently used survey methods such as GPS receivers. The setup time required and ease of use of the system will also be evaluated qualitatively. The accuracy of the system was also evaluated.

TECHNOLOGY DESCRIPTION

The developed system is a GPS SDR that makes use of vector tracking techniques to improve the receiver's ability to track and reacquire weak signals. The GPS position is blended with the output of a commercial IMU to provide attitude measurements and allow brief periods of dead-reckoning during complete GPS outages. A chip scale atomic clock (CSAC) is used as the receiver clock to further improve reacquisition time and the receiver's ability to operate with a limited number of satellites. The SDR based design allows the receiver algorithms to be defined completely in software, allowing an easy upgrade path as more advanced algorithms are developed. This design also drastically reduces development cost when compared to a traditional application-specific integrated circuit (ASIC).

Vector Tracking Architecture

In this work, the tracking loops used in traditional receivers are replaced with a vector tracking architecture. Vector tracking loops are an advanced receiver architecture that combine signal tracking and position, velocity, and time (PVT) estimation into a single process. The vector tracking algorithm used is based on a vector delay / frequency locked loop (VDFLL). This architecture differs from a standard commercial receiver in two main areas: (1) a vector tracking architecture is used in place of the scalar tracking architecture and (2) the phase locked loop (PLL) is replaced with a frequency locked loop (FLL). An overview of the receiver algorithm as implemented in this work is given in the following sections.

Scalar vs Vector Tracking Loops

Standard GPS receivers use scalar tracking loops to process the received satellite signals. As shown on the left in Figure 1, the tracking loops in different channels of the receiver operate independently of each other. Measurements are generated in each channel and then fed into a navigation processor for determining a position solution. No information is shared between channels and there is no feedback from the navigation processor to the tracking loops. Vector tracking exploits the correlations between the received satellite signals and receiver position to improve tracking performance. The right side of Figure 1 below shows a generic block diagram of the vector tracking architecture. In a vector tracking architecture, the navigation filter directly drives the correlators, combining the navigation solution estimation and tracking loops into a single operation. This allows the different channels of the receiver to share information, so that strong signals can assist in the tracking of weaker signals.

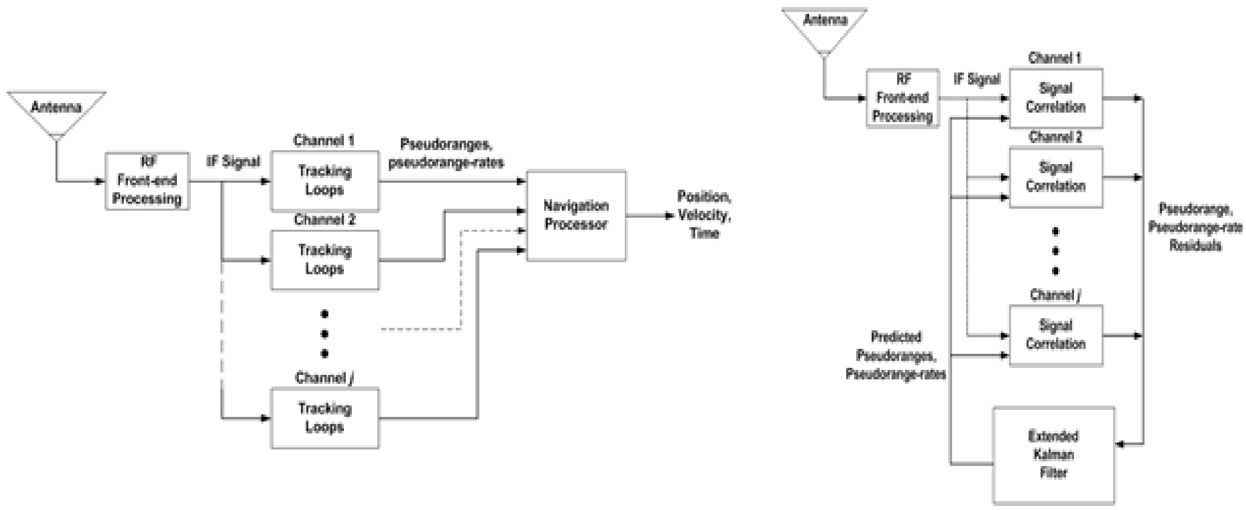

Figure 1. [Left] Standard, Scalar GPS Tracking Loop Architecture [Right] Vector Tracking GPS Receiver Architecture

The phase and frequency of the received signals are predicted from the receiver's estimated position and velocity. Residuals are formed in each channel by taking the difference between the predicted and received signals. The residuals are then used to update the estimates of the receiver's position and velocity. The vector tracking approach exploits the coupling between the receiver's dynamics and the dynamics seen by the tracking loops. Instead of every channel of the receiver tracking the dynamics of the individual signals, the user dynamics that are causing the change in the signals are tracked. Since the code phase and frequency of each channel are calculated based on the current navigation solution, rather than tracking an individual satellite signal, these values can continue to be estimated even when the satellite is not in view allowing for near instant reacquisition when the satellite comes back into view.

Hardware Implementation

A typical, commercial GPS receiver is based around a custom designed ASIC with most of the receiver functionality implemented in custom designed hardware. While this approach allows for substantial cost savings in mass production, the significant development and manufacturing setup costs make it an unsuitable approach for an experimental or prototype receiver. Field Programmable Gate Arrays (FPGAs) provide an effective method for prototyping devices before converting to an ASIC design, or for low-volume applications can be a cost-effective production platform. FPGAs can be programmed after production using Hardware Description Languages (HDL) similar to those used to develop ASICs and can be programmed to perform most any function that can be developed in an ASIC.

A real-time implementation of the vector-tracking receiver described above has been developed based on a Xilinx Zynq All-Programmable System-on-Chip (SoC). The Zynq SoC features an FPGA, a dual-core ARM Cortex-A9 processor, and several peripheral devices on a single chip. An overview of the Zynq SoC is shown in Figure 2. It provides an ideal development platform for a real-time, GPS SDR.

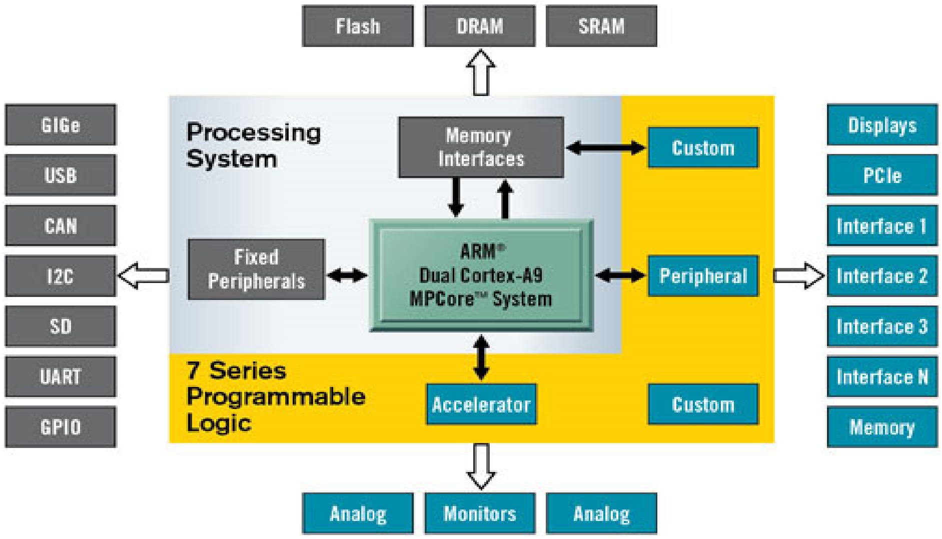

Figure 2. Xilinx Zynq Architecture

The SoC based design allows the FPGA and processor to maintain the same tight coupling seen with soft-core processors while gaining the performance from including a hard-core processor with two cores. The block diagram in Figure 3 shows the components of the VTRx receiver including peripheral sensors (i.e., CSAC, HG1930, Microstrain IMU). The Zynq SOC is represented by the dark blue SDR Processor block.

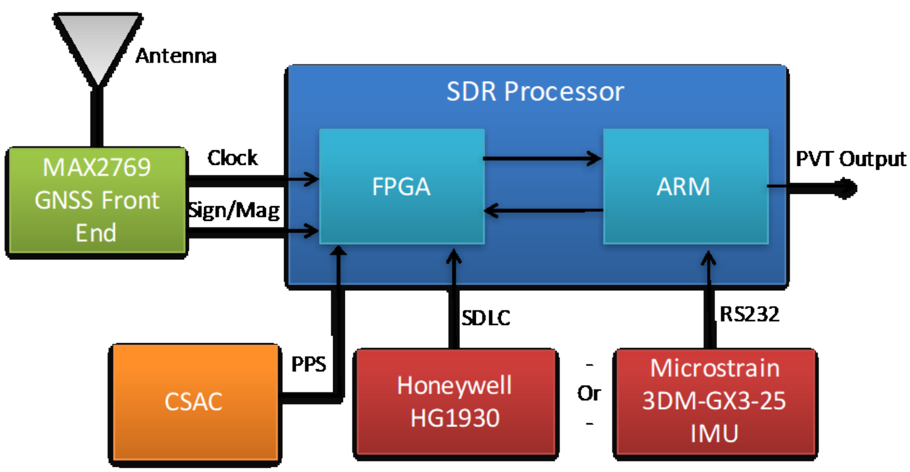

Figure 3. Block Diagram of Hardware Components for the VTRx Receiver.

RF data is received by the antenna and then down-converted to an intermediate frequency (IF) and sampled by a Maxim Integrated Circuits MAX2769 front-end integrated circuit (IC). The samples are then processed in the Zynq and the position, velocity, and time (PVT) estimate output over either a serial or Ethernet port. Acquisition and correlator functions are implemented as Xilinx custom peripherals in the programmable logic (PL) of the Zynq. These peripherals are interfaced to the ARM based processing system (PS) through an Advanced Microcontroller Bus Architecture (AMBA) Advanced eXtensible Interface (AXI) bus. The tracking loop filters and navigation filter are implemented in C++ on the PS and are run without an operating system.

Pictures of the final printed circuit board (PCB) hardware and enclosure are shown in Figure 4. A MicroZed development board contains the Zynq 7020 and various input/output (I/0) including ethernet, USB, and serial connections. The Microzed is attached to a custom board that provides power and CSAC/IMU interfaces. The unit requires 3W of power excluding the IMU power requirement. The enclosure has dimensions of 6.5x5x2.2 inches or roughly the size of a Novatel Propak V3.

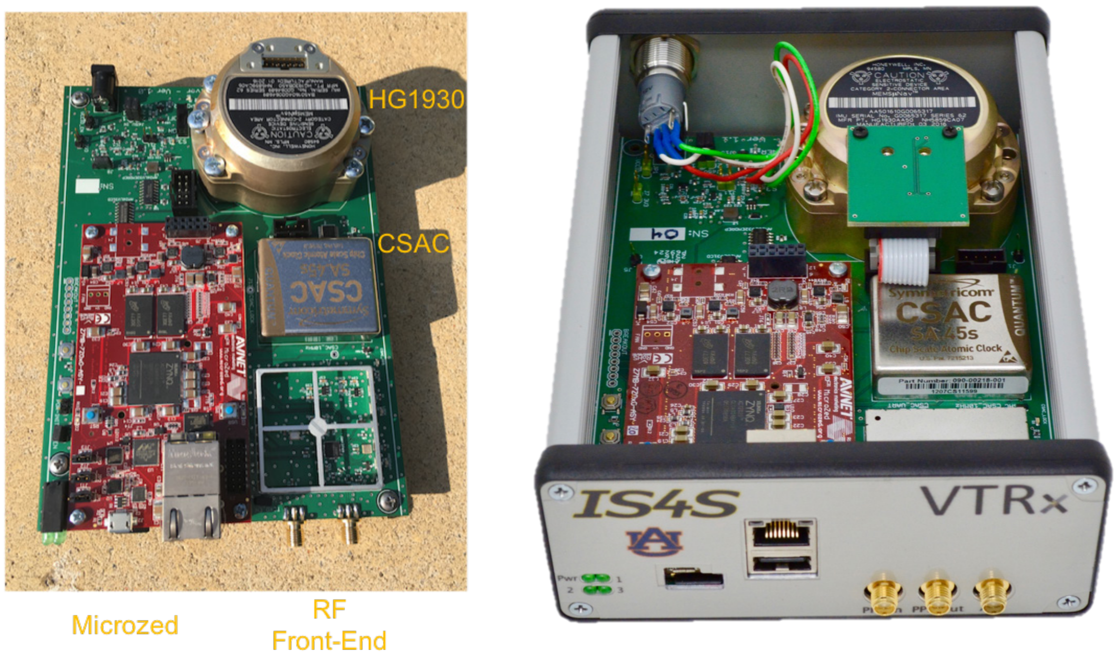

Figure 4. Final Prototype Hardware

PERFORMANCE ASSESSMENT

Fields tests were conducted to determine the positioning performance of the proposed system in a realistic environment and allow the performance to be compared to existing systems. The prototype VTRx system as well as a Novatel RTK capable GPS receiver were installed in a survey backpack. A Trimble Integrated Surveying (IS) system consisting of a Trimble R8 GPS receiver and a Trimble VX Total Station provided truth data. Tests are repeated numerous times in two different sites on Redstone Arsenal in Huntsville, AL.

An example result from Site 9 is provided below. Site 9 featured both open sky areas and dense foliage allowing the system to be tested in a wide range of environments. Representative pictures of the site are shown in Figure 5.

Figure 5. Site 9 Open Sky Areas [Left] and Dense Foliage [Right]

An example run in the dense portion of the site is shown in Figure 6.

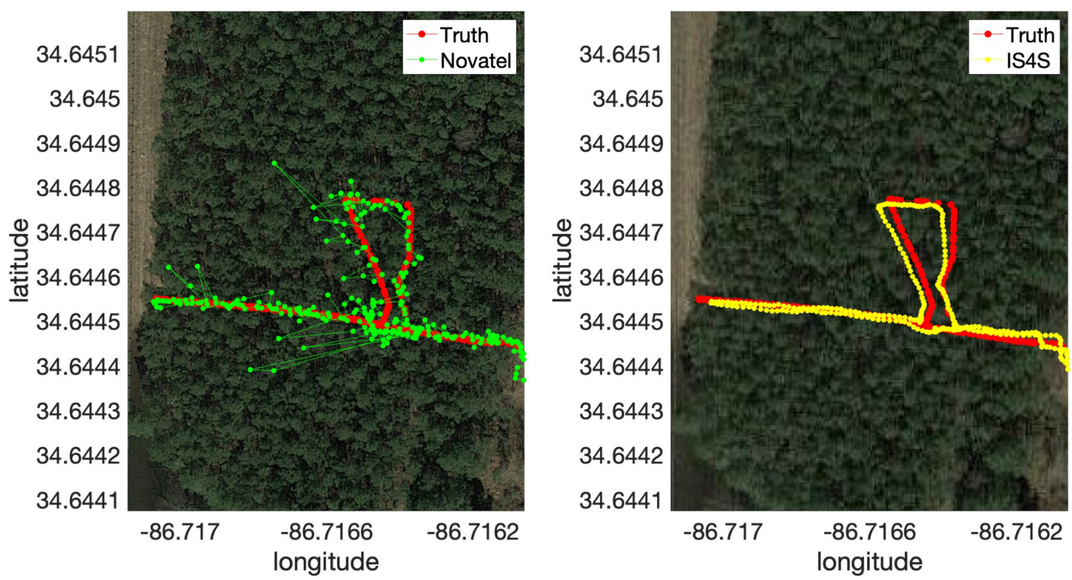

Figure 6. Receiver Outputs in Dense Foliage Portion of Site 9

The error from both the Novatel and VTRx receiver are shown in the plot and table below. While both receivers showed a bias with respect to the truth data, the VTRx receiver produced a solution 100% of the time through the heavy foliage section with an error standard deviation more than three times smaller than that of the Novatel.

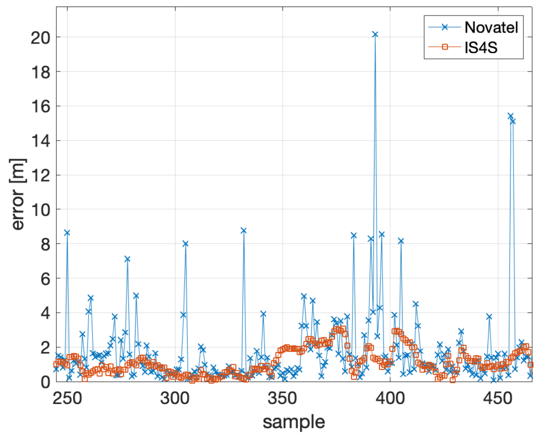

Figure 7. VTRx and Novatel Error for Sample Run on Site 9

Table 1. Error Mean and Standard Deviation for Site 9 Sample Run

Receiver	Mean [m]	Std. Dev [m]
VTRx	1.13	0.74
Novatel	1.8	2.47

COST ASSESSMENT

The primary cost associated with the system is the cost of the receiver and other hardware components. In standalone (non-differential) mode the produces real-time outputs and is designed to replace the GPS receiver typically used in surveys. No additional setup or calibration is required beyond what is required for currently used receivers and so survey costs are expected to be unchanged when replacing an existing GPS based setup.

The costs of the system components are given in the Table 2. A base system requires a VTRx receiver and a GPS antenna for an approximate total cost of $2500. This cost is based on using the dual-frequency Novatel Pinwheel antenna used in the demonstration. Since the VTRx only receives on the L1 band, a lower-cost antenna could be substituted without changing performance. The CSAC and IMU can be optionally added to the system to improve performance, particularly when less than three satellites are visible.

Table 2. System Component Costs

Component	Cost
VTRx Receiver	$1,500
CSAC [Optional]	$4,500
HG1930 IMU [Optional]	$7,000-10,000
Novatel Pinwheel Antenna	$1,000

A primary driver of the cost effectiveness of the system is the amount of GPS challenging terrain (such as heavy foliage areas) that is present on the site. For sites with areas that a traditional GPS receiver cannot reliably track satellites and produce an accurate position, the VTRx provides significant cost savings over other alternatives such as robotic total stations or systems containing high-end IMUs.

The primary cost benefit of the VTRx system is in the ability to use GPS based survey methods in areas where a standard GPS receiver would not provide acceptable availability. The ability to continue to use GPS deeper into foliage areas provides a significant cost benefit over alternatives such as robotic total stations. The system hardware is less expensive than most robotic total stations or other alternative systems containing high-end IMUs. Additionally, in contrast to a robotic total station, no additional setup is required greatly improving productivity and reducing the per-acre survey cost.

IMPLEMENTATION ISSUES

The demonstrated system consists primarily of a custom-built prototype that makes use of COTS components to the extent possible. The prototype system was developed exclusively for this effort and is not currently commercially available. Six prototype systems have been built to date and two are available as deliverables on this effort.

Since the conclusion of this effort, however, IS4S has developed a next generation software receiver (VTRx V2) based on lessons learned in this effort and demand from other DoD customers. While not yet a commercial product, approximately 25 of the receivers have been built and a significant portion of those delivered to customers. The VTRx V2 hardware is shown in Figure 8. This system improves on the demonstrated platform in several areas:

- RF front-end replaced by a wide-band front-end capable of receiving signals with bandwidths up to 36 MHz on L1, L2, or L5
- Two RF receive chains for multi-band operation.
- Improved enclosure and mechanical designs improve robustness and reduces assembly costs.
- Improved channel manager drastically reduces acquisition time and tracking robustness.

Figure 8. VTRx V2 SDR Platform

1.0 INTRODUCTION

1.1 BACKGROUND

Geophysical mapping is a key step in the process of remediating sites contaminated with unexploded ordnance (UXO). In order to accurately locate UXO, accurate measurements of the positions of the geophysical sensors are needed. The need for accurate, real-time pose (position and attitude) estimates has increased in recent years as more advanced sensors are developed that are capable of not only detecting anomalies, but also discriminating items of interest from cultural debris. A combination of a global positioning system (GPS) receiver and an inertial measurement unit (IMU) is a common method of determining the position and orientation of these sensors. GPS signals are extremely low power, however, and the performance of GPS receivers degrades rapidly when these signals are attenuated or blocked by nearby buildings or foliage. An example survey in a heavy foliage environment is shown in Figure 1-1.

Figure 1-1. Geophysical Survey Under Heavy Foliage in Culebra, Puerto Rico

Currently, in areas where there are strong or frequent attenuations or blockages of the GPS signal alternative methods of positioning such as laser or RF based ranging systems or odometry are used. Ranging based systems such as robotic total stations, such as the example shown in Figure 1-2, that are traditionally used in surveying applications or more developmental RF based ranging systems are capable of providing very accurate position measurements in GPS denied areas. They often, however, require line of sight to the receiver and are cumbersome and time consuming to set up. Systems such as total stations are also generally considerably more expensive than a GPS receiver. Odometry solutions, based on wheel encoders or IMUs, have error characteristics that grow over time and require prohibitively expensive sensors to provide accurate positions for periods longer than a few minutes.

Figure 1-2. Surveyor Operating a Robotic Total Station

This work will attempt to improve the accuracy and availability of position measurements for geophysical surveys by providing a GPS/INS system capable of providing positions in environments where standard GPS receivers provide a poor solution or fail to provide a solution at all. A GPS software defined receiver (SDR) will be developed that is capable of providing a position solution in degraded GPS environments such as under heavy foliage by making use of vector tracking techniques. The GPS position will be blended with the output of a commercial IMU to provide attitude measurements and allow brief periods of dead-reckoning during complete GPS outages. A chip scale atomic clock (CSAC) will be used as the receiver clock to further improve reacquisition time and the receiver's ability to operate with a limited number of satellites.

1.2 OBJECTIVE OF THE DEMONSTRATION

The objective of the demonstrations performed under this effort was to validate the proposed GPS receiver under controlled conditions and compare its performance to GPS navigation systems currently used for geophysical surveys. Additionally, a ranging based positioning system such as a robotic total station was used to provide "truth" measurements allowing the absolute performance of the system to be determined in addition to comparing it to a traditional GPS receiver. These demonstrations validate the utility of the developed system and can be used to aid in transition of the technology to end users.

1.3 REGULATORY DRIVERS

This project is primarily motivated by the desire for more efficient and accurate survey operations, to achieve better technical performances at reduced cost. The ability to perform GPS/INS based surveys in areas that previously required systems with tedious setup requirements or reduced accuracy will support faster, better and cheaper detection, characterization, and anomaly removal. Regulatory issues do not directly affect the need for this technology.

2.0 TECHNOLOGY

2.1 TECHNOLOGY DESCRIPTION

The system developed and demonstrated in this effort is a GPS SDR that makes use of vector tracking techniques to improve the receiver's ability to track and reacquire weak signals. The GPS position can also be optionally blended with the output of a commercial IMU to provide attitude measurements and allow brief periods of dead-reckoning during complete GPS outages. A chip scale atomic clock (CSAC) can also be optionally integrated to further the receiver's ability to operate with a limited number of satellites. This combination of techniques provides a receiver that is capable of tracking signals at lower carrier to noise ratios, "instantly" reacquire satellites after brief outages, and navigate for periods with less than 4 satellites in view.

The receiver is shown in Figure 2-1 and Figure 2-2. The hardware consists of a combination of commercial off-the-shelf (COTS) components combined with custom electronics. The software receiver based design allows the receiver algorithms to be defined completely in software, allowing an easy upgrade path as more advanced algorithms are developed. This design also drastically reduces development cost when compared to a traditional application-specific integrated circuit (ASIC). Details on the receiver algorithms, software and hardware are provided in the following sections.

Figure 2-1. VTRx Receiver

Figure 2-2. VTRx Receiver Internal Components

2.1.1 GPS Receiver Architecture

Traditional GPS receivers use scalar tracking loops to process received satellite signals. A block diagram showing a standard GPS receiver architecture is shown in Figure 2-3. The GPS receiver performs several operations to produce the position, velocity, and time (PVT) output on the far right of the figure. First, the signal is received at the antenna and processed by the RF front-end. In this step, a local oscillator offset from the signal frequency (e.g., GPS L1) by an amount equal to the intermediate frequency (IF) is used to mix the signal down to the IF frequency.

An analog-to-digital converter then produces a set of digital samples of the IF signal. Once the satellites signals are acquired (not shown), a tracking loop is used to track the signal from each satellite by generating a local replica of the signal and minimizing the offsets between the received signal and this local replica. It should be noted that in a traditional architecture the tracking loops in different channels of the receiver operate independently of each other. The outputs of the tracking loops are then used to generate range and range rate measurements (typically referred to as pseudorange and pseudorange rates due to the receiver clock bias inherent in the measurements). The navigation processor combines range and range rate measurements from multiple channels to generate the PVT solution. In Figure 2-3, notice that the tracking channels and navigation processor are distinct operations with one-way data flow from the tracking channel to the navigation processor.

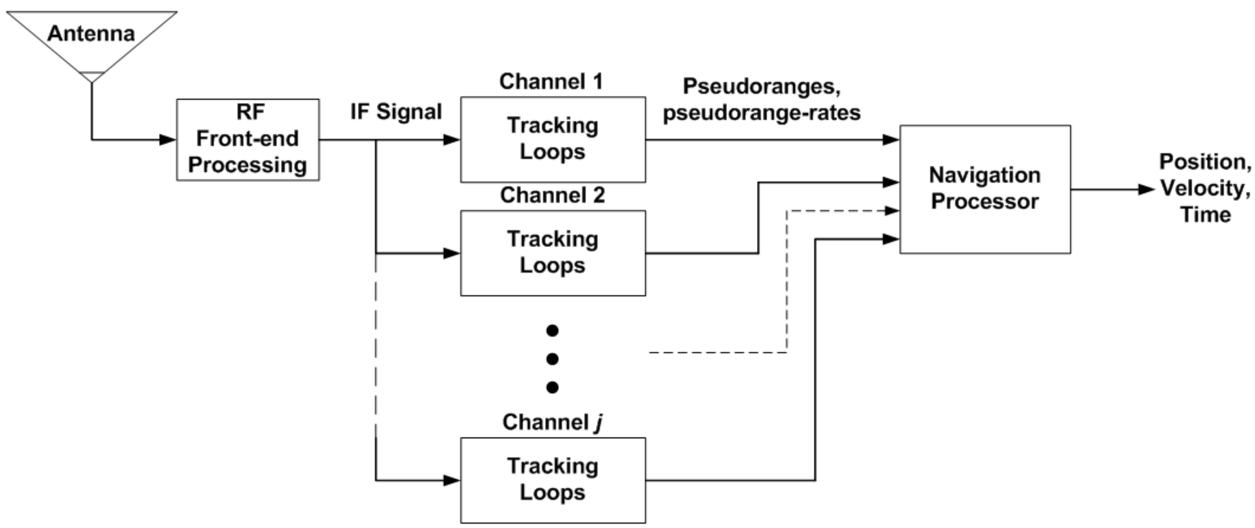

Figure 2-3. Block Diagram Showing the Operations of Traditional Scalar Tracking GPS Receiver.

To improve the performance of the GPS receiver in low signal strength environments, the VTRx receiver developed for this effort combines the tracking and navigation step to form a vector tracking receiver. A block diagram of the vector tracking process is shown in Figure 2-4. In the figure, the range and range-rate measurements from the tracking channels are replaced by range and range-rate error values, and feedback from the navigation processor to the tracking channels is added. Conceptually, the signal tracking is performed in the position, velocity, and time domain rather than along the line-of-sight to each visible satellite. This reduces the number of unknowns and allows the receiver to share signal power across channels so that the channels tracking weak signals are aided by the channels tracking strong signals resulting in an improvement in tracking performance. Additional, since the signal parameters are generated based on the navigation processors PVT estimate, it is possible to continue to estimate the parameters for a satellite that is no longer in view, allowing “instant reacquisition” when the signal returns. As a result, the vector tracking receiver provides improved performance when signals are attenuated or temporarily blocked by foliage.

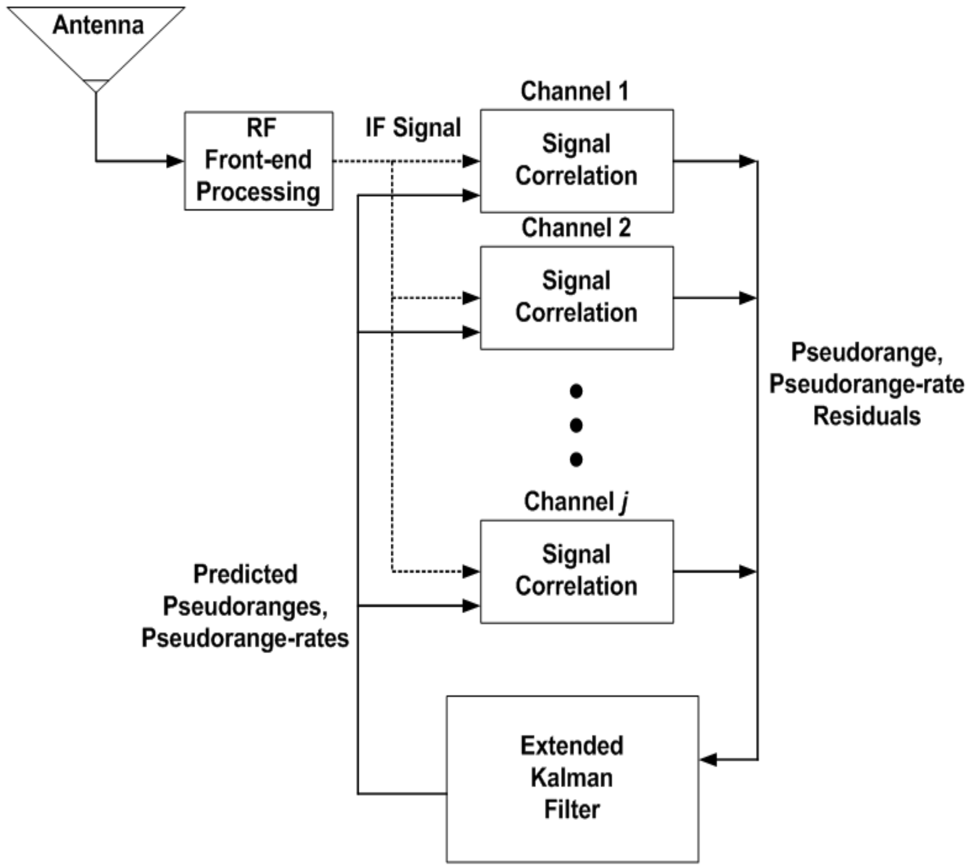

Figure 2-4. Block Diagram Showing the Modified Architecture of a Vector Tracking GPS Receiver.

In the remainder of this section, classical GPS signal tracking and advanced vector tracking receiver architectures are discussed in detail. Equations for implementing classical tracking (e.g., "scalar" tracking) and vector tracking are provided. Next, there is a discussion of integrating Inertial Measurement Unit (IMU) measurements in the tracking architecture. The hardware implementation is described along with design constraints associated with real-time operation. Finally, the performance of the vector tracking receiver is compared to the traditional approach in simulation and experimentally.

A block diagram showing the basic functions of a tracking channel in a GPS receiver is provided in Figure 2-5. The tracking channel is responsible for maintaining an accurate replica of the received signal. The replica is comprised of the binary pseudorandom noise code (PRN) and sinusoidal carrier. The tracking channel must track the phase of the PRN code and the frequency of the sinusoidal carrier to provide the navigation processor with range and range rate measurements. The local replicas are compared to the received signal in the integrate and dump cycle of the tracking channel.

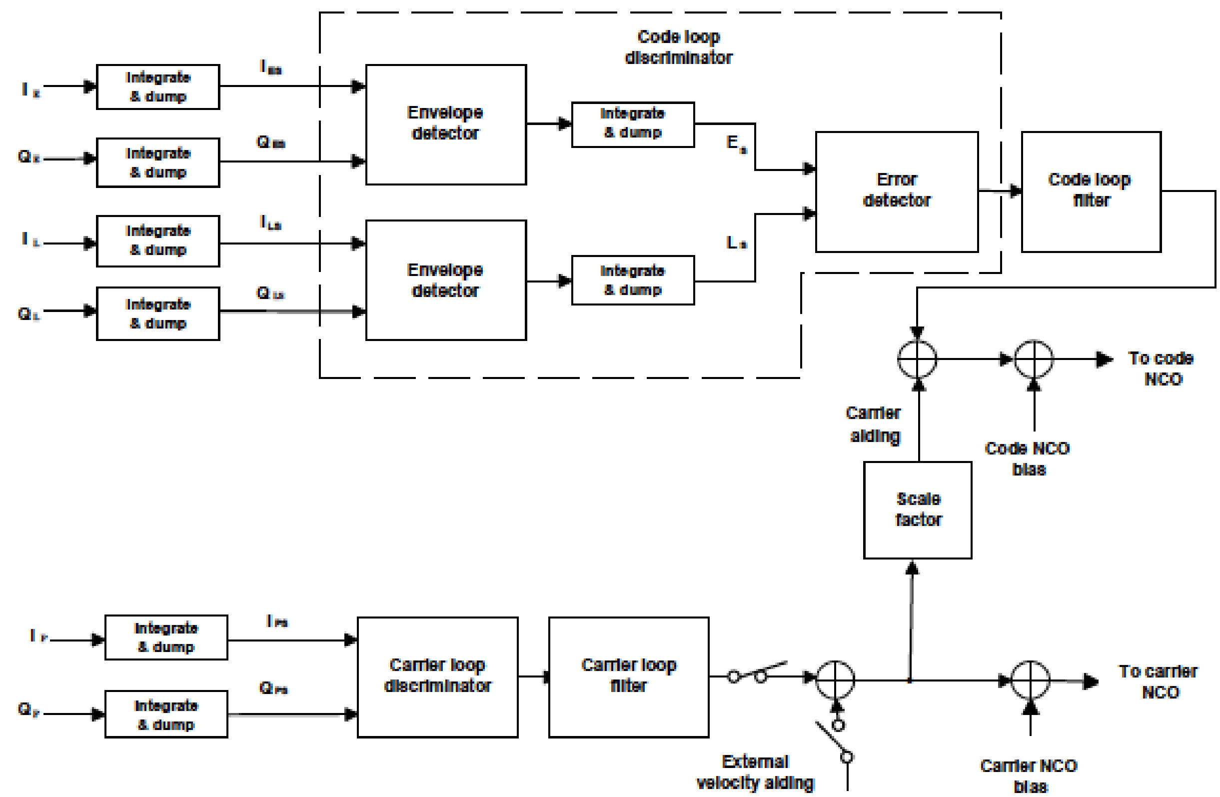

Figure 2-5. Block Diagram of Traditional Receiver Tracking Design [Brown].

After the integrate and dump cycle, the correlator outputs are passed through discriminator functions where observations of the code and carrier replica error are generated. These errors are passed through loop filters, and the outputs are used to update the code and carrier numerically controlled oscillators (NCOs). The fi gure also shows carrier aiding to the delay lock loop tracking the code phase. The Doppler frequency must be appropriately scaled by the relative frequency of the CA code and GPS L1. The order and bandwidth of the code and carrier loop filters have a significant impact on tracking performance. In particular, the selection of the noise equivalent bandwidth of the loop filters is a trade-off between tracking rapid signal changes and filtering noisy discriminator outputs.

2.1.1.1 Classical Receiver Design

As shown in Figure 2-5, for a traditional receiver the tracking channel updates the code and carrier NCO values in a two-step process. First, a discriminator function is used to measure the error in the replica. Next, the error is passed through a loop filter to determine the appropriate correction to the NCO value. The software-defined GPS receiver design presented in this report uses a normalized early minus late power discriminator to measure the code phase error. The discriminator is shown in Equation (1).

$$\delta c = \frac{\sqrt{IE^2 + QE^2} - \sqrt{IL^2 + QL^2}}{\sqrt{IE^2 + QE^2} + \sqrt{IL^2 + QL^2}} \qquad (1)$$

In the equation, the IE, IL, QE, and QL represent the in-phase early, in-phase late, quadrature early, and quadrature late correlator outputs respectively. The correlator spacing is plus and minus ½ chip.

The delay lock loop (DLL) is implemented by a 2nd order loop filter with carrier aiding. A block diagram showing the delay lock loop architecture is shown in Figure 2-6. Note that the loop filter gains are fixed and are calculated following the formulation in [Kaplan] as a function of the desired noise equivalent bandwidth. The integration period (T) for the delay lock loop is 20 ms which is the maximum coherent integration period possible due to the 50 Hz navigation message modulated on GPS L1.

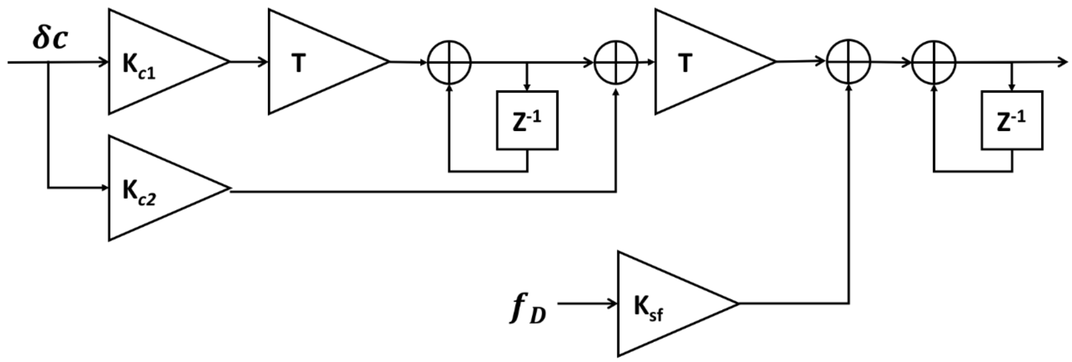

Figure 2-6. Block Diagram of Second Order Carrier Aided Delay Lock Loop

A frequency lock loop (FLL) is used to track the received carrier signal. The frequency lock loop is more robust than a phase lock loop when the tracking loop is stressed to its limits by the dynamics of the platform. A four-quadrant arctangent frequency discriminator seen in Equation (2) is used to measure the carrier frequency error.

$$\delta f = \frac{atan2\left(\frac{IP_1 QP_2 - IP_2 QP_1}{IP_1 IP_2 + QP_1 QP_2}\right)}{\pi T} \tag{2}$$

Note that two consecutive 10 ms integration periods are used to generate the first and second in-phase prompt (IP_1, IP_2) and quadrature prompt (QP_1, QP_2) correlator outputs. Two frequency lock loop implementations are common for carrier frequency tracking in low signal strength environments – a 2nd order and 3rd order tracking loop. Block diagrams of the 2nd order and 3rd order frequency lock loops are shown in Figure 2-7 and Figure 2-8, respectively.

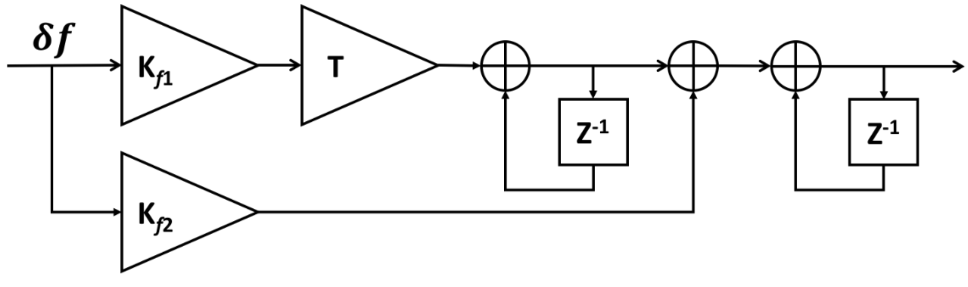

Figure 2-7. Block Diagram of Second Order Frequency Lock Loop

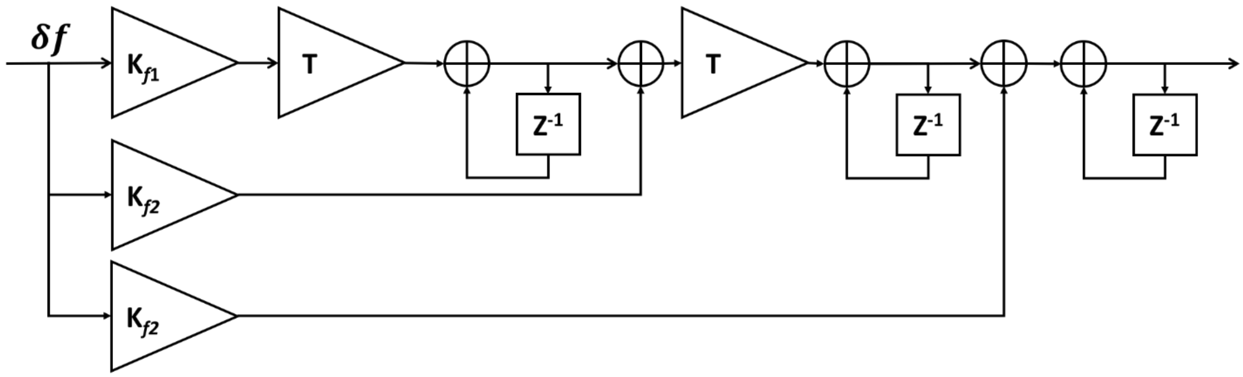

Figure 2-8. Block Diagram of Third Order Frequency Lock Loop

Again, the filter coefficients are calculated based on the desired noise equivalent bandwidth as shown in [Kaplan].

2.1.1.2 Vector Tracking Receiver Design

The alternative to the traditional fixed gain scalar tracking channel is the vector tracking Kalman filter based loop filters that were implemented in the VTRx receiver. The Kalman filter iteratively determines the optimal loop filter gain based on the statistical properties of the signal model and the correlator noise model. The Kalman loop filter may be implemented on each channel independently, or it may be implemented in the position, velocity, and time domain in a formulation (i.e., vector tracking). In the vector tracking architecture, the correlator output or the discriminator outputs are used to directly update the navigation processor state estimates. The code and carrier NCO values are then derived from the state estimates, the satellite position, velocity, and time. A block diagram of the vector tracking receiver is shown in Figure 2-9. The figure depicts a vector delay and frequency lock loop (VDFLL) architecture. In this formulation, the code phase and carrier frequency discriminators (seen in Equations (1) and (2)) are used to update the estimated position, velocity, clock bias, and clock drift of the receiver. The code and carrier frequency used to drive the NCO values are calculated based on the current best estimates of the navigation processor.

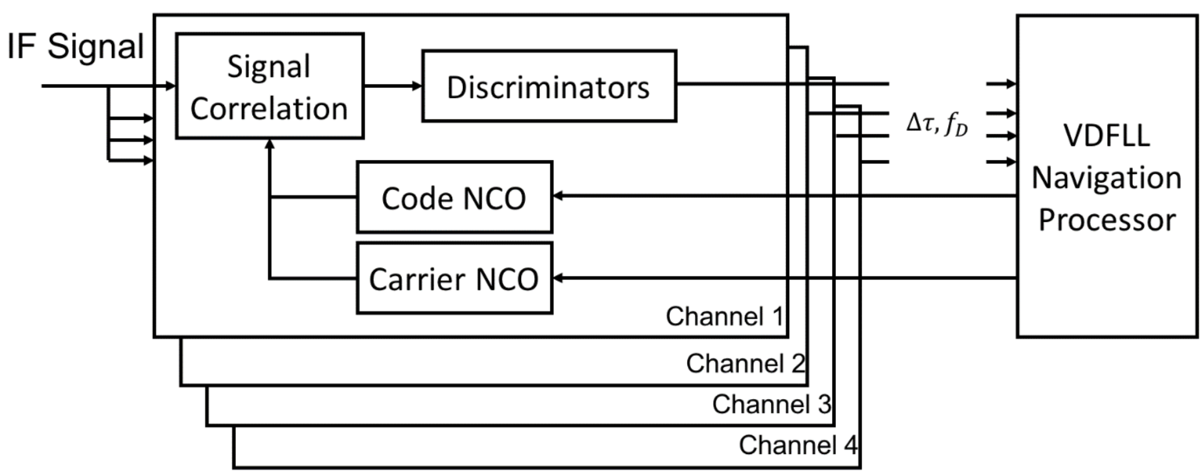

Figure 2-9. Block Diagram of Vector Delay/Frequency Lock Loop

The navigation processor shown in Figure 2-9 is responsible for estimating the receiver position and velocity in Earth-Centered-Earth-Fixed (ECEF) coordinates. The state vector of the navigation processor Kalman filter is given in Equation (3). The state vector consists of the receiver's position (x, y, z), velocity $(\dot{x}, \dot{y}, \dot{z})$, clock bias (b) and clock drift $(\dot{b})$.

$$\mathrm{X} = [x \quad \dot{x} \quad y \quad \dot{y} \quad z \quad \dot{z} \quad b \quad \dot{b}]^{\mathrm{T}} \tag{3}$$

A dynamic model is required to propagate the estimated state vector between measurement updates. One option is a kinematic model that assumes that the acceleration of the GPS antenna can be modeled as zero mean Gaussian random noise. This model is sufficient for many platforms. It is easily extended to high order by adding an acceleration state in the x, y, and z coordinate directions and assuming that the platform jerk can be modeled as zero mean Gaussian noise. The random acceleration model results in the following state transition matrix.

$$\Phi = \begin{bmatrix} \alpha_{2x2} & 0_{2x2} & 0_{2x2} & 0_{2x2} \\ 0_{2x2} & \alpha_{2x2} & 0_{2x2} & 0_{2x2} \\ 0_{2x2} & 0_{2x2} & \alpha_{2x2} & 0_{2x2} \\ 0_{2x2} & 0_{2x2} & 0_{2x2} & \alpha_{2x2} \end{bmatrix} \tag{4}$$

The α matrices relate the position and velocity along each coordinate axis as seen in Equation (5).

$$\alpha = \begin{bmatrix} 1 & \Delta T \\ 0 & 1 \end{bmatrix} \tag{5}$$

The process noise covariance matrix is used to capture the increased uncertainty due to the unknown platform acceleration. The matrix is calculated as seen in Equation (6).

$$Q = \begin{bmatrix} Q_x & 0_{2x2} & 0_{2x2} & 0_{2x2} \\ 0_{2x2} & Q_y & 0_{2x2} & 0_{2x2} \\ 0_{2x2} & 0_{2x2} & Q_z & 0_{2x2} \\ 0_{2x2} & 0_{2x2} & 0_{2x2} & Q_b \end{bmatrix} \tag{6}$$

In practice, the acceleration uncertainty can be defined uniquely for each coordinate direction based on known platform constraints.

$$Q_x = Q_y = Q_z = \begin{bmatrix} \sigma^2 \dfrac{\Delta T^3}{3} & \dfrac{\sigma^2 \Delta T^2}{2} \\ \dfrac{\sigma^2 \Delta T^2}{2} & \sigma^2 \Delta T \end{bmatrix} \tag{7}$$

The process noise matrix also includes parameters for modeling the uncertainty in the clock bias and clock drift due to oscillator variations. Variations in the frequency of the oscillator create signal dynamics that must be tracked by the receiver tracking loops. This means that the frequency spectrum of the receiver oscillator should be considered when modeling the receiver clock uncertainty.

Phase noise specifications for commercial oscillators are typically provided at several key frequencies offset from the nominal frequency and allow the end user to reconstruct an approximate single sideband noise spectrum. Using the data from the oscillator specifications, a polynomial is fit to the phase noise spectrum to determine the power law parameters normally used to characterize oscillators. The power law coefficients complete the model for the oscillator power spectral density seen in Equation (8).

$$S_{\phi}(f) = N^2\left(h_0 + \frac{h_1}{f} + \frac{h_2^2}{f^2} + \frac{h_3^3}{f^3} + \frac{h_4^4}{f^4}\right) \tag{8}$$

Based on the clock specification for a typical temperature compensated crystal oscillator (TCXO) the h_2 and h_4 parameters were found to be $2.8\text{x}10^{-23}$ and $2.4\text{x}10^{-23}$ respectively. The h_2 and h_4 parameters are used to model the uncertainty in the clock bias and clock drift states as seen in Equation (9).

$$Q_b = \begin{bmatrix} \frac{h_2}{2}\Delta T + \frac{2}{3}\pi^2 h_4 \Delta T^3 & \pi h_4 \Delta T^2 \\ \pi h_4 \Delta T^2 & 2\pi h_4 \Delta T \end{bmatrix} \tag{9}$$

The Kalman filter state and covariance estimates are propagated during the time update using the models described above and the time update equations given in Equation (10).

$$\begin{aligned} \mathrm{X} &= \Phi \mathrm{X} \\ \mathrm{P} &= \Phi \mathrm{P} \Phi^{\mathrm{T}} + Q \end{aligned} \tag{10}$$

At the end of the integrate and dump period for each channel, the code and carrier discriminators are used to update the navigation solution. The CA code chip width (λ_c) and the wavelength of the carrier (λ_{L1}) are used to transform the signal errors into pseudorange and pseudorange rate residuals. The measurement vector is shown in Equation (11).

$$z = \begin{bmatrix} \delta c * \lambda_c \\ \delta f * \lambda_{L1} \end{bmatrix} \tag{11}$$

The pseudorange and pseudorange rate residuals map to the state domain through the unit vectors from receiver to satellite and an identity matrix relating the clock bias and clock drift estimates. The Kalman measurement matrix is given in Equation (12).

$$H = \begin{bmatrix} u_x & 0 & u_y & 0 & u_z & 0 & 1 & 0 \\ 0 & u_x & 0 & u_y & 0 & u_z & 0 & 1 \end{bmatrix} \tag{12}$$

The Kalman measurement covariance matrix is calculated as a function of the carrier-to-noise density ratio (C/N_0) and the integration period (T) using Equation (13).

$$R = \begin{bmatrix} \frac{\lambda_c{}^2}{2T\frac{C}{N_0}}\left(\frac{1}{2}+\frac{1}{T\frac{C}{N_0}}\right) & 0 \\ 0 & \left(\frac{\lambda_{L1}}{\pi T}\right)^2 \frac{2}{T\frac{C}{N_0}}\left(1+\frac{1}{T\frac{C}{N_0}}\right) \end{bmatrix} \tag{13}$$

Once the residual vector, measurement matrix, and measurement covariance matrix have been calculated, the Kalman filter measurement update is performed using Equation (14).

$$\begin{aligned} K &= PH^T(HPH^T + R)^{-1} \\ \mathrm{X} &= \mathrm{X} + K\mathrm{z} \\ \mathrm{P} &= (I - KH)\mathrm{P} \end{aligned} \tag{14}$$

The *a posteriori* state estimates are used to predict the received time of the start of the next code period and calculate the desired code frequency for the code NCO. First, a prediction of the state vector at the end of the *k+1* integrate and dump period is calculated using the state transition matrix. Note that the state (mean and covariance) estimates are not propagated forward in this step because the filter time update is performed at the end of each integration period. The state vector prediction and the predicted satellite positions are used to calculate a prediction of the pseudorange at the end of the current integration period as seen in Equation (15).

$$\hat{\rho}_{k+1} = \left|\vec{r}_{s_{k+1}} - \hat{r}_{r_{k+1}}\right| + \hat{b}_{k+1} \tag{15}$$

The subscript *k+1* is used to denote the end of the current integration period where *k* is the current time. The three-dimensional satellite position ($\vec{r}_{s_{k+1}}$) is calculated using the decoded ephemerides. The predicted three-dimensional receiver position is represented by ($\hat{r}_{r_{k+1}}$) and ($\hat{b}_{k+1}$) represents the predicted clock bias. The operator | | represents the Euclidean norm.

The transmission time ($t_{t_{k+1}}$) of the start of a code period is synchronized to GPS time, and is a known quantity based on the decoded navigation message and the code period counter in the receiver. The received time of the first sample of the code period starting at time *k+1* is calculated using Equation (16).

$$\hat{t}_{r_{k+1}} = t_{t_{k+1}} + \hat{\rho}_{k+1} \tag{16}$$

At this point, the start time (i.e., current receiver time $t_{r_{k+1}}$) and the predicted end time (i.e., current receiver time $\hat{t}_{r_{k+1}}$) of the current integration period are available. The CA code chipping rate is 1.023x10^6, and the integration period is 20 milliseconds. Therefore, the desired code frequency is calculated by dividing the number of chips by delta time as seen in Equation (17).

$$f_{code} = \frac{1.023\text{x}10^6\ \mathrm{T} - \theta_{c_k}}{\hat{t}_{r_{k+1}} - t_{r_k}} \tag{17}$$

The CA code chip transition does not happen on a whole sample from the front end, therefore the current code phase (θ_{c_k}) is subtracted from the total number of chips in the 20 milliseconds integration period.

The carrier NCO command is calculated as a function of the predicted satellite and receiver relative velocities and the predicted receiver clock drift. The line-of-sight relative velocity is calculated using Equation (18).

$$v_{los} = [u_x \quad u_y \quad u_z][\vec{v}_{s_{k+1}} - \hat{v}_{r_{k+1}}] \tag{18}$$

With the line-of-sight velocity and the predicted receiver clock drift, the carrier NCO value is calculated with Equation (19).

$$f_{carrier} = \frac{\left(1 - \frac{v_{los}}{c}\right) f_{L1}}{1 + \frac{\hat{\dot{b}}}{c}} - f_{L1} + f_{IF} \tag{19}$$

2.1.1.3 INS Aided Loop Filters

An inertial measurement unit (IMU) is often paired with GPS to provide a robust navigation solution. IMU measurements are mechanized to estimate the position, velocity, and orientation of the platform using angular velocity and translational acceleration measurements. The resulting navigation system is referred to as an inertial navigation system (INS). INS estimates may be combined with GPS estimates of position and velocity at a loose, tight, or deep integration level. In each implementation, the navigation filter states are propagated in time using the IMU angular rate and acceleration measurements (i.e., IMU measurements replace the zero mean Gaussian acceleration assumption of the GPS Kalman filter described above). The three approaches are differentiated by the way the GPS receiver interacts with the updated navigation solution. In a loose-integration, the GPS position and velocity estimates are used to update the navigation solution. The tightly-integrated system typically uses the GPS pseudorange and pseudorange rate measurements to update the navigation solution, and the deeply-integrated system uses the discriminator outputs from the tracking channel to correct the navigation solution. It is possible to use the INS solution to aid the tracking channels. Deep integration requires that the navigation solution be used to generate the code and carrier NCO values as shown in the VDFLL implementation described above. This requirement ensures that the code and carrier discriminator values accurately represent the error in the navigation solution.

As stated above, the INS navigation solution may be used to aid the GPS tracking loops in either a scalar or vector formulation. In the case where a tradition scalar tracking loop is used to maintain the code and carrier replica, the INS information enters the tracking loop similarly to the carrier aided code loop implementation shown in Figure 2-6. The INS velocity estimates are combined with the satellite trajectory information and the receiver clock drift estimates to predict the Doppler frequency of the received signal. The predicted Doppler is then added as a feedforward term to the tracking loop as seen in Figure 2-10. With the appropriate scalar factor (Ksf), the Doppler may be added to the code and/or carrier loop.

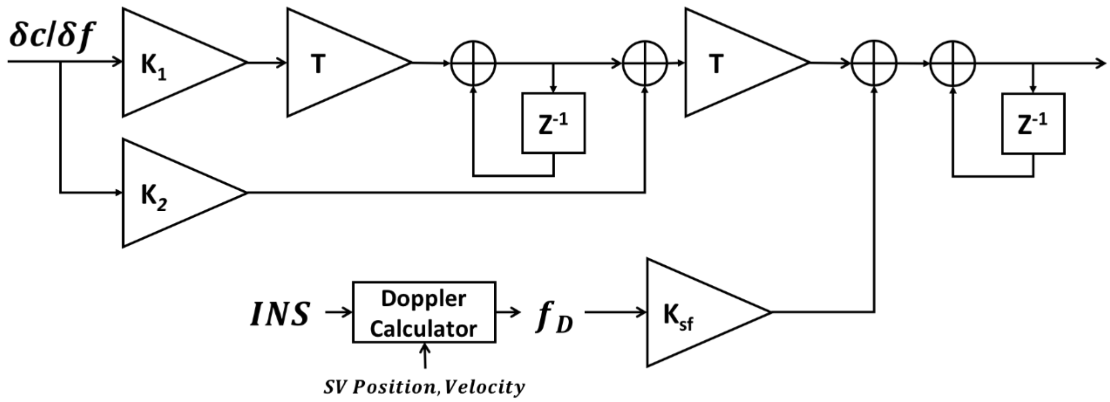

Figure 2-10. Block Diagram of INS Aided Scalar Tracking Loop

When formulating a deeply-integration GPS/INS navigation solution, the IMU and the GPS share a common navigation processor. The IMU measurements are used in the time-update step of the Kalman filter are described above, and the code and carrier discriminator values are used to perform the measurement-update. The code and carrier NCO are updated using the same procedure as the VDFLL implementation described in Equations (15) through (19). A block diagram showing the architecture is shown in Figure 2-11.

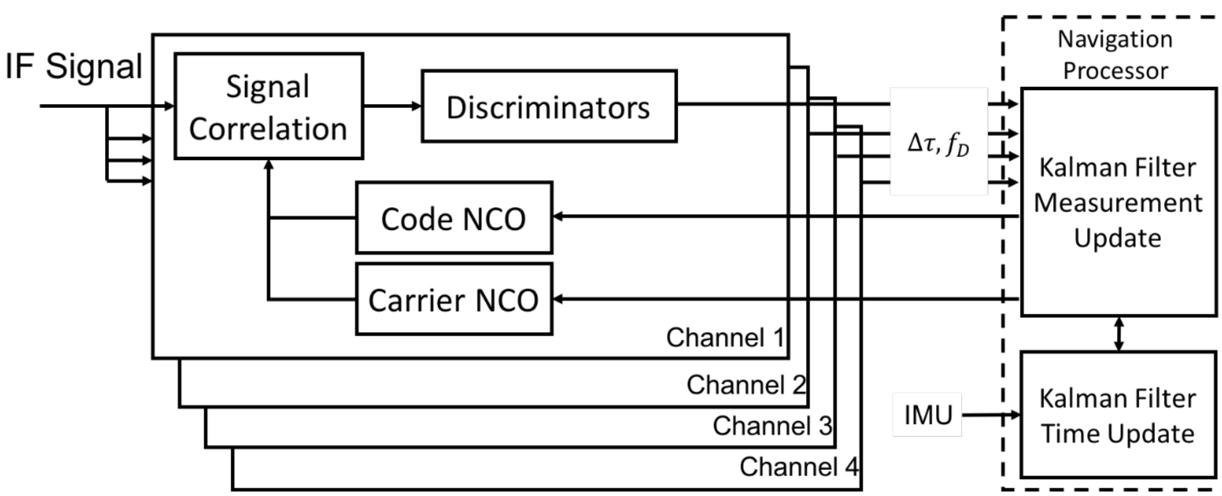

Figure 2-11. Block Diagram of INS Aided Vector Delay/Frequency Lock Loop

2.1.2 Real-Time Implementation

The VTRx receiver is implemented on a Xilinx Zynq 7020 all-programmable platform. The Zynq is a System-on-Chip (SOC) that incorporates an Artix 7 FPGA with a dual-core ARM Cortex A9 processor on a single chip. This allows the FPGA and processor to maintain the same tight coupling seen with soft-core processors while gaining the performance from including a hard-core processor with two cores. The block diagram in Figure 2-12 shows the components of the VTRx receiver including peripheral sensors (i.e., CSAC, HG1930, Microstrain IMU). The Zynq SOC is represented by the dark blue SDR Processor block.

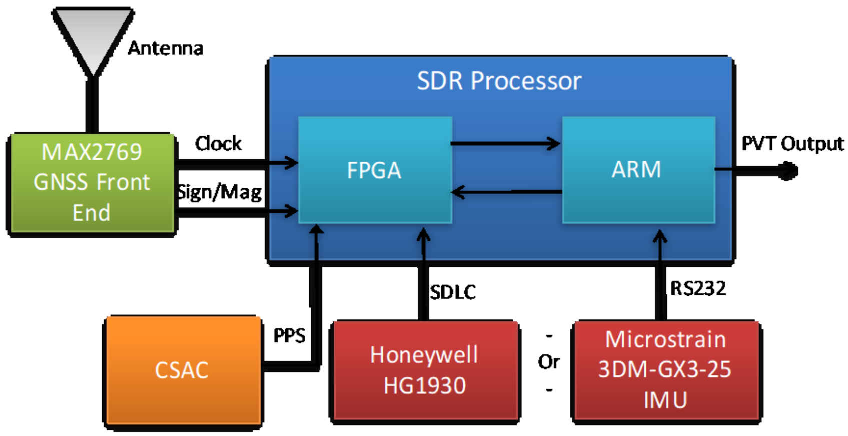

Figure 2-12. Block Diagram of Hardware Components for the VTRx Receiver.

Pictures of the final printed circuit board (PCB) hardware and enclosure are provided in Figure 2-13. A MicroZed development board contains the Zynq 7020 and various input/output (I/0) including ethernet, USB, and serial connections. The Microzed is attached to a custom board that provides power and CSAC/IMU interfaces. The unit requires 3W of power excluding the IMU power requirement. The enclosure has dimensions of 6.5x5x2.2 inches or roughly the size of a Novatel Propak V3.

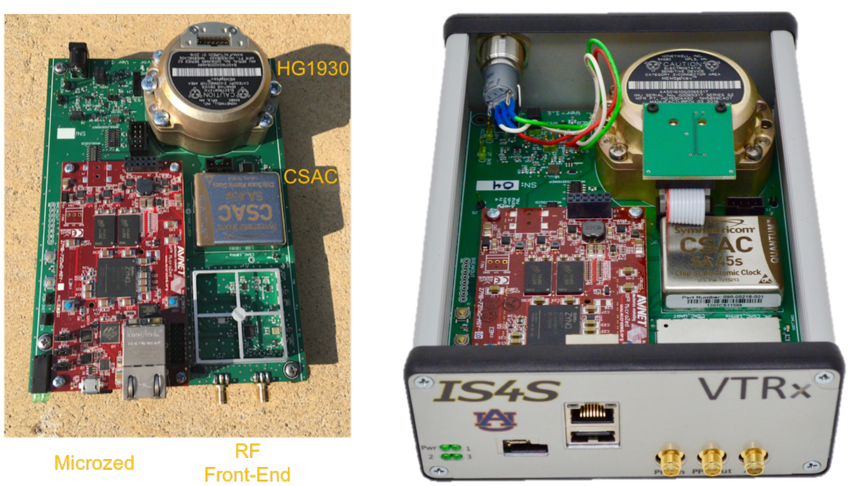

Figure 2-13. Picture of Final Hardware Including the Microzed Development Board, Custom Interface Board, and Enclosure.

The RF front end for this receiver is a MAX2769 from Maxim Integrated Circuits. It may be used to track GPS, GLONASS, or GALILEO. There are also many configurable parameters such as intermediate frequency (IF), filter type and order, automatic gain control (AGC) settings, and sampling frequency (Maxim 2014). Some of the settings used for the VTRx receiver are shown in Table 2-1.

Table 2-1. GPS Front-End Specifications

Sampling Frequency	16.368 MHz
Intermediate Frequency	4.092 MHz
IF Filter Bandwidth	2.5 MHz
IF Filter Order	5th

As described previously, the IF processing includes generating the local signal replica and correlating it with the incoming signal. Any counters or other modules used for book-keeping are also considered part of the IF processing. This must all be done at or above the sampling frequency of the ADC in the front-end to meet real-time requirements. The sampling frequency for the receiver constructed here is 16.368 MHz. In addition to the operating frequency being high, the channels must run in parallel. In commercial receivers, this is often accomplished on application specific integrated circuits (ASICs). However, FPGAs can be used to efficiently perform these high frequency parallel tasks on a reprogrammable platform.

The baseband processing includes the updates for the tracking loops, as well as the navigation solution calculations. The tracking loop updates operate at frequencies from 50 Hz to 1 kHz. With an understanding of the processing requirements of the receiver, the operations of the receiver can also be broken off into different parts of the hardware. The organization of the Zynq is described in Figure 2-14.

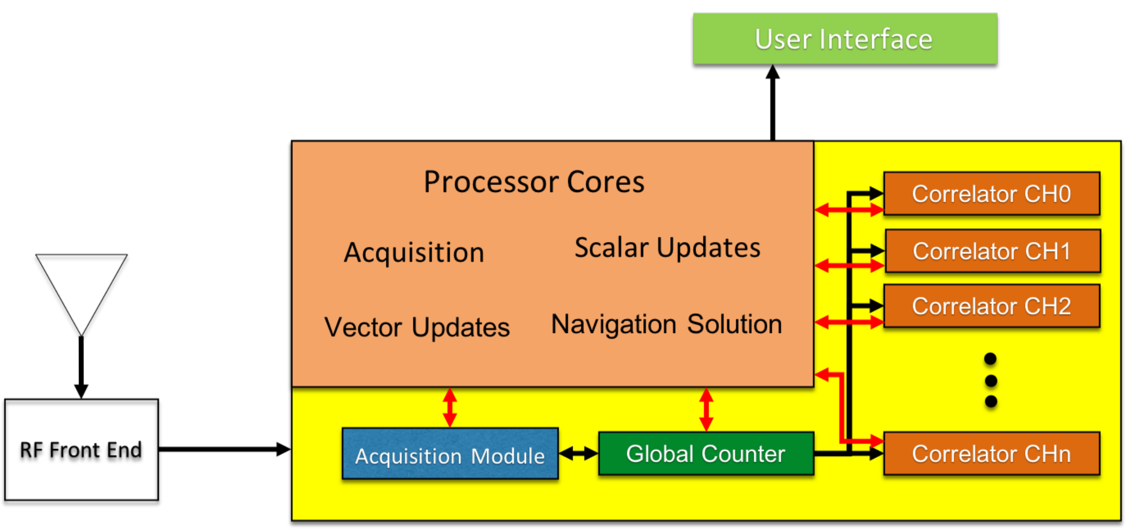

Figure 2-14. Block Diagram Showing the Distribution of Tasks Between Fabric (Yellow Box) and Soft Cores (Orange Box) on Zynq 7020.

The yellow portion indicates the FPGA and the orange indicates the processor. In the FPGA, there are different modules for the different operations of the receiver. The Acquisition module handles the tasks associated with the acquisition algorithm; the Global Counter handles scheduling and synchronization; and the Correlator channels operate as tracking loops. The black arrows in the FPGA indicate signals that pass between modules. Because FPGAs allow for easy routing of signals between these modules, information can be shared between the sections of the FPGA. The red arrows indicate communication from each of the modules to the processor. This is an example of one of the major benefits of the system-on-chip architectures: each module on the FPGA holds register space in the memory of the processor. This allows for easy access to these register spaces from either the FPGA or the processor.

While the scalability of the Zynq architecture gives freedom to select larger hardware if needed, the final hardware implementation relies on the Zynq 7020 found on the Microzed. Thus, the resource utilization of a 12 and 16 channel vector tracking receiver was studied; the results are shown in the table.

Table 2-2. Resource Utilization for Two Configurations of the VTRx Implemented on Zynq 7020

	12 Channel	**16 Channel**
Registers	31%	42%
LUTs	58%	77%
Occupied Slices	84%	96%
DSP Slices	0%	0%
36KB BRAM	1%	1%
18KB BRAM	4%	6%
Processor Cores	50%	50%

The 16 channel approaches utilization of all available logic slices, however without occupying almost 25% of look-up tables and almost 60% of the registers. The implementation leaves free many of the available block RAMs as well as all of the DSP slices. While the DSP slices would be very effective if used for the Correlator modules, their lack of use here simply shows room for further optimization (such as in the Acquisition module). Also, to complete the tracking loop updates and navigation solution, only one of the processor cores has been utilized, freeing up the other processor for other tasks.

As described in the vector tracking section above, the loop closure process is a unique formulation when the receiver operates in the vector tracking mode. Because the outputs of each active channel become measurements in the Kalman filter, completed integration periods from each channel are desired prior to computing the loop update. This becomes difficult due to the fact that each channel will complete integration periods at different times. This can be explained graphically in Figure 2-15.

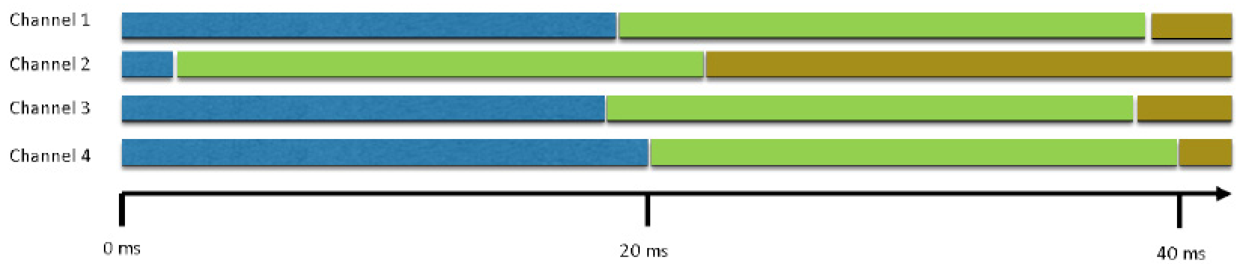

Figure 2-15. Diagram of Asynchronous Loop Closure and Kalman Filter Updates in Real-Time Vector Tracking Implementation.

For vector tracking updates, the interrupts trigger every 20 ms. Each color in Figure 2-15 represents the same transmitted 20 ms signal from each satellite. Due to differences in distances from satellite to user, the integration periods are misaligned. In order to get all of the measurements for a particular integration period, the measurements must be taken after the last of the channels has finished that integration period. In the example shown in Figure 2-15, Channel 4 completes the blue integration period last and will thus be used as the trigger for the vector tracking loop update.

A key issue with this method is illustrated in Figure 2-15. It is known that transit time for satellite signals range from 65 to 83 ms. Because this difference is less than 20 ms, it can be assumed that received signals will not overlap by a whole data bit. However, as illustrated above, as little as 2 ms can be left for overlap. Notice how the blue integration period of Channel 4 ends very near to the beginning of the brown integration period of Channel 2. Ideally, the NCO adjustments based on the blue integration period should be made to the green integration period. If the Kalman filter equations can be updated quick enough, then these updates may be applicable for the green integration period for Channels 1, 3, and 4. However, once the updates have been calculated, the green integration period for Channel 2 will be nearly over. To overcome this issue, the receiver uses the Correlator outputs from the blue integration period and predict the NCO adjustments required for the brown integration period. Thus, the NCO adjustments is applied one integration period late, however they will be calculated based on a prediction of the values of the Kalman filter states at the point that the brown integration period begins.

2.1.3 RTK Vector Phase Locked Loop

High precision RTK GPS receivers require continuous carrier phase lock on multiple satellite signals by the rover and base receiver. The traditional scalar tracking GPS receiver normally maintains phase lock on several signals in environments where the rover receiver has a clear line of sight to the sky, and where the received signal is not disrupted by interference due to atmospheric affects or signal jammers. Applications such as precision surveying in heavy foliage, and autonomous vehicle operation in urban canyons strain the capabilities of the scalar tracking receiver. In this section, a software receiver vector tracking architecture is derived for improved code and carrier tracking in environments that disrupt the operations of a traditional receiver. The receiver combines a Doppler aided vector delay locked loop (VDLL) with an RTK vector phase locked loop (VPLL). A conceptual drawing of the system design is shown in Figure 2-16. The vector tracking software receiver is mounted on the rover vehicle (the tractor in the figure), and a local base station receiver is mounted in the area with a clear view of the sky.

The carrier tracking algorithms of the software vector tracking receiver on the rover uses measurements from the base antenna and the relative position vector, $\vec{r}$, to predict the received signal from each satellite. When measurements are available at the rover, the relative position vector estimates are updated.

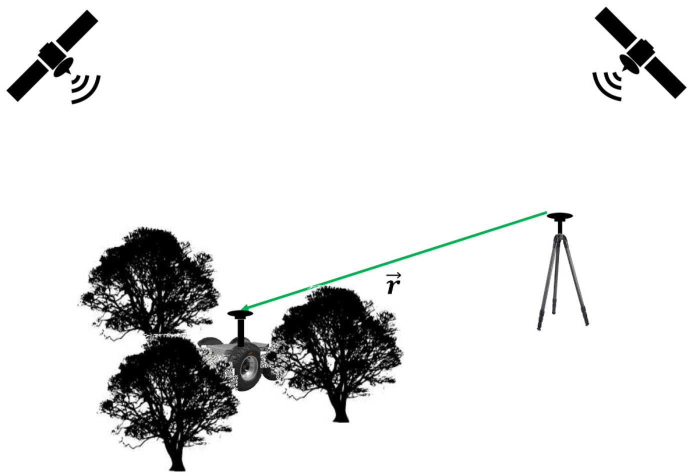

Figure 2-16. The RTK-VPLL Receiver Uses Differential Carrier Phase Positioning and Base Station Measurements to Improve Phase Tracking in Degraded Environments.

The software receiver combines vector code and carrier tracking. In a vector receiver, the local replicas are driven by the navigation solution directly. Due to the differences in the precision of the discriminator-based measurements used to update the navigation solution and possible code/carrier divergence due to ionospheric affects, the vector tracking receiver is designed with two navigation processors. A block diagram of the receiver architecture is shown in Figure 2-17.

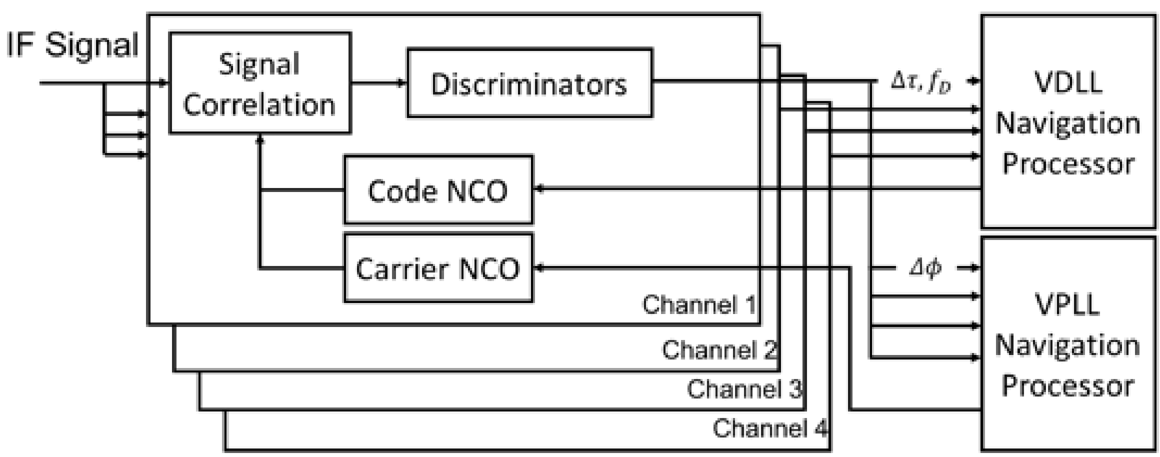

Figure 2-17. The Software Vector Tracking Receive for the Rover Uses Two Navigation Processors to Track Code and Carrier Phase Independently.

In the figure, the code discriminator and Doppler frequency from each channel feed the VDLL navigation processor. The carrier phase discriminator is used to update the VPLL navigation filter.

The VDLL drives the code NCO, and the VPLL drives the carrier NCO. This architecture prevents the less accurate code discriminator measurements from degrading the accuracy of the carrier phase navigation solution. The Doppler measurements are used to improve the velocity and clock drift state estimates in the VDLL navigation filter, and act like carrier smoothing or Doppler aiding in traditional scalar receivers. Also, the VDLL is not a differential navigation filter, meaning that the pseudorange measurements from the base station receiver are not used in the update or prediction step. This design was selected based on the following criteria: the VDLL navigation processor is quite robust without need of external data, the VDLL can maintain a navigation solution during a communication disruption since it does not rely on base station measurements, and the required communication bandwidth can be reduced by removing pseudorange measurements from the payload.

In a vector receiver, the code and carrier NCO values are set using predictions derived directly from the navigation solution. The VDLL navigation processor is only responsible for updating the NCO value used to generate the local code replica. A separate navigation processor is used to drive the carrier NCO. As stated earlier, this architecture is chosen to prevent a degradation in the high precision navigation solution that would result from code phase error measurement updates. The block diagram of the separation of the code and carrier generation was shown previously in Figure 2-17. The block diagram in Figure 2-18 isolates the modules used in the RTK vector phase locked loop (VPLL) and highlights the different modes of the receiver from initialization through to vector operation.

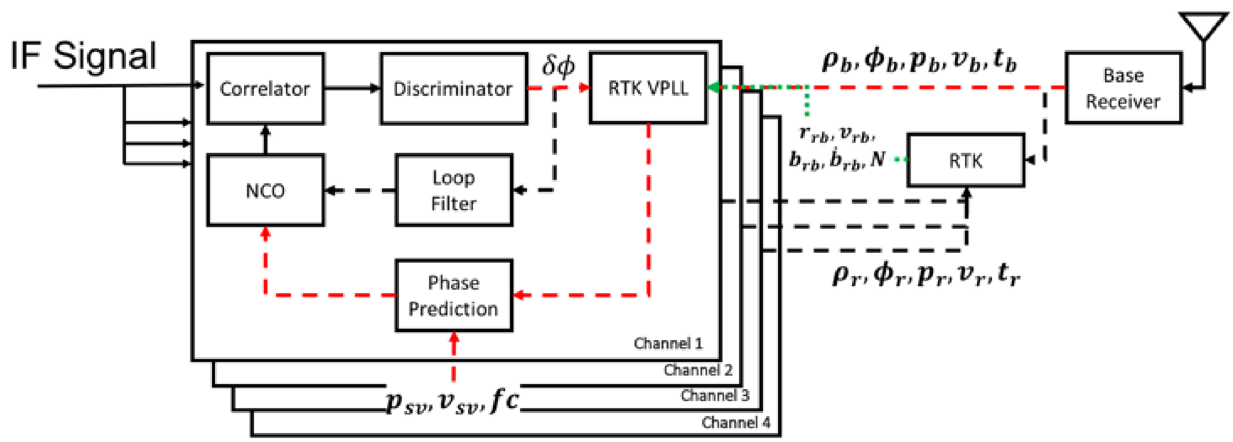

Figure 2-18. Block Diagram of the RTK-VPLL Receiver Architecture Using Data from Base Station and Relative Position Estimates to Close the Carrier Loop.

In the figure, the solid black lines represent the receiver operations that continue at all times, including the correlation and discrimination blocks. The black dashed lines connect the elements that are required to calculate the first receiver position and form the initial high precision relative position vector. The initialization of the RTK-VPLL requires a scalar PLL in the rover receiver, measurements from the base receiver, and a differential carrier phase positioning (RTK) algorithm. The green dotted line shows the outputs of the RTK algorithm that are used to initialize the RTK-VPLL, and the red dashed lines map the route of data through the RTK-VPLL receiver components.

2.1.3.1 RTK-VPLL Kalman Filter

The navigation filter designs in this chapter use code and carrier phase errors calculated from correlator outputs to update the state estimates. Therefore, it is advantageous to review the correlator output model at this time. The mathematical model of the in-phase and quadrature correlators are given by Equation (1).

$$I(k,\gamma) = AR(\epsilon+\gamma)D(k)\cos(\pi f_e T + \delta\phi) + \eta_I(k) \tag{1.a}$$

$$Q(k,\gamma) = AR(\epsilon+\gamma)D(k)\sin(\pi f_e T + \delta\phi) + \eta_I(k) \tag{1.b}$$

In the equations A is the received signal amplitude, ϵ is the code phase error, f_e is the carrier frequency error, and $\delta\phi$ is the carrier phase error. γ is the offset for the early and late replicas used to generate the code phase error measurement. Code phase and carrier phase error observables are used to update the VDLL and VPLL navigation processors.

A Kalman filter is used to maintain high precision relative position estimates in RTK-VPLL navigation processors. The state vector, seen in Equation (2), includes the three-dimensional ECEF relative position vector errors, the relative velocity errors, the relative clock bias error, and the relative clock drift error.

$$X = [\delta x \quad \delta y \quad \delta z \quad \delta\dot{x} \quad \delta\dot{y} \quad \delta\dot{z} \quad \delta cb \quad \delta c\dot{b}]^{\mathrm{T}} \tag{2}$$

2.1.3.2 Initialization

An RTK algorithm is used to estimate the relative position, velocity, and clock states used to initialize the RTK-VPLL navigation processor. After the first integer fix is calculated using the LAMBDA method, the high precision relative position vector (HPRPV) is calculated using the double difference least squares solution. The relative position states of the RTK-VPLL are initialized with the HPRPV. The relative velocity and relative clock states are initialized using the RTK Kalman filter estimates. The vector of fixed integer single difference carrier ambiguities, seen in Equation (3), is recorded and is used as a known quantity in the carrier phase prediction step of the RTK-VPLL algorithm that is described later in this section

$$N = \begin{bmatrix} N_{r,b}^{1} \\ \vdots \\ N_{r,b}^{m} \end{bmatrix} \tag{3}$$

Since the relative velocity and relative clock states are estimated in the RTK algorithm along with the decimal estimates of the carrier ambiguities, the RTK-VPLL navigation solution is updated several times before the loop closure aspect of the vector PLL is initiated. The updates are performed at the update rate of the original RTK algorithm using the single difference carrier phase measurements from the rover and base receivers. This step allows the clock bias estimate in particular to converge to a more precise value that may be used to predict the received carrier phase and close the phase tracking loop.

2.1.3.3 Time Update

The RTK-VPLL is designed assuming that the base receiver is stationary with good sky visibility. Accordingly, the change in the relative position and velocity are the result of the motion of the rover receiver. Therefore, the dynamic model used in the Kalman filter time update is generally the same in the VDLL and the RTK-VPLL. The discrete dynamic model used to propagate the RTK-VPLL navigation solution is shown in Equation (4).

$$X_{k+1} = \Phi_{k,k+1} X_k + Q_k \tag{4.a}$$

$$\Phi_{k,k+1} = \begin{bmatrix} \alpha_k & 0_{2x2} & 0_{2x2} & 0_{2x2} \\ 0_{2x2} & \alpha_k & 0_{2x2} & 0_{2x2} \\ 0_{2x2} & 0_{2x2} & \alpha_k & 0_{2x2} \\ 0_{2x2} & 0_{2x2} & 0_{2x2} & \alpha_k \end{bmatrix} \tag{4.b}$$

$$\alpha_k = \begin{bmatrix} 1 & \Delta t \\ 0 & 1 \end{bmatrix} \tag{4.c}$$

$$Q_k = \begin{bmatrix} Q_x & 0_{2x2} & 0_{2x2} & 0_{2x2} \\ 0_{2x2} & Q_y & 0_{2x2} & 0_{2x2} \\ 0_{2x2} & 0_{2x2} & Q_z & 0_{2x2} \\ 0_{2x2} & 0_{2x2} & 0_{2x2} & 2Q_{cb} \end{bmatrix} \tag{4.d}$$

$$Q_x = Q_y = Q_z = \begin{bmatrix} \frac{\sigma^2 \Delta t^3}{3} & \frac{\sigma^2 \Delta t^2}{2} \\ \frac{\sigma^2 \Delta t^2}{2} & \sigma^2 \Delta t \end{bmatrix} \tag{4.e}$$

$$Q_{cb} = \begin{bmatrix} \sigma_b^2 T + \frac{\sigma_r^2 T^3}{3} & \frac{\sigma_r^2 T^2}{2} \\ \frac{\sigma_r^2 T^2}{2} & \sigma_r^2 T \end{bmatrix} \tag{4.f}$$

Equation (4) is derived from the kinematic relationship of the states and assumes that the velocity states are driven by zero mean Gaussian white noise. Equation (4.e) shows that the variance on the platform acceleration is assumed to be the same in all directions. In practice, it may be possible to use platform constraints when selecting these values. Notice that the process noise matrix reflects the fact that the relative clock bias and drift includes the effects of both the rover and base clocks. Equation (4.f) assumes that the clock model parameter (e.g. σ_b, σ_r) are the same for the rover and base clocks and that the stochastic errors are uncorrelated.

2.1.3.4 Measurement Update

The navigation solution of the RTK-VPLL is initialized with position information that is accurate enough to predict the received carrier phase. To maintain this level of accuracy, the Kalman filter residuals must be as accurate as the single difference carrier phase measurements used to estimate the HPRPV. The carrier phase discriminator provides a range error measurement with an accuracy of a few millimeters. The RTK-VPLL Kalman filter residual is shown in Equation (5).

$$\delta\phi = \lambda_{L1}\,\mathrm{atan}\left(\frac{QP}{IP}\right) \qquad 5$$

The Costas carrier discriminator is used to calculate the residual carrier phase error, and the wavelength of the GPS L1 signal is used to convert to units of meters. The primary error source in the carrier tracking loop is thermal noise. Accordingly, the measurement uncertainty of the carrier discriminator is calculated as a function of the C/N0 ratio of the signal from each channel. Carrier phase error measurement noise is modeled based on the suggestion in [Borre] and is given in Equation (6).

$$\sigma_\phi^2 = \frac{\left(\frac{\lambda_{L1}}{2\pi}\right)}{2T\left(\frac{C}{N_0}\right)} \qquad 6$$

The RTK-VPLL measurement updates are performed at the end of the integrate and dump period on each channel. Therefore, the measurement vector only includes a single carrier phase discriminator for the current channel as seen in Equation (7).

$$z = [\delta\phi_1] \qquad 7$$

The measurement matrix maps the state errors into the measurement domain using the line of sight unit vectors from satellite to receiver. The matrix is defined in Equation (8).

$$H = [a_x \quad 0 \quad a_y \quad 0 \quad a_z \quad 0 \quad -1 \quad 0] \qquad 8$$

The column of negative one relates the relative clock error to the carrier phase residual. The Kalman filter measurement update is performed using the traditional equations defined in Equation (9).

$$K_k = P_k H^T (H P_k H + R_k)^{-1} \qquad 9.a$$

$$P_k = (I - K_k H) P_k \qquad 9.b$$

$$X_k = X_k + K_k z_k \qquad 9.c$$

2.1.3.5 Carrier Loop Closure

To close the carrier tracking loop, the RTK-VPLL state estimates and the carrier phase and Doppler measurements from the base station receiver are used to predict the carrier phase of the received signal at the end of the current integration period. The current integration period refers to the integration period that begins directly after the VPLL measurement update. The prediction step begins with the propagation of the base station carrier phase from the time of the measurement to the end of the current integration period. The updated base station carrier phase is calculated by Equation (10).

$$\hat{\phi}_{b_{k+1}} = \tilde{\phi}_{b_t} + f_{D_{b_t}}(t_{k+1} - t) \qquad 10$$

The *k* notation is not used with the base station carrier phase measurement because the base station measurements are synchronized to GPS time and are not synchronous with the end of an integration period in the rover tracking channels. In Equation (10), ϕ_{b_t} is the most recent base station carrier phase measurement, $f_{D_{b_t}}$ is the most recent Doppler measurement from the base station, and t_{k+1} is the receive time of the end of the current integration period.

Next the RTK-VPLL navigation states are projected forward to time t_{k+1} using the state transition matrix defined in Equation (4.b). The error state (mean and covariance) are not updated at this time. The predicted states are used along with the base receiver predicted carrier phase and the carrier ambiguity to calculate the predicted carrier phase at the rover at time t_{k+1} using Equation (11).

$$\hat{\phi}_{r_{k+1}} = \hat{\phi}_{b_{k+1}} + \frac{1}{\lambda}\left(\vec{a}_{k+1}\hat{\vec{r}}_{r,b_{k+1}} + c\hat{b}_{r,b_{k+1}}\right) + N_{r,b} \qquad 11$$

The predicted state estimates are used to calculate the line of sight phase difference between the rover and base represented in the equation by the middle term of the right-hand side. Note that $\vec{a}_{k+1}$ is the three dimensional line of sight unit vector, $\hat{\vec{r}}_{r,b_{k+1}}$ is the predicted three dimensional relative position vector, and $c\hat{b}_{r,b_{k+1}}$ is the predicted relative clock bias. The carrier ambiguity is initialized using the scalar RTK algorithm is assumed to be constant during RTK-VPLL operation.

The total phase change during the integration period of the sampled signal includes both the Doppler affect and the intermediate frequency of the GPS front end. To calculate the desired carrier frequency setting for the carrier NCO, the total phase change over the integration period is divided by the change in receiver time. The formula is defined in the Equation (12).

$$f_{\phi} = \frac{f_{IF}(t_{k+1} - t_k) - \left(\hat{\phi}_{r_{k+1}} - \phi_{r_k}\right)}{t_{k+1} - t_k} \qquad 12$$

In the equation, f_{IF} is the intermediate frequency of the GPS front end and ϕ_{r_k} is the current carrier phase measurement of the rover receiver. Note that the change in carrier phase is subtracted because the Doppler frequency decreases for increasing range between transmitter and receiver.

2.1.4 Vector Tracking Simulation and Experimental Results

As described previously, the robustness of the vector tracking receiver architecture can be attributed to a sharing of signal power across the tracking channels. The sharing of power improves the tracking performance of the receiver in part because the number of states that are estimated in the navigation processor does not increase with the number of visible satellites. This means that as the number of visible satellites increases the system becomes more overdetermined resulting in more robust navigation and tracking as signal strength decreases. Alternatively, the number of tracking parameters in a scalar tracking receiver does increase with increasing numbers of visible satellites. Since there is no sharing of information across channels in the scalar receiver, all channels degrade equally as the C/N$_0$ ratio of the received signal decreases.

When analyzing the tracking performance of the receiver, it is common to evaluate the ability to maintain lock on the frequency of the sinusoidal carrier as this is typically the weakest link in the tracking channel (as opposed to the code phase tracking). A simulation study was performed to compare the performance of the vector tracking receiver to the scalar tracking receiver. The results are summarized in Figure 2-19. There are two plots in the figure showing results of the vector receiver with 5 visible satellites (left) and 9 visible satellites (right). The plots show the one sigma frequency jitter as a function of the C/N0 ratio for different receiver configurations. The blue line shows vector tracking results, and the green line shows the scalar tracking results. The threshold line at 8.33 Hz jitter is the boundary at which the frequency locked loop typically fails. As shown in the figure, the scalar tracking performance remains the same with either 5 or 9 satellites. Three FLL configurations are shown with bandwidths ranging from 2 to 18 Hz. Lower bandwidths improve noise rejections but are limited to scenarios where the platform dynamics are expected to low (i.e., low accelerations). The simulation shows that scalar tracking receiver cannot maintain frequency lock at C/N_0 ratios less than 20 dB-Hz in the best-case scenarios (i.e. low platform dynamics). By comparison, the vector tracking receiver is able to maintain frequency lock at 17 dB-Hz C/N_0 in the worst scenario when only 5 satellites are visible, and the platform acceleration variance is 125 m^2/s^4. Under the most benign dynamic conditions that were simulated (acceleration variance is 2 m^2/s^4) and when 9 satellites were visible, the vector tracking receiver is able to track signals with a C/N_0 of 11 dB-Hz representing a significant improvement over scalar tracking.

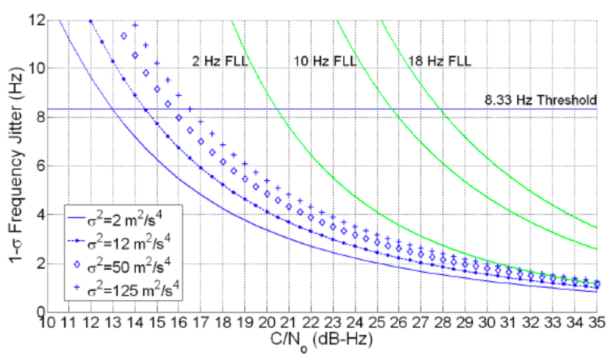

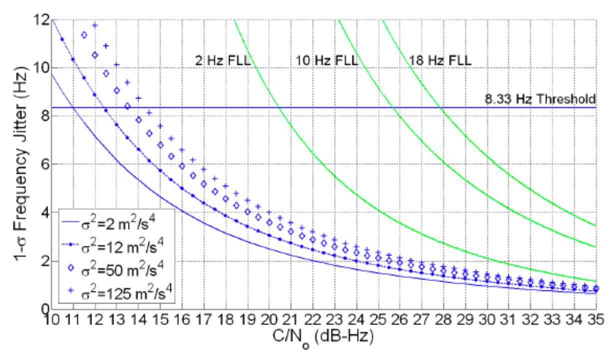

Figure 2-19. Plots of Vector Frequency Tracking (Blue) with 5 Satellites (Left) and 9 Satellites (Right) and Scalar Frequency Tracking (Green) as a Function C/N_0 Ratio for Different Platform Dynamics. [Lashley]

In addition to improved weak signal tracking, the VTRx architecture also provides instant signal re-acquisition after a brief blockage of the line-of-sight to the satellite. Recall that the receiver must maintain replica signals with the correct code phase and carrier frequency to generate range and range rate measurements. When a signal is blocked, the discriminator does not accurately capture the true signal errors but reports a random value dependent on thermal noise. As a result, the replica signal that is maintained by a traditional scalar tracking loop wanders at random during the outage. This effect was demonstrated in simulation and is shown in the green plots in Figure 2-20. The dot red-line in the figure at the 27 second mark shows the beginning of the signal outage. At that point, the code phase and carrier frequency of the traditional tracking loop begins to drift away from the true values due to the discriminator noise. The scalar tracking loop is unable to resolve the code and carrier errors affectively after the signal returns at the 39 second mark.

The traditional receiver would have to perform a board acquisition search to re-acquire the signal after the outage. The vector tracking receiver is able to predict the expected signal frequency and phase during the outage from the navigation solution. This is particularly clear in the right plot showing the carrier frequency prediction during the outage. Once the signal returns, the replica errors are accurately measured by the discriminator function and the vector tracking loop continues to operate without disruption.

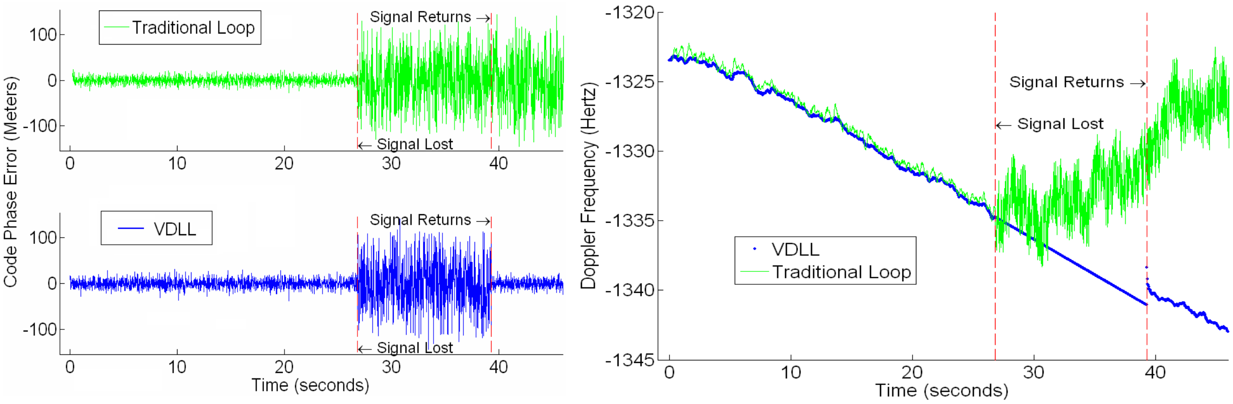

Figure 2-20. Plots of Instant Re-acquisition of Code Phase and Carrier Frequency After a 12 Second Signal Outage.

Experimental data was collected in urban areas and heavy foliage environments to analyze the performance of the vector tracking receiver compared to a commercial-off-the-shelf (COTS) receiver. The plots in Figure 2-21 show the positioning results of each receiver with satellite imagery for reference. In each scenario, the vector tracking receiver is able to track satellites and report a position solution for 100% of the test. The COTS receiver is unable to maintain track on at least 4 satellite in many areas and cannot report a position solution.

Figure 2-21. Plots of the Vector Tracking Position Solution Compared to a COTS GPS Receiver in Urban and Heavy Foliage Environments Showing the Improved Performance of the Vector Receiver.

2.1.5 RTK-VPLL Simulation and Experimental Results

The performance of the RTK-VPLL receiver was analyzed in the simulation and experimentally. First, a nonlinear simulator was used to analyze the performance of the RTK-VPLL algorithm as a function of the C/N_0 ratio of the received signal. Three different acceleration variances were simulated to analyze the response of the receiver to variable platform dynamics. The acceleration was modeled as a zero mean Gaussian random variable with standard deviations of either 0, 1, or 3 m/s^2. The three scenarios represent a static platform, a slow-moving platform like a pedestrian or small robot, and a moderately dynamic platform like a ground vehicle. The C/N_0 ratio of the received signal was held constant during each simulation, and all channels were simulated with the same ratio. Simulations were performed with C/N_0 ratios ranging from 30 dB-Hz to 20 dB-Hz. During the simulations, it was assumed that the base station receiver had clear lines of sight to the satellites and that the receiver signals were quite strong. The C/N0 ratios of the signals received by the base station receiver were set to 45 dB-Hz. Twenty simulations of each combination of acceleration variance and C/N0 ratios were performed. Figure 2-22 summarizes the results of the simulation study. Note for comparison, a scalar tracking receiver can typically maintain phase lock at approximately 28 dB-Hz. The threshold of 15 degrees is the representative of the limits of tracking for any Costas PLL. The figure shows the RTK-VPLL provides improved tracking in all scenarios with modest improvement at higher dynamics (approximately 1.5 dB-Hz) and more significant improvement at lower dynamics (approximately 5.5 dB-Hz).

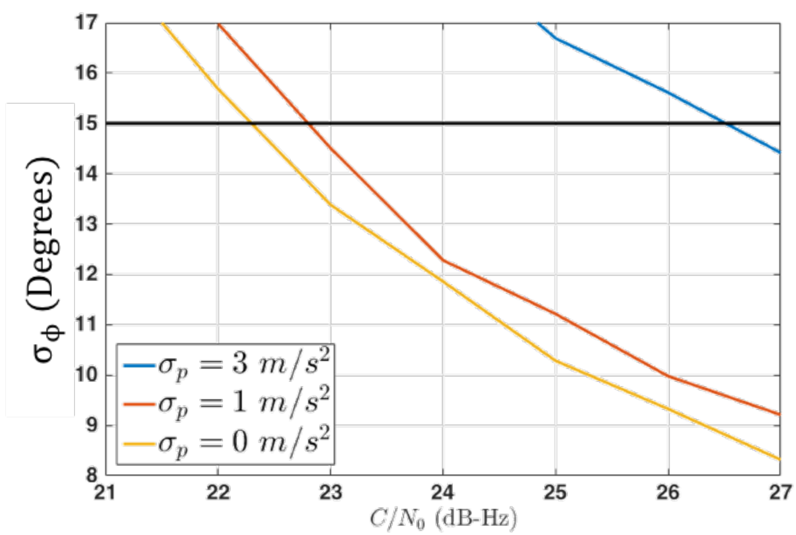

Figure 2-22. A Plot of Carrier Phase Error as a Function of C/N_0 Ratio and Platform Dynamics.

Experimental data was collected to analyze the accuracy and tracking performance of the RTK-VPLL receiver compare to a Novatel receiver operating in RTK mode. First, a static clear sky environment was select to analyze the positioning accuracy of the RTK-VPLL receiver. Figure 2-23 shows the location of the base and rover receivers and error of the VPLL position solution compared to the Novatel RTK solution. The horizontal (North and East) positioning error of the VPLL is zero mean with a variance of less than 1 cm^2. This is consistent with the limitation of RTK GPS positioning. This verifies that the RTK-VPLL receiver provides RTK accuracies in benign conditions.

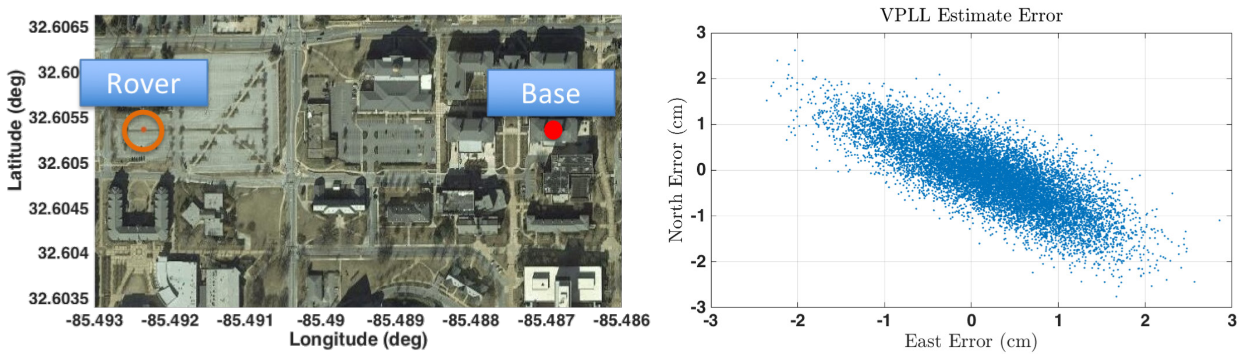

Figure 2-23. Picture of Locations of the Two Antennas During Test with a Plot of RTK Position Error Relative to RTK Novatel Reference.

Additional data was collected while driving a route through moderate and heavy foliage near the Auburn University campus to analyze the performance of the RTK-VPLL in a degraded signal environment. The position solutions of the RTK-VPLL receiver are shown along with the Novatel RTK position solution in Figure 2-24. In several section of the route, the Novatel RTK solution was unavailable (note that in most cases the standard Novatel position was available) because the receiver did not maintain carrier phase lock on a sufficient number of channels. The RTK-VPLL continuously reported the carrier phase position solution throughout the route. It should be noted that there were cycle slips in several tracking channels of the RTK-VPLL receiver as the vehicle passed the football stadium and was unable to maintain lock on at least 4 satellites.

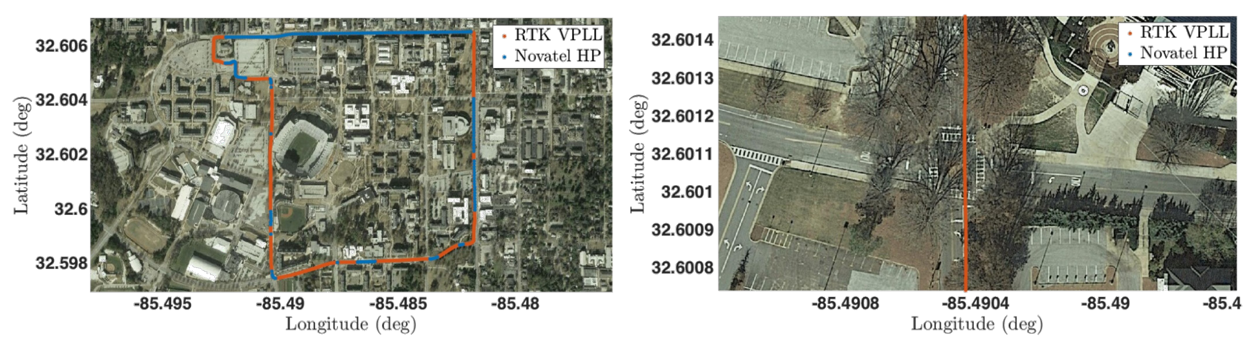

Figure 2-24. Experimental Results of RTK-VPLL Receiver Operating in Moderate to Heavy Foliage Compared to RTK Novatel Reference.

The number of phase locked channels for each receiver is shown in Figure 2-25. Clearly, the RTK-VPLL outperforms the Novatel receiver by maintaining phase lock on more channels in the difficult environments. There are three brief periods between 1700 and 1850 seconds when the RTK-VPLL receiver is unable to maintain phase lock on at least 4 satellite. During this period, the receiver slipped cycle on several channels resulting in a degraded navigation solution (i.e., position bias of 1 to 3 meters). Overall, the RTK-VPLL receiver maintained vector phase lock (i.e. phase lock on 4 or more channels) 98.7% of the time.

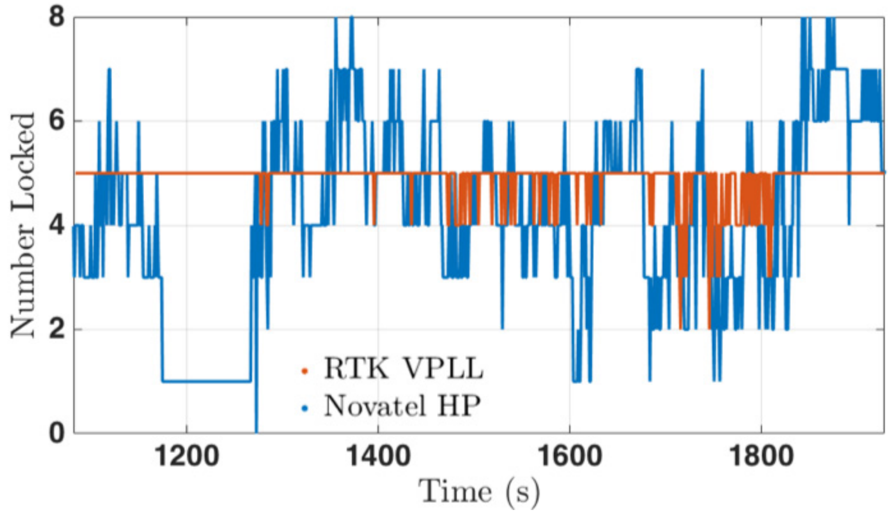

Figure 2-25. Comparison of Tracking Performance of RTK-VPLL Receiver Compared to RTK Novatel Reference Based on the Number of Phase Locked Channels.

In Table 2-3, the phase lock performance of the Novatel receiver and the RTK-VPLL receiver are quantitatively characterized by the percentage of time during the test that each channel was phase locked. The results are shown for 5 satellites that were tracked by each receiver during the test. On average, the RTK-VPLL receiver lost lock 1.9 percent of the time compared to 26.0 percent of the time for the Novatel receiver. The RTK-VPLL receiver maintained phase lock more often than the reference receiver on every channel during the test. The improvement ranged from 2 percentage points to 43 percentage points.

Table 2-3. Percent of Time Phase Locked By Channel

PRN	Novatel	RTK-VPLL
2	54.3%	97.5%
6	97.4%	99.3%
17	76.4%	98.2%
19	84.3%	98.4%
28	57.5%	96.4%

2.2 ADVANTAGES AND LIMITATIONS OF THE TECHNOLOGY

The primary advantage of the positioning system currently developed is the ability to perform GPS based surveys in areas where GPS was previously unavailable or unreliable. RTK GPS positioning is the preferred positioning method for most surveys due to its relatively low cost, ease of setup and use, and high accuracy. GPS, however, as discussed previously is very susceptible to signal interference and attenuation making it unavailable in many locations due to signal blockage or attenuation from foliage or cultural obstructions.

There are several existing methods for determining position in GPS degraded/denied environments. One method commonly used in surveys is to integrate wheel odometry to provide a position estimate.

While this method is inexpensive and has availability almost anywhere, it is inaccurate and can only measure distanced traveled, not a global position. Another alternative is to combine a GPS receiver with an inertial navigation system (INS). A GPS/INS system integrates IMU measurements when GPS is not available. The accuracy of these systems is highly dependent on the quality of the IMU used. Inexpensive IMUs provide position estimates with errors on the order of meters within only a few seconds with no GPS. High-end IMUs are available that provide accurate positions after hours of integration time. These sensors are, however, prohibitively expensive. A final option is a laser based system such as a robotic total station, commonly used in surveys. These systems are more expensive than a GPS receiver, but not prohibitively so and produce very accurate measurements. The main limitation of a total station is that an optical transmitter must be setup in a known location and line of sight must be maintained to this transmitter. For areas with numerous obstructions this requires frequently relocating the transmitter, resulting in significant setup time.

A vector tracking based GPS receiver has many of the advantages of a standard GPS receiver. It provides a very accurate solution when used with differential corrections. It is reasonably priced and requires little to no setup time. The vector tracking receiver has improved availability over a standard receiver due to its ability to track signals at lower C/N0 and to perform near instant reacquisition. While the developed receiver technology can continue to provide accurate positions in areas where current commercial receivers fail, it still requires available satellite signals to operate and so will eventually fail to provide a position when blockages/attenuation becomes significant enough. It is also not able to acquire GPS signals any weaker than those acquired by a standard receiver. The receiver must, therefore, be initialized in an area with sufficiently strong signals to acquire before moving into more degraded environments. Like a standard GPS receiver, the availability of the VTRx solution can be further improved when the optional CSAC and IMU components are included.

A summary of the trade-offs between the various options discussed is given in Table 1. This table provides a relative, qualitative comparison between the various methods. The techniques are compared in four categories: availability, accuracy, setup time, and cost.

Table 2-4. Geophysical Survey Positioning Solutions

Technology	Availability	Accuracy	Setup Time	Cost
VTRx	★★★☆☆	★★★★☆	★★★★☆	★★★★☆
VTRx with CSAC and IMU	★★★★★	★★★★☆	★★★★☆	★★★☆☆
Standard GPS Receiver	★★☆☆☆	★★★★☆	★★★★☆	★★★★★
Wheel Odometry	★★★★★	★★☆☆☆	★★★★☆	★★★★★
High-end GPS/INS	★★★★★	★★★★★	★★★☆☆	★☆☆☆☆
Standard GPS/INS	★★★☆☆	★★★★☆	★★★☆☆	★★★☆☆
Total Station	★★★☆☆	★★★★★	★☆☆☆☆	★★☆☆☆

Availability addresses the percentage of time the technology is expected to produce a useable navigation solution. Technologies that provide a solution by integrating a stand-alone sensor such as an IMU or wheel encoder that does not require any external measurements provide a solution 100% of the time. GPS receivers or other ranging based solutions such as a laser based total station require line of sight to an infrastructure components, thus reducing the amount of time a position is available. A standard GPS/INS solution was also given a lower rating on availability because with an inexpensive IMU, errors grow rapidly in the absence of GPS resulting in a position solution that is not meaningful or useful after a short period of time. Even though a solution is "available" 100% of the time, the solution has an error so large that it cannot be used. It should also be noted that a vector-tracking receiver could also be paired with a high-end IMU to increase its availability.

Accuracy evaluates the position accuracy of that solution. GPS receivers (both with and without an IMU) can provide centimeter level accuracy when operating in RTK mode with clear sky. A total station can provide comparable or better accuracy (down to millimeters). Wheel odometry, which has no absolute measurement capability, provides the worst position accuracy of the listed options. The vector-tracking receiver is given one less star for accuracy than a standard receiver due to the fact that the FLL used in the vector-receiver will degrade carrier measurements resulting in less accurate differential positions in degraded environments. The accuracy will, however, match that of a standard receiver in clear sky environments.

Setup time is a measure of the amount of time needed to setup and configure the technology, including any infrastructure components that might need to be installed. A stand-alone (standard or vector-tracking) GPS receiver provides the shortest setup time of the available options. Adding an IMU to the receiver adds a small amount of time to the initial setup since the IMU must be mounted and the level arm between the IMU and receiver must be calibrated. While the setup time for wheel odometry itself is generally short, flags must often be measured out and placed at the end of each line to be surveyed in order to provide a lateral position measurement, which adds significant time to the survey setup. Finally, a total station requires the longest setup time since the base must be installed in a surveyed location and potentially moved frequently to maintain line of sight to the receiver.

Finally cost evaluates the purchase price of the system. More stars indicate a less expensive option. The proposed vector-tracking receiver is comparable in cost to a standard, survey grade receiver. Both are much less expensive than a total station. A GPS combined with a high-end IMU is the most expensive option compared.

3.0 PERFORMANCE OBJECTIVES

The primary performance objective for the system demonstration is to improve the availability of position measurements for geophysical surveys when compared to currently used survey methods such as GPS receivers. The setup time required and ease of use of the system will also be evaluated qualitatively. A summary of performance objectives is given in Table 3-1. Details of each objective are given in the following sections.

Table 3-1. Performance Objectives

Performance Objective	Metric	Data Required	Success Criteria	Results
Quantitative Performance Objectives				
Improve position availability in light to medium foliage environments	Percent increase over currently used receiver	• Position status from standard receiver • Position status from vector tracking receiver	20%	Mixed: The VTRx receiver consistently increased position availability with respect to the Novatel. The Novatel, however, performed well in the moderate foliage present resulting in less than 20% improvement for many runs.
Maintain position availability in clear sky environments	Percent increase over currently used receiver	• Position status from standard receiver • Position status from vector tracking receiver	0%	Success: The VTRx receiver was able to successfully provide positions in all areas where the Novatel produced a solution.
Qualitative Performance Objectives				
Decrease Setup / Use Complexity		• Feedback from Army Corp representatives on ease of setup and time required in comparison to current methods.	Decrease setup time / complexity when compared to current GPS denied solutions.	Success: The VTRx solution took less time to setup and configure than the total station used for truth measurements.

3.1 OBJECTIVE: IMPROVE POSITION AVAILABILITY IN LIGHT / MEDIUM FOLIAGE ENVIRONMENTS

The effectiveness of the proposed technology for providing positioning information for geophysical surveys can be most directly measured by comparing the amount of time the proposed system produces a valid position solution to the percent of time currently used GPS receivers produce a valid position solution. The primary hindrance to availability for a standard receiver is the presence of foliage or cultural obstructions. This objective will therefore seek to improve the positioning performance in these scenarios.

3.1.1 Metric

Position availability is calculated as the number of measurements with a valid position divided by the total number of measurements for both the proposed and current systems. A percent improvement is then be calculated showing the improvement in position availability of the proposed system over the position availability of a currently used GPS receiver.

3.1.2 Data Requirements

Measurements from both the proposed vector tracking receiver and a standard GPS receiver are needed at each epoch that contain the fix status of the receiver.

3.1.3 Success Criteria

The objective will be considered met if more than a 20% improvement in the availability is seen when compared to a currently used GPS receiver. It should be noted, however, that the percent improvement is likely to be highly dependent on the density of foliage and the current geometry of the satellite constellation. Numerous runs with varying foliage densities and satellite geometries were performed in order to minimize this effect.

3.1.4 Criteria Evaluation

The VTRx receiver consistently increased position availability with respect to the Novatel. The Novatel, however, performed well in the moderate foliage present resulting in less than 20% improvement for many runs. A future demonstration at a more challenging site would allow the potential improvements from the technology to be better assessed.

3.2 OBJECTIVE: MAINTAIN POSITION AVAILABILITY IN CLEAR-SKY ENVIRONMENTS

The developed system seeks to improve position availability in degraded environments as discussed in Objective 1. It does not provide any benefits over a standard receiver in clear-sky environments. To be a viable alternative to a standard receiver, however, it should not degrade performance over a standard receiver in open areas.

3.2.1 Metric

As given in Section 3.1.1, position availability is again be calculated as the number of measurements with a valid position divided by the total number of measurements for both the proposed and current systems. A percent improvement is then calculated showing the improvement in position availability of the proposed system over the position availability of a currently used GPS receiver.

3.2.2 Data Requirements

Measurements from both the proposed vector tracking receiver and a standard GPS receiver are needed at each epoch that contain the fix status of the receiver.

3.2.3 Success Criteria

The objective will be considered met if there is a 0% or greater improvement in position availability. Any degradation in position availability (negative percent improvement) would indicate that the system performs worse in open sky than a standard receiver. The cause of this degradation would need to be determined and addressed before proceeding.

3.2.4 Criteria Evaluation

The VTRx receiver was able to successfully provide positions in all areas where the Novatel produced a solution.

3.3 OBJECTIVE: DECREASE SETUP / USE COMPLEXITY

The developed system seeks to provide accurate position information in areas where commercial GPS receivers fail to provide a solution, while not increasing setup or use complexity above that of a standard GPS receiver and significantly reducing setup time / complexity when compared to currently GPS denied solutions such as a robotic total station.

3.3.1 Metric

This metric is qualitative and consists of observations made by Army Corp and other personnel involved in the demonstration. Observations will be made on the setup time and complexity of the three positioning systems used in the demonstration.

3.3.2 Data Requirements

Notes on the setup time and complexity of the vector tracking receiver, standard receiver, and total station truth system will be kept during the demonstration.

3.3.3 Success Criteria

The objective will be considered met if the setup time and complexity of the proposed system is no longer than that of the currently used receiver and better than that of the total station.

3.3.4 Criteria Evaluation

The VTRx solution took less time to setup and configure than the total station used for truth measurements.

4.0 SITE DESCRIPTION

The demonstration was performed at Redstone Arsenal (RSA). RSA is located in southern Madison County, Alabama, and is bounded by the City of Huntsville to the north and east, and by the Tennessee River to the south. The towns of Madison and Triana are northwest and southwest of the facility, respectively.

4.1 SITE SELECTION

Three sites were selected on the western-most part of the RSA installation for testing. These areas are shown on the map in Figure 4-1. The site contains a range of environments from open sky, to light foliage, to dense wooded areas. Testing the proposed positioning system in this wide range of environments allowed its performance and limits to be thoroughly analyzed.

Figure 4-1. Map Showing Location of Testing Sites on Western Edge of Redstone Arsenal

The areas were cleared of brush, ordnance and surveyed for CWM (Chemical Warfare Munitions) prior to the ESTCP project tests by CEHNC. These sites represent the target dense foliage use case for this technology demonstration in varying degrees. At the starting point of each site is an area of clear sky to ensure a good navigation solution prior to beginning the run.

Due to inclement weather on the days designated for testing, only two of the sites were used for in the data collection event. These two testing sites will be presented in the order that the data collection was performed.

4.1.1 Site 13

Site 13 begins at the roadside in clear sky. The location of the starting point is 34°38'39.8"N 86°42'53.3"W and is shown by the blue star in Figure 4-2.

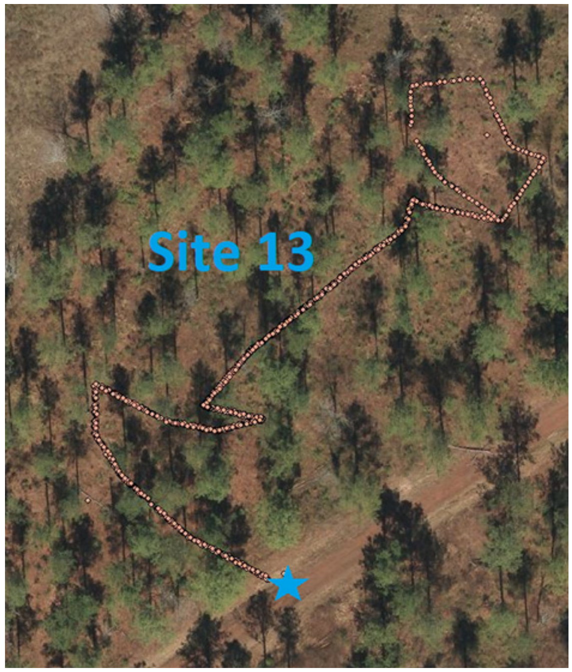

Figure 4-2. Surveyed Positions of Test Site 13 with Starting/Ending Point Shown with a Star

The course is characterized by consistently light to mid-level foliage as shown in Figure 4-3. The course starts at the road and is walked to the circle at the northeast side. The expected course is for the tester to walk the full circle and then double back on the original path to the beginning of the course back to the road. The course features very sharp direction changes, reducing the effectiveness of interpolation techniques.

Figure 4-3. Representative Pictures of Site 13

Figure 4-4. View of Site 13 from the Ground

4.1.2 Site 9

Site 9 begins at the roadside in clear sky. The location of the starting point is 34°38'38.6"N 86°42'55.5"W and is shown by the blue star in Figure 4-5.

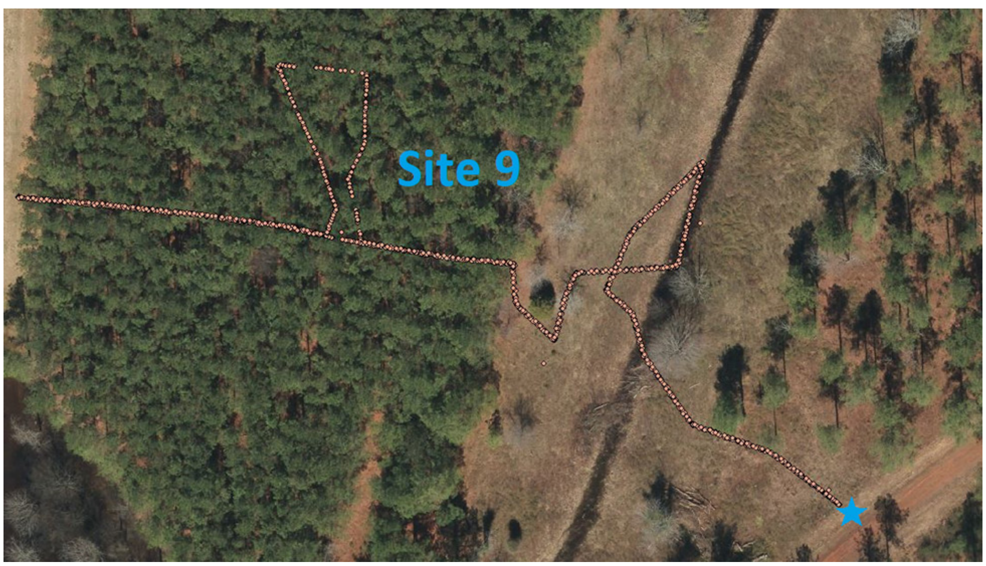

Figure 4-5. Surveyed Positions of Test Site 9 with Starting/Ending Point Shown with a Star

The course is characterized by areas of consistent clear sky (Figure 4-6 - Left) followed by areas of very dense foliage (Figure 4-6 - Right). The foliage on this site was primarily pine trees. The course starts at the road and is walked through an open area, changing direction sharply at multiple points. About halfway through the course, the area of dense foliage is entered. A sharp set of turns in the dense foliage takes place in the middle of the dense foliage. The course then continues through the dense foliage to another area of clear sky on the easternmost side of the course. The tester then turned and repeated the steps in reverse order.

Figure 4-6. Representative Pictures of Site 9.

4.1.3 Site 5

Site 5 begins at the roadside in clear sky. The location of the starting point is 34°38'46.5"N 86°42'30.5"W and is shown by the blue star in Figure 4-7. The course features a loop through moderately dense foliage that ends back at its starting point. Inclement weather prevented a survey of Site 5 from being completed. Only one data collection run was completed on Site 5.

Figure 4-7. Test Site 5 with Starting/Ending Point Shown with a Star.

4.2 SITE HISTORY

RSA encompasses approximately 38,300 acres, and the Department of the Army controls 36,459 acres of that total, of which approximately 15,500 acres are woodlands, 5,360 acres are leased for agricultural use, and approximately 12,000 acres are used for test ranges. The National Aeronautics and Space Administration was granted 1,841 acres in the central part of RSA for the Marshall Space Flight Center. Prior to this land grant in 1960, the area occupied by Marshall Space Flight Center was used by the Army. A portion of RSA in the southeastern part of the facility was previously used to develop solid rocket propellants as a government-owned, contractor-operated facility. This area is now referred to as the RARE (Redstone Arsenal Rocket Engine) facility. Approximately 2,900 acres owned by the Tennessee Valley Authority and 4,100 acres of the Wheeler National Wildlife Refuge are within the boundaries of RSA.

There is no documented survey history of these sites that specifically applies to the technology demonstration. Existing ordnance is located throughout RSA at various locations, but the testing sites were cleared of all ordnance. The site was chosen for its representative dense foliage environment. Previous munitions use and surveys on the site are not applicable as geophysical surveys are not being conducted as part of this demonstration.

4.3 SITE GEOLOGY

Site geology is not applicable to the demonstration of a positioning system as geophysical surveys are not being conducted.

4.4 MUNITIONS CONTAMINATION

The area was cleared of existing ordnance. Other information pertaining to munitions contamination is not applicable to the demonstration of a positioning system.

5.0 TEST DESIGN

5.1 CONCEPTUAL EXPERIMENTAL DESIGN

Fields tests were conducted to determine the positioning performance of the proposed system in a realistic environment and allow the performance to be compared to existing systems. The prototype VTRx system as well as a Novatel RTK capable GPS receiver were installed in a survey backpack. A Trimble Integrated Surveying (IS) system consisting of a Trimble R8 GPS receiver and a Trimble VX Total Station provided truth data. Tests are repeated numerous times in two different sites on RSA as described in Section 4.0.

The required demonstration hardware included a single GPS antenna split to both the vector tracking SDR and a Novatel receiver, a laptop used for data collection, a Trimble VX Total Station, and a survey backpack, as shown in Figure 5-1.

Figure 5-1. Demonstration Hardware

As much as possible, the vector tracking and Novatel receivers were installed on the platform before arrival at the site to minimize setup time. Once on site, the remainder of the survey backpack was assembled and tested for power and connectivity with the host laptop. The prism for the Trimble truth hardware was installed on the backpack. The base station was set up to collect data from the roadside near the testing sites. A GPS base station was set up and the Trimble IS system setup and tested. Known monument points were measured with the truth system to verify its operation.

The physical setup required a tester to wear the survey backpack and walk the outlined course. The course was marked using path guides and the tester walked in an orientation such that the backpack antenna was centered on the path guide as much as possible. Both the vector tracking receiver and the Novatel receiver were physically located in the survey backpack connected to the same antenna using an RF splitter. The Trimble Total Station always maintained line of sight to the prism which was connected just below the antenna. The physical setup is shown in Figure 5-2.

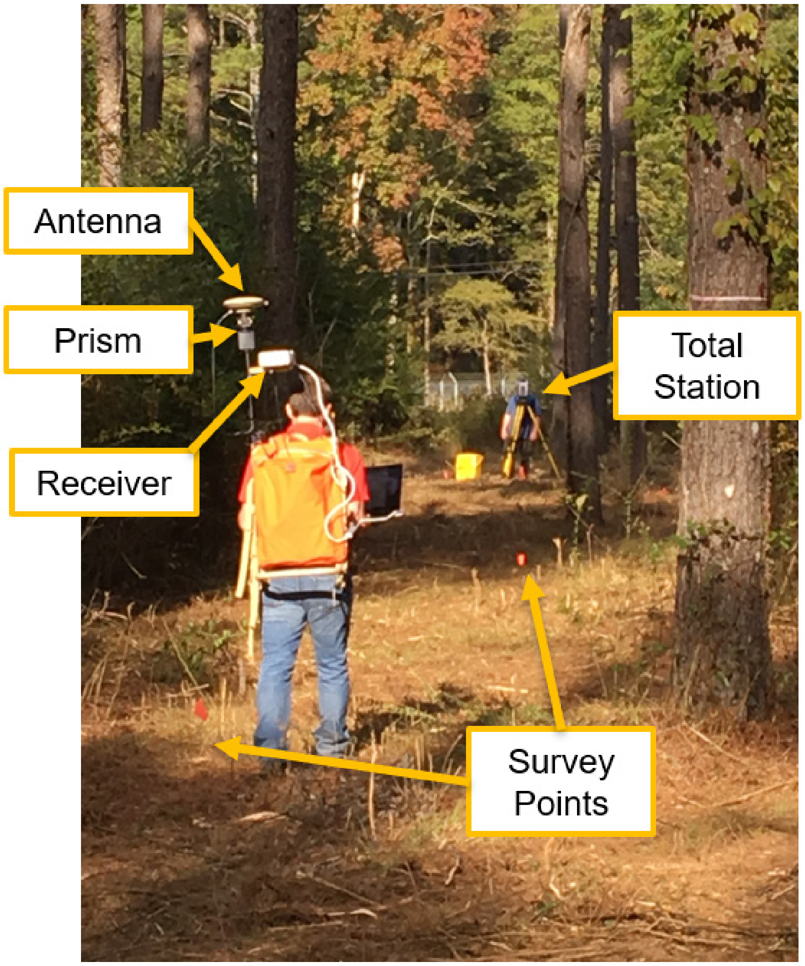

Figure 5-2. Testing Physical Setup

Vector tracking receiver operation was tested in a live sky environment to ensure operation. An acquisition procedure was repeated until enough satellites were captured, then scalar operation began. Once a position solution was reached, the software receiver transitioned to vector tracking mode. In a live sky environment, the Novatel was able to also get a reliable position fix. This open sky environment testing ensured both the proper receiver operation and as a decision point to begin further testing on the sites.

To begin every test, the tester turned on all logging and remained static in an open sky environment. This ensured that a position fix was achieved from the vector tracking receiver, the Novatel, and that the truth system was locked onto a position. After about one minute of static operation, the tester began walking the pathway into the foliage-covered testing sites.

The Trimble truth station was set up in a position that covered as much of the ground course as possible. However, in both of the sites tested, blockages prevented the truth system from covering the entire course. The Trimble system was moved at least once during each of the testing sites to ensure coverage of truth data. Testing scenarios were designed to frequently enter and exit wooded areas as well as sharp turns under foliage. This eliminates the benefit of any navigation solution interpolation and requires that lock is maintained on the satellites without the benefit of an inertial device.

The first site that was chosen was Site 13 as described in Section 4.1.1. This site features open areas followed by light-to-medium foliage. The success of the testing at Site 13 was a decision point for moving to the next site for more strenuous testing. Once the testing was shown to perform well at Site 13, tests continued at Site 9, described in Section 4.1.2, which features dense foliage. Finally, a short data collection was performed at Site 5 before ending the collection activities early due to weather.

5.2 SITE PREPARATION

Since munitions or seed items are not involved in this demonstration, little to no site preparation is required. All three test sites described in Section 4.0 the areas were cleared of brush and ordnance. They were surveyed for chemical warfare munitions (CWM) prior to the ESTCP project tests by the Corps of Engineers – Huntsville Center (CEHNC).

Several points along the predefined paths were surveyed. The path was defined by string run between stakes that marked these surveyed spots. The tester was positioned along the path such as to center the antenna over the string as much as possible. These survey points and string are shown in Figure 5-3.

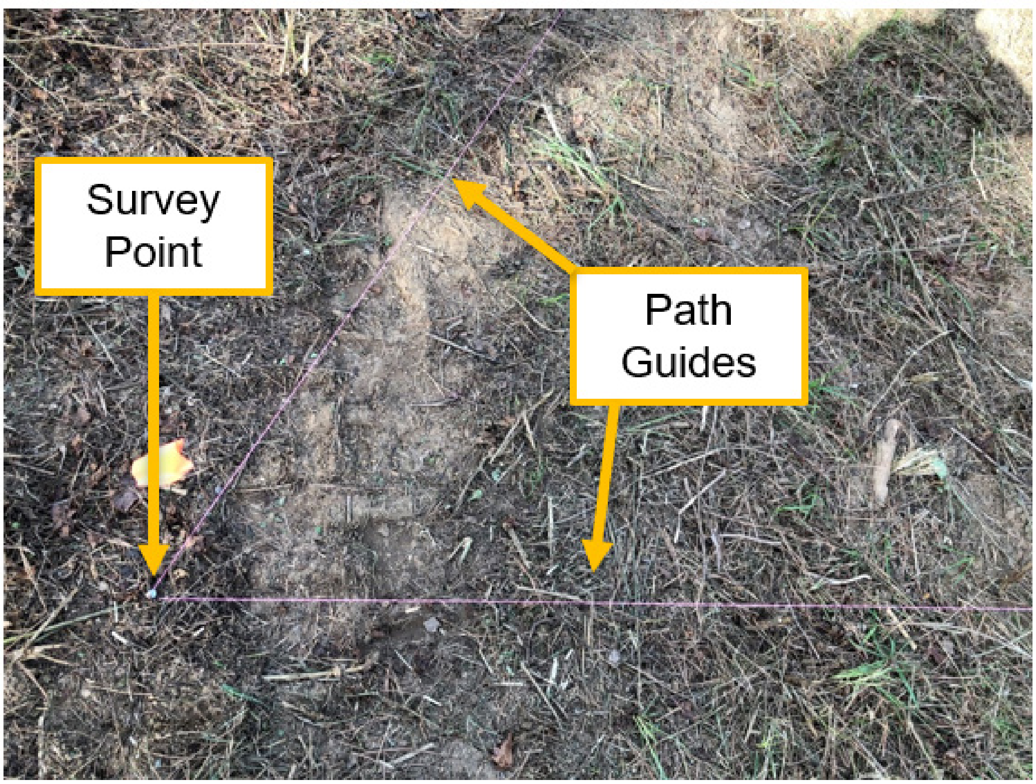

Figure 5-3. Path Definition Using Survey Points and Path Guide Strings

5.3 SYSTEM SPECIFICATION

The system used in the field tests consisted of three main components: 1) the prototype and standard receivers to be tested, 2) a base platform that will be used to house and move the system, and 3) a truth measurement system. Each component is described in detail in the sections below.

A schematic of the receiver systems is shown in Figure 5-4. In order to provide the most direct comparison possible between the existing (Novatel) receiver and the proposed system, a single antenna was used to provide data to each. An RF splitter was used to split the received signal to the two receivers. Solutions from both receivers were recorded.

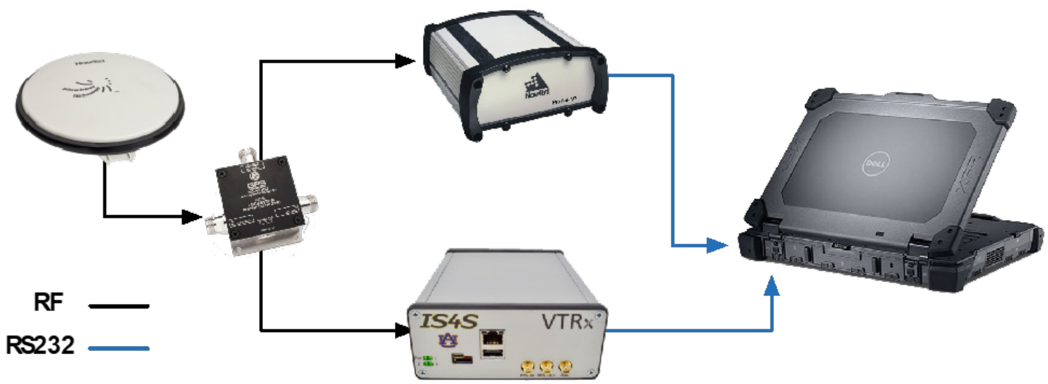

Figure 5-4. Test Setup Showing VT Receiver and Standard GPS Receiver for Comparison

The receivers and truth system prism were installed on a survey backpack as shown in Figure 5-5. The VTRx receiver, prism, and antenna were mounted on a pole extending up from the backpack. The antenna splitter, Novatel receiver, and power components were installed in the backpack. A data collection laptop was carried by the operator. Additional details on each component are provided in the following sections.

Figure 5-5. Data Collection Setup

5.3.1 GPS Antenna

A Novatel Pinwheel 702-GG L1/L2 antenna was used to feed both receivers.

5.3.2 Antenna Splitter

A GPS Networking powered splitter was used to power the antenna and split the signal to the two receivers. The splitter was powered using a battery installed in the survey backpack.

5.3.3 Vector Tracking Receiver

The proposed vector-tracking receiver was installed in the survey backpack. The receiver hardware is described in detail in Section 2.1.

5.3.4 Standard GPS Receiver

A Novatel Propak OEMV GPS receiver was used as an example of a currently used system for comparison purposes. In order to provide a more direct comparison to the prototype system, the receiver was used in standalone mode with no RTK corrections and receiving only L1 signals. Satellite based differential corrections will also be disabled. These settings only affect the accuracy of the receiver, and not its ability to obtain and maintain a position solution.

5.3.5 Data Collection System

A laptop was used to collect data from both receivers for later analysis. Real-time positions and status from each receiver were viewed on the laptop during the tests to monitor system operation. The user interface for the vector tracking receiver provided real-time feedback during the runs. A sample screenshot of this user interface is shown in Figure 5-6. Truth data was logged separately and combined with the receiver data in post-process.

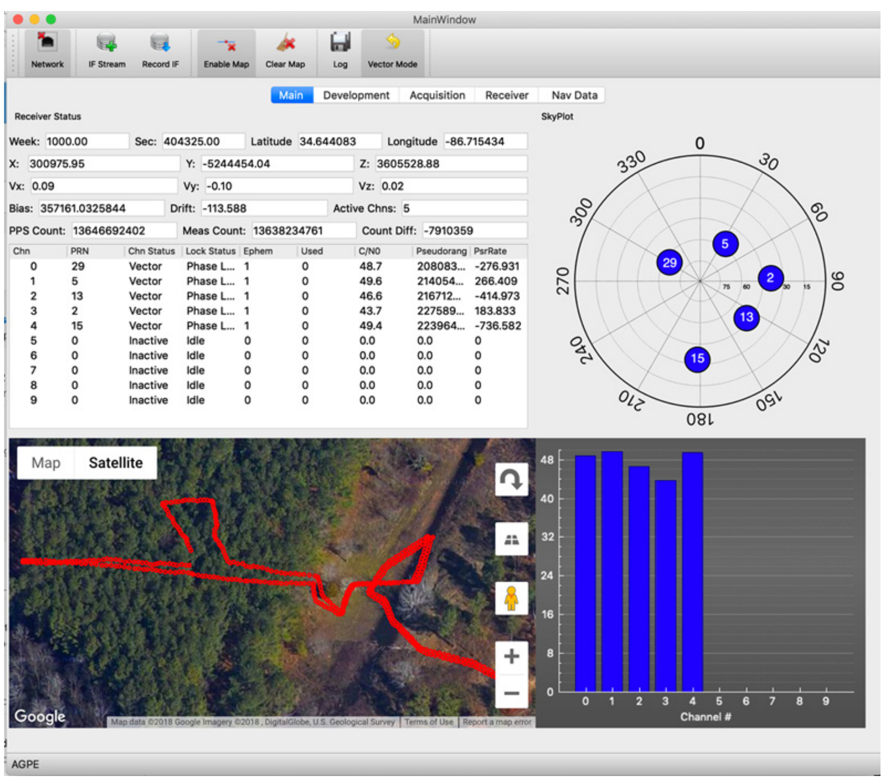

Figure 5-6. Vector Tracking Receiver User Interface

5.3.6 Truth Data System

A Trimble robotic total station system was used to provide truth information for the tests. The total station was installed on predetermined surveyed points and used to track a prism installed on the data collection backpack. A Trimble data logger was used to record the data from the total station. The system in operation at the test site is shown in Figure 5-7. In order to maintain line of site the total station had to be moved during tests to cover the entire site. Multiple runs were performed at each site with the total station in various location ensuring that truth data was provided for the entire course over all the runs, while not being available for all of any individual run.

Figure 5-7. Trimble IS System Including Trimble Controller / Data Logger and Trimble VX Total Station

5.4 CALIBRATION ACTIVITIES

No calibration of the system was needed. In order to ensure meaningful data was collected, however, the receiver output was checked for reasonableness before starting each data collection run. The system was placed in a clear sky environment and allowed to acquire satellites. The satellites acquired and positions were compared between the proposed system and the standard GPS receiver used for comparison.

5.5 DATA COLLECTION

Data from the Novatel receiver and VT receiver were recorded on the laptop using custom data collection software. Data was taken from the VT receiver using two different methods. In real-time mode, the vector tracking receiver reported navigation solution and channel status at 1 Hz to the host computer. In this mode, the receiver fully implemented the vector tracking navigation solution and returns the processed outputs. In raw data collection mode, the receiver does not perform any processing. Instead, the RF data was sampled at the intermediate frequency and stored on the host computer for post-processing. The sampling rate for this data was 16.368 MHz at 2 bits per sample.

All recorded data was logged with a GPS derived timestamp so that the various data files could be synchronized for analysis. Log files were organized and named using the date and time recording began as well as the name of the sensor being recorded to eliminate ambiguity. Detailed notes were maintained to indicate the test being performed during each log file. Truth data from the Trimble IS system was recorded using the Trimble controller / data logger shown in Figure 5-7.

5.6 VALIDATION

Data quality checks were performed during data collection to ensure time was not lost to sensor or recording issues. Log files were recorded in an ASCII format so that they could be visually scanned to give a quick check of the reasonableness of the data. This check was performed after every run. Processed data from the VT receiver was checked in real-time using the graphical interface shown in Figure 5-6.

Although truth data were collected and will allow the position accuracy of the system to be evaluated, the primary goal of the demonstration was to analyze the improvement in position availability.

6.0 DATA ANALYSIS AND PRODUCTS

6.1 PREPROCESSING

Two types of data collection runs were performed during the demonstration. For some runs, the VTRx was run in a real-time mode and produced a PVT estimate that was directly recorded during the run. For other runs, the receiver was placed in a data collection mode and raw IF data samples were recorded. These data files allow the receiver to be run later in post-process to produce a PVT estimate. The receiver is not currently capable of both logging raw data and producing a real-time solution at the same time due to its limited processing capability. The raw data runs were performed to collect data that could be used to further analyze and improve system performance by testing parameter changes and algorithm improvements in post-process. The results shown in Section 7 were generated by post-processing the No performance differences were seen between the real-time and post-processed runs.

Data from the various log files was processed in MATLAB. Scripts were developed to read the various log file formats and synchronize the data from the various sensors for each run. Data was trimmed from the beginning and ends of files as necessary to ensure that the data from every sensor was available over the time period of interest. The synchronized data was then be saved for later analysis. No filtering or other modification of the data was performed, with the exception of conversion of the data to common coordinate systems.

6.2 TARGET SELECTION FOR DETECTION

No applicable to this demonstration.

6.3 PARAMETER ESTIMATES

No applicable to this demonstration.

6.4 CLASSIFIER AND TRAINING

No applicable to this demonstration.

6.5 DATA PRODUCTS

Data including position estimates and tracking status was recorded from both the VTRx and Novatel receivers. Raw data samples were also recorded from the VTRx for some runs. Position data was recorded from the truth system. A list of all data captured for analysis from the demonstration is provided in Table 6-1. These data files were then processed to determine position error in both the VTRx and Novatel position estimates based on the survey data. Position availability was also calculated.

Table 6-1. Data Collected During Demonstration

Type	Thing	Description
Meta	Telemetry Metadata File	File containing information about each run, the associated filenames or file pointers for each run, and notes from each run
VTRx	Processed data from navigator (rcvr_output.csv, rcvr_channels.csv)	Navigator and channel output data for each run stored in human readable format
VTRx	Raw data (if_data.ini, if_data.max)	Raw 2-bit samples collected at 16.368MHz and intermediate frequency of 4.092MHz collected in binary format. Data metafile with sample offsets and other information necessary to process data.
Novatel Receiver	Bag file ([run_name].bag)	Date and timestamped rosbag file with odometry and nav fix messages logged. Parsing requires access to ROS library
Surveyor	Original surveyor points (Points with timestamp.xlsx)	Data from Trimble truth station showing vertical and horizontal distance and azimuth and elevation from a fixed reference point
Surveyor	Converted surveyor points (Global Point File Export.xlsx and AL State Plane East Zone Point File Export.xlsx)	Truth data converted to WGS84 latitude-longitude-altitude and local state plane (Alabama East, 0101) Easting-Northing-Elevation

7.0 PERFORMANCE ASSESSMENT

A performance analysis was performed using data collected during the demonstration. The following sections provide the performance results for each run performed. The runs are labelled by the day they were collected and whether the receiver was operating in real-time mode or in data collection mode. When the run was performed in data collection mode, the results were generated in post-process.

A robotic total station was used to provide truth data. Due to the need to maintain line of site to the total station during the survey, there are portions of each run where truth data is not available. For each course, the total station was moved between runs to ensure that truth data was available for all portions of the course on at least some of the data runs. The portions of the runs where truth data is not available is not included in the error analysis. The analysis of position availability includes the entire run.

7.1 RUN COMPARISON

7.1.1 Site 13 – Light Foliage

7.1.1.1 Run: Day 1 – Real-time 1 (14:49 10/24/2018)

In this run, the truth system was unable to track the back portion of the course due to obstruction by foliage. The back portion of course was also walked in the reverse direction of the expected path. This should not affect results except repeatability versus other runs.

An overhead map comparison of the Novatel and IS4S VTRx receiver vs truth for this run is shown in Figure 7-1.

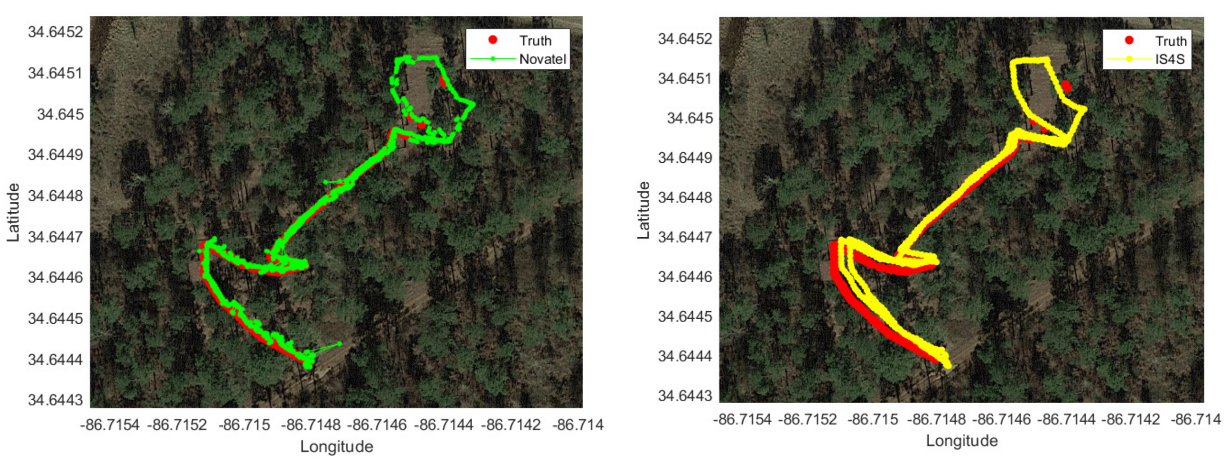

Figure 7-1. Point Map Showing Whole Course

A zoomed-in version of the plot on the area of truth coverage is found in Figure 7-2.

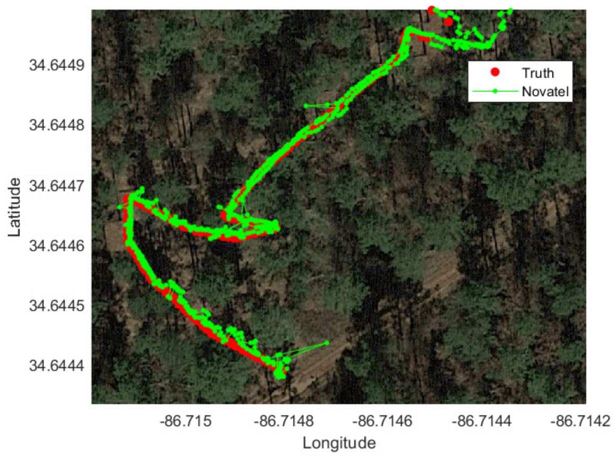

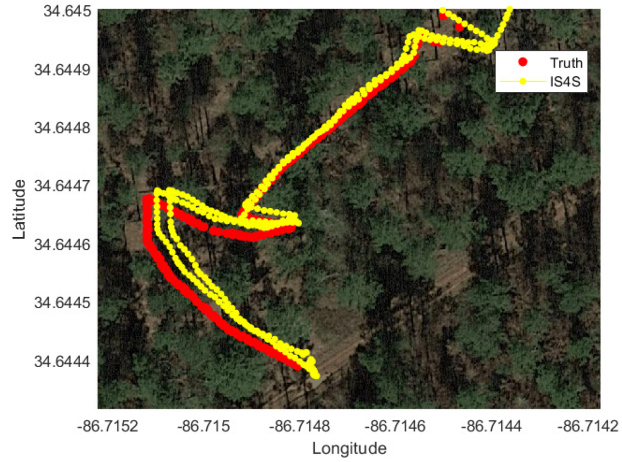

Figure 7-2. Point Map Showing Zoomed Area of Truth Coverage

A total position error plot between the receiver and the truth data is shown in Figure 7-3. The portions for which truth data was not available were omitted from this plot.

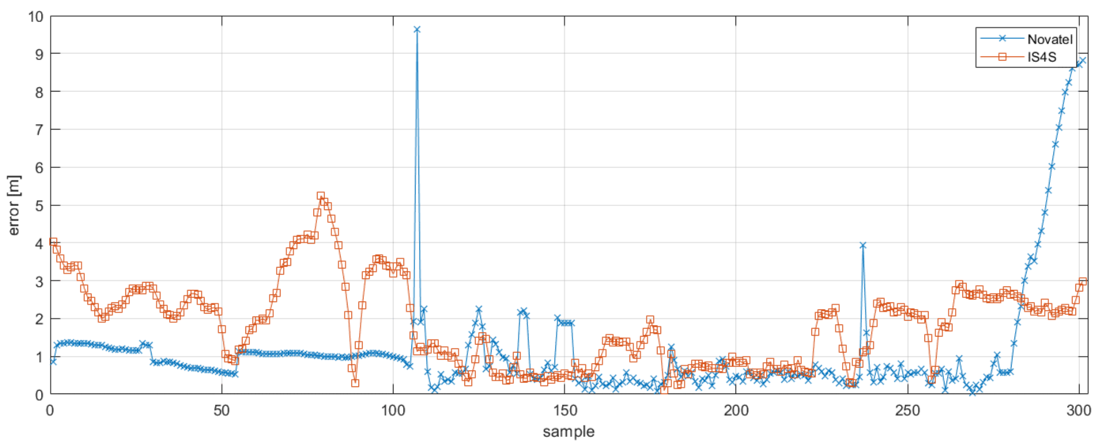

Figure 7-3. Position Error of Test Receivers versus Truth

Table 7-1 shows the statistics of the error between the truth data and the receiver output data for this run. The information below excludes the points for which the truth data was not available.

Table 7-1. Error Statistics for Run

Receiver	Mean [m]	Std Dev [m]
VTRx	1.83	1.10
Novatel	0.73	0.49
Improvement	-150%	-124%

Table 7-2 shows the percentage of the samples that each receiver had a valid position solution.

Table 7-2. Percentage Fix for Run

Receiver	Percentage Fix
VTRx	100%
Novatel	100%

This data run exhibited a position bias from the beginning of the run with the VTRx that skews the results error results. While the VTRx receiver performed well on this run, the Novatel also performs very well in this area of light foliage.

7.1.1.2 Run: Day 1 – Real-time 2 (16:06 10/24/2018)

In this run, the truth system was moved to the northeast portion of the course.

An overhead map comparison of this run is shown in Figure 7-4.

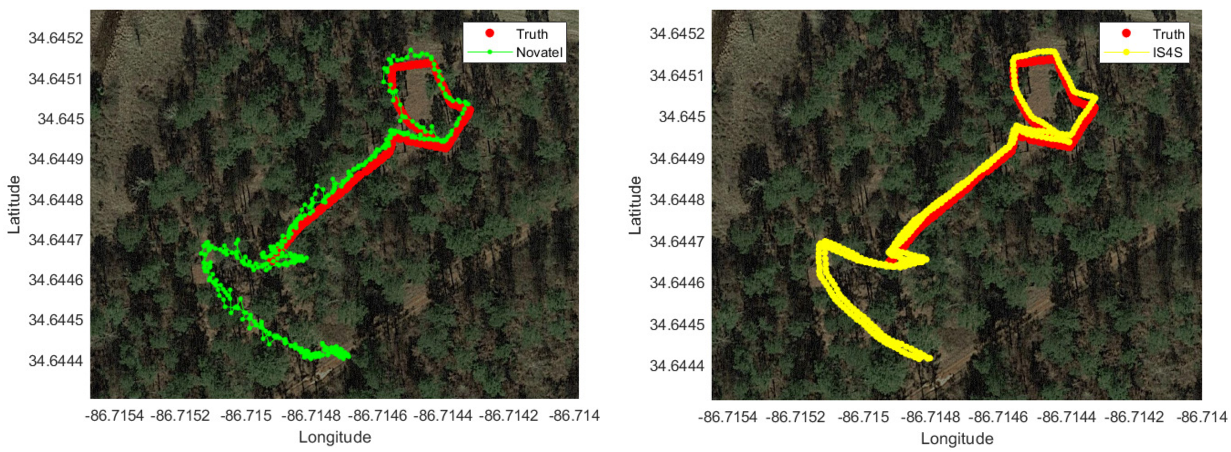

Figure 7-4. Point Map Showing Whole Course

A zoomed-in version of the plot on the area of truth coverage is found in Figure 7-5.

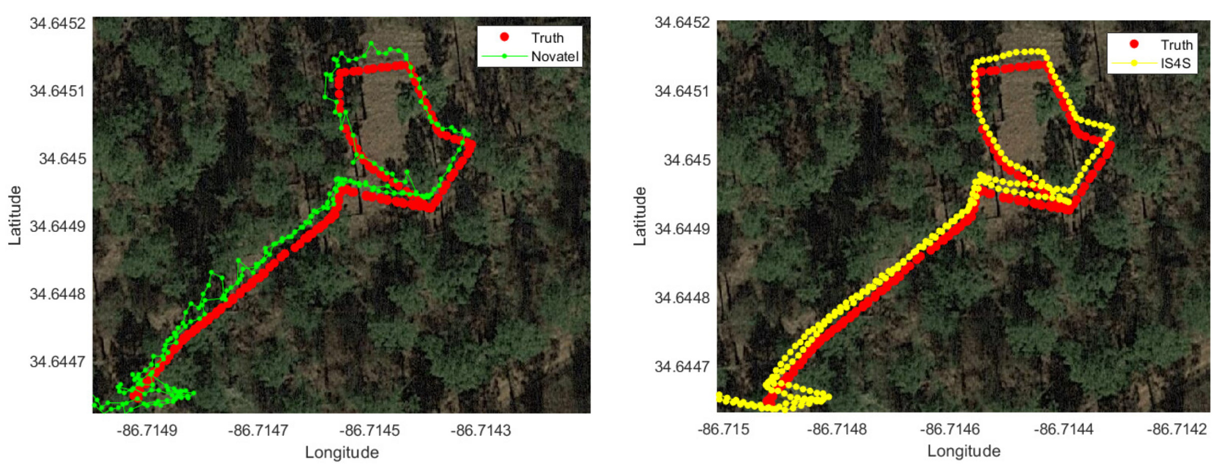

Figure 7-5. Point Map Showing Zoomed Area of Truth Coverage

A total position error plot between the receiver and the truth data is shown in Figure 7-6. The portions of the run that were covered by truth data were contiguous in time, so the error plot is shown zoomed into that area.

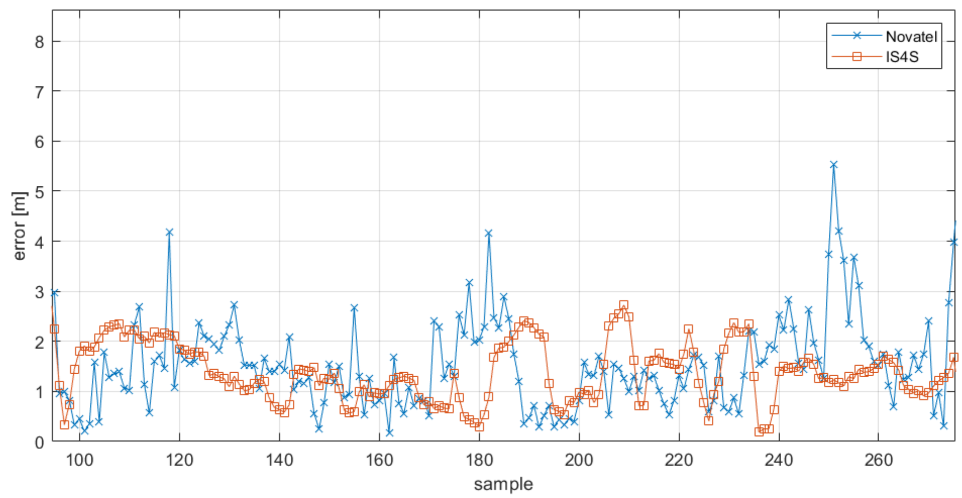

Figure 7-6. Position Error of Test Receivers versus Truth

Table 7-3 shows the statistics of the error between the truth data and the receiver output data for this run. The information below excludes the points for which the truth data was not available.

Table 7-3. Error Statistics for Run

Receiver	Mean [m]	Std Dev [m]
VTRx	1.37	0.58
Novatel	1.51	0.86
Improvement	9.27%	32.56%

Table 7-4 shows the percentage of the samples that each receiver had a valid position solution.

Table 7-4. Percentage Fix for Run

Receiver	Percentage Fix
VTRx	100%
Novatel	100%

This data run highlights the smoothing effect of the vector tracking solution on the navigation position.

7.1.1.3 Run: Day 1 – Processed Raw Data 1 (09:13 10/25/2018)

In this run, the truth system was not yet set up. In addition, the data was captured raw and processed by the software-only version of the receiver. This eliminates much of the position bias seen in other captures, which also suggests that the bias could be removed with tuning in the VTRx.

An overhead map comparison of this run is shown in Figure 7-7.

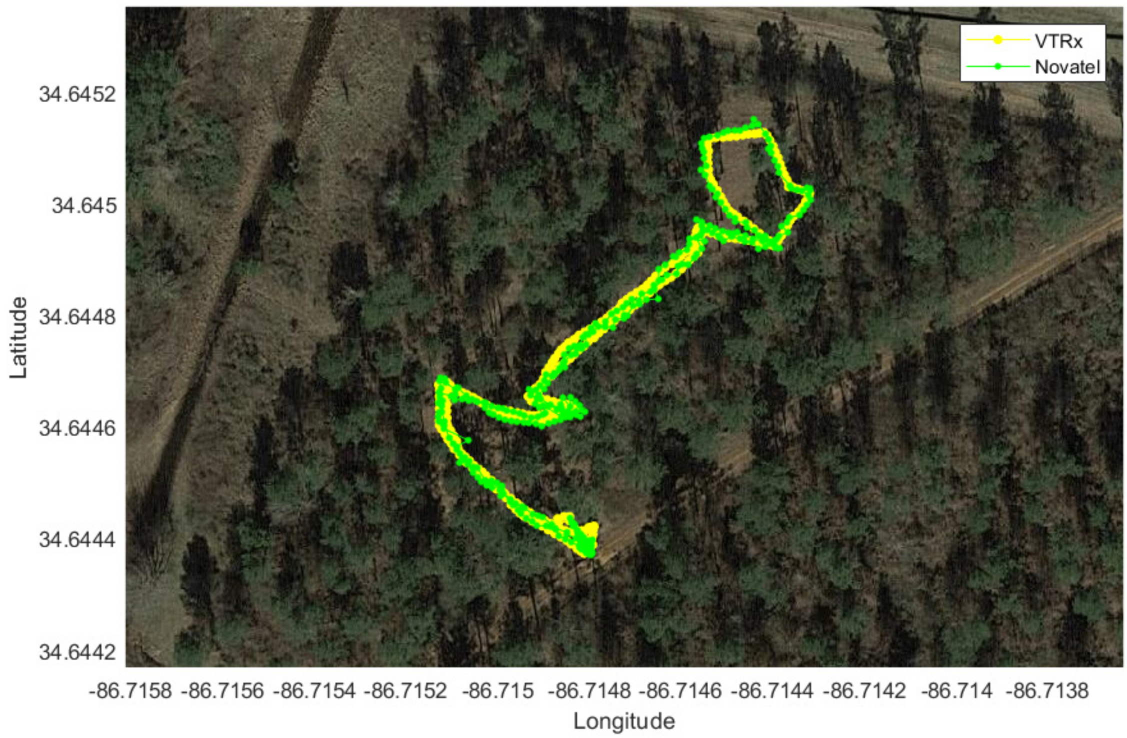

Figure 7-7. Point Map Showing Whole Course

A zoomed-in version of the plot on the area of receiver coverage is found in Figure 7-8.

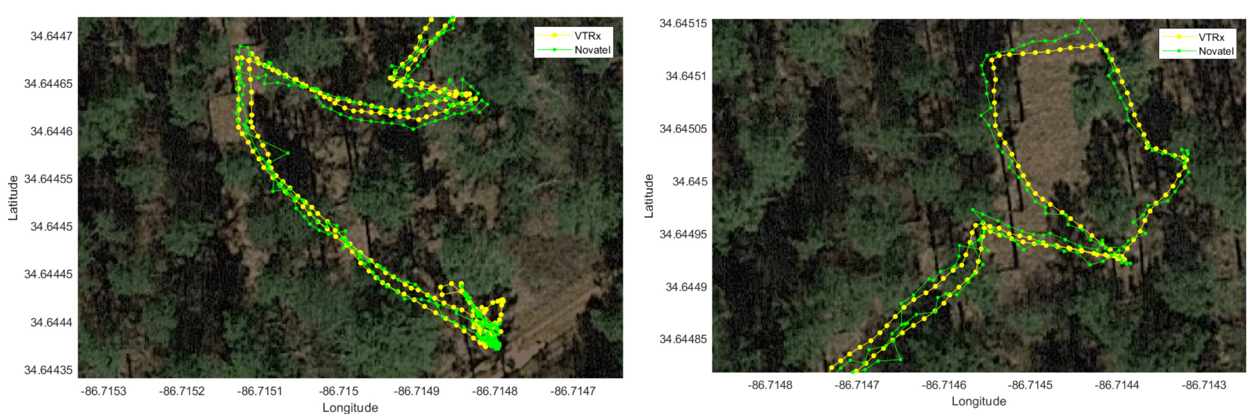

Figure 7-8. Point Map Showing Zoomed Area with Signal Reception on Both Receivers

Since truth data is not available the receivers' absolute performance could not be determined. Instead they were compared by looking at the smoothness of their position outputs as an indicator of the vector tracking receiver's tracking performance compared to the Novatel receiver. Figure 7-9 shows the change in position for each receiver for the time that both receivers tracked. This was computed by calculating the norm of the difference in sequential positions for each receiver. The position "jumps" seen in Figure 7-8 can also be seen in the larger delta position measurements for the Novatel in Figure 7-9. While this does not provide any absolute measure of performance it does likely indicate that the Novatel receiver was having a more difficult time tracking the available SVs and maintaining a stable position solution.

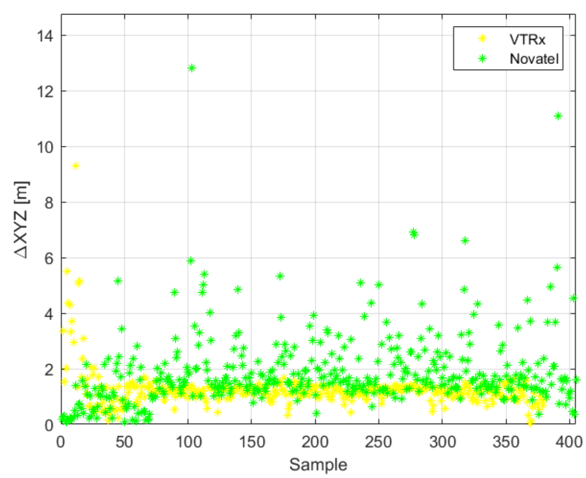

Figure 7-9. Sample-to-sample Position Difference Magnitude

Table 7-5 shows the statistics of the point-to-point variability between each datapoint with outliers omitted.

Table 7-5. Sample-to-sample Error Statistics for Run

Receiver	Mean	Std Dev
VTRx	1.14	0.28
Novatel	1.94	1.24
Improvement	41%	77%

Table 7-6 shows the percentage of the samples that each receiver had a valid position solution.

Table 7-6. Percentage Fix for Run

Receiver	Percentage Fix
VTRx	100%
Novatel	100%

This is an important run for analysis. The raw data was processed by the software version of the VTRx given updated tuning parameters. If these same tuning parameters had been used on the real-time runs, the expected output would also be the same. This suggests that the position bias seen in the real-time runs can be eliminated in the future.

7.1.2 Site 9 – Dense Foliage

7.1.2.1 Run: Day 2 – Real-time 1 (09:45 10/25/2018)

In this run, the truth system was not yet set up and only a partial recording of the vector tracking receiver was logged. In this run, the vector tracking receiver did not track through the course. Only four satellites were initially acquired, and one was dropped as the receiver entered the heavy foliage area. An overhead map comparison of this run is shown in Figure 7-10.

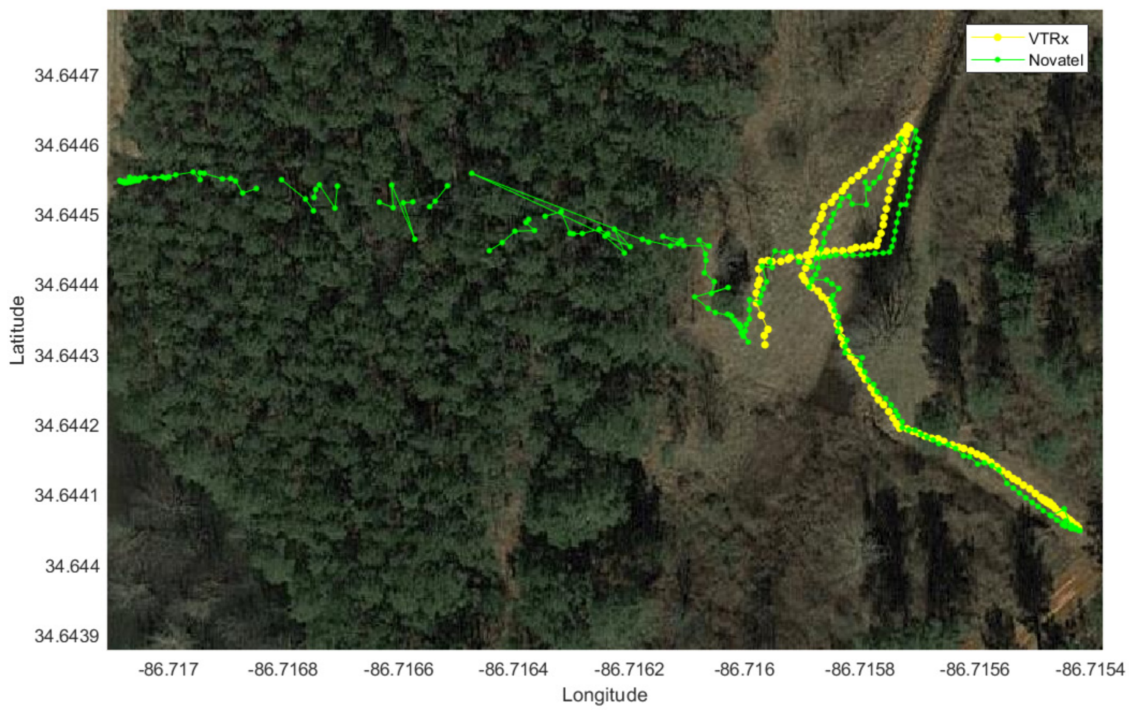

Figure 7-10. Point Map Showing Whole Course

A zoomed-in version of the plot on the area of both receiver coverage is found in Figure 7-11.

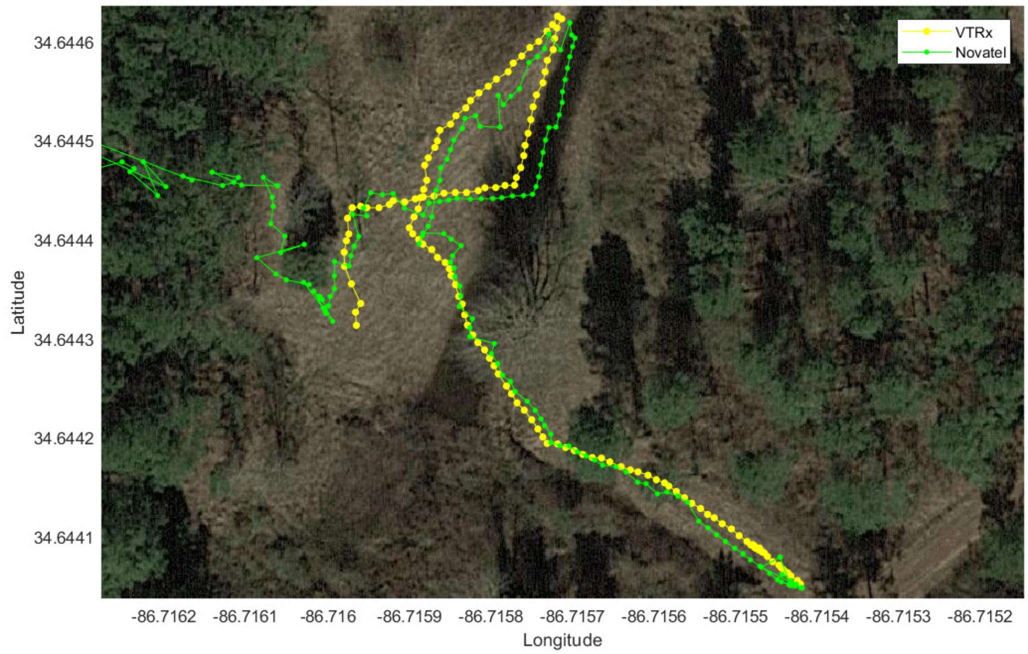

Figure 7-11. Point Map Showing Zoomed Area with Signal Reception on Both Receivers

Figure 7-12 shows the total distance difference in ENU between the two receivers for the time that both receivers tracked. Since truth data is not available, this metric is an indicator of the vector tracking receiver's tracking performance compared to the Novatel receiver.

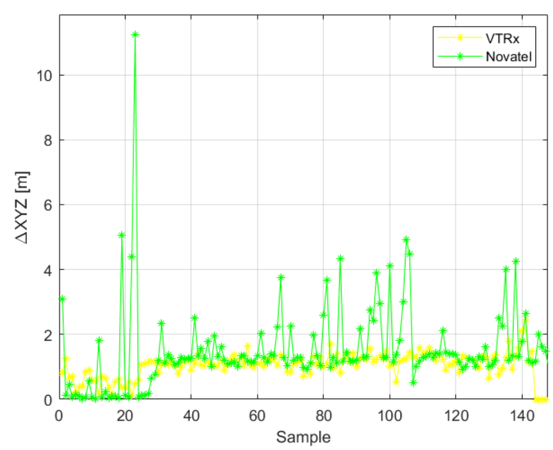

Figure 7-12. Sample-to-sample Position Difference Magnitude

Table 7-7 shows the statistics of the point-to-point variability between each datapoint.

Table 7-7. Sample-to-sample Error Statistics for Run

Receiver	Mean [m]	Std Dev [m]
VTRx	1.06	0.34
Novatel	1.52	1.34
Improvement	30%	75%

Table 7-8 shows the percentage of the samples that each receiver had a valid position solution.

Table 7-8. Percentage Fix for Run

Receiver	Percentage Fix
VTRx	51%
Novatel	97%

This run shows the room for improvement of the vector tracking receiver. In its state at the test event, the VT receiver was not able to continuously acquire or reacquire after signals were lost.

7.1.2.2 Run: Day 2 – Real-time 2 (10:52 10/25/2018)

In this run, the truth system was not yet set up. A comparison of the two receiver solutions is shown.

An overhead map comparison of this run is shown in Figure 7-13.

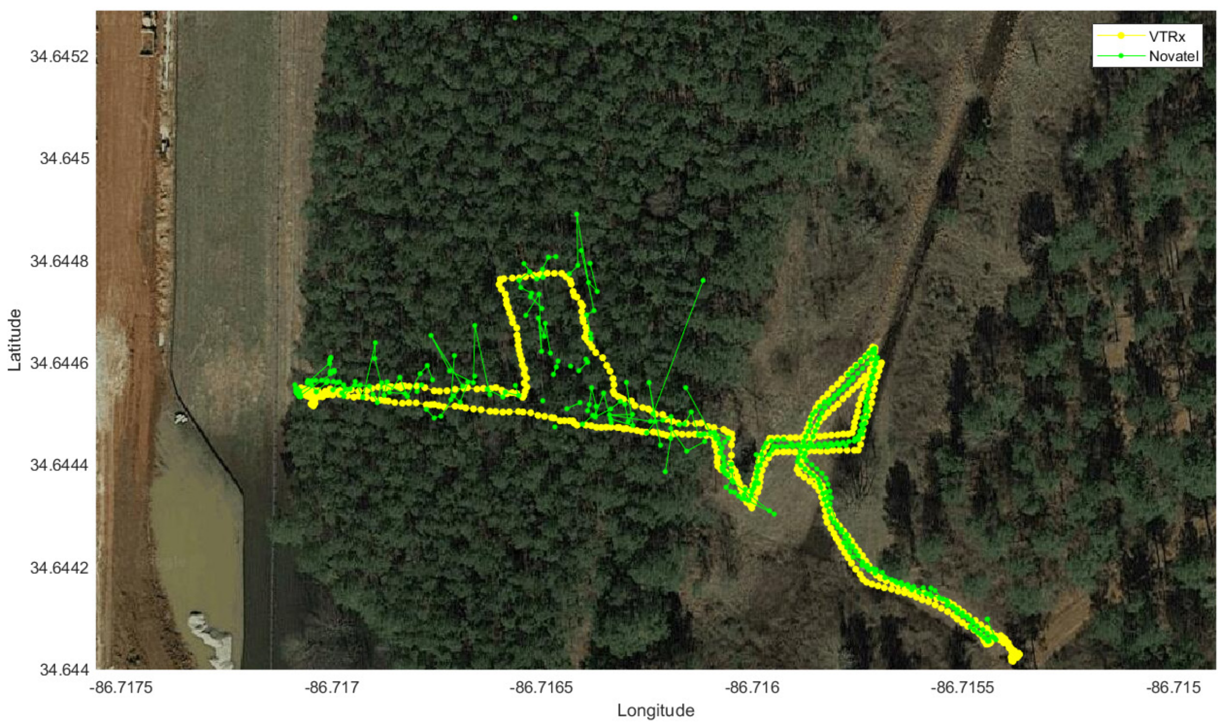

Figure 7-13. Point Map Showing Whole Course

A zoomed-in version of the plot on the area of both receiver coverage is found in Figure 7-14.

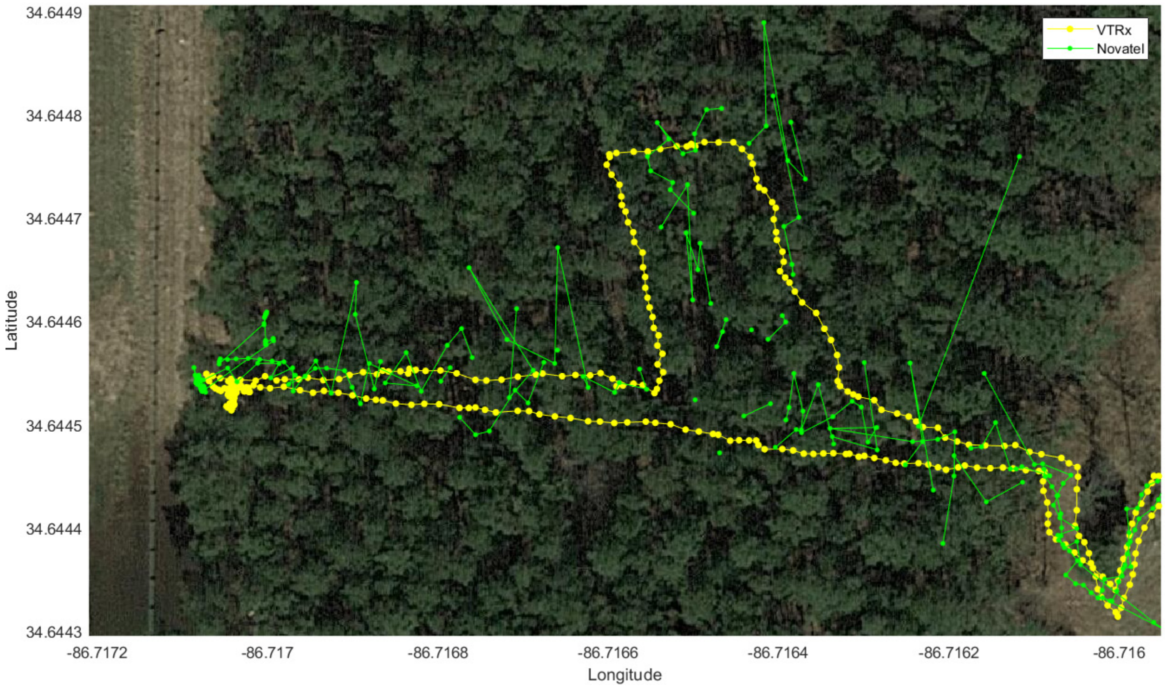

Figure 7-14. Point Map Showing Zoomed Area in Dense Foliage

Figure 7-15 shows the total differenced distance in ENU between the two receivers. Since truth data is not available, this metric is an indicator of the vector tracking receiver's tracking performance compared to the Novatel receiver. The figure on the right shows a zoomed in version with the large outliers from the Novatel removed.

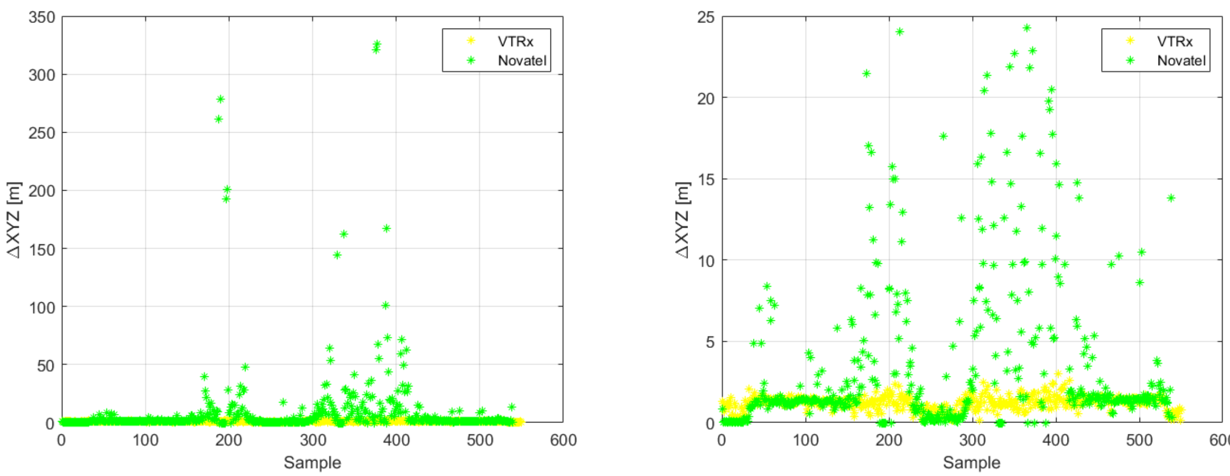

Figure 7-15. Sample-to-sample Position Difference Magnitude

Table 7-9 shows the statistics of the point-to-point variability between each datapoint with and without the outliers (defined as >25m).

Table 7-9. Sample-to-sample Error Statistics for Run

Receiver	Mean | (no outliers) [m]	Std Dev | (no outliers) [m]
VTRx	1.21 (1.21)	0.44 (0.44)
Novatel	9.57 (3.50)	31.81 (4.82)
Improvement	65%	91%

Table 7-10 shows the percentage of the samples that each receiver had a valid position solution.

Table 7-10. Percentage Fix for Run

Receiver	Percentage Fix
VTRx	100%
Novatel	91%

This data run highlights the performance of the vector tracking receiver in a dense foliage environment.

7.1.2.3 Run: Day 2 – Real-time 3 (11:09 10/25/2018)

In this run, the truth system was activated. The vector tracking receiver tracked 5 satellites throughout the entire course. The truth system was only able to cover a portion of the run due to obstruction by placement.

An overhead map comparison of this run is shown in Figure 7-16.

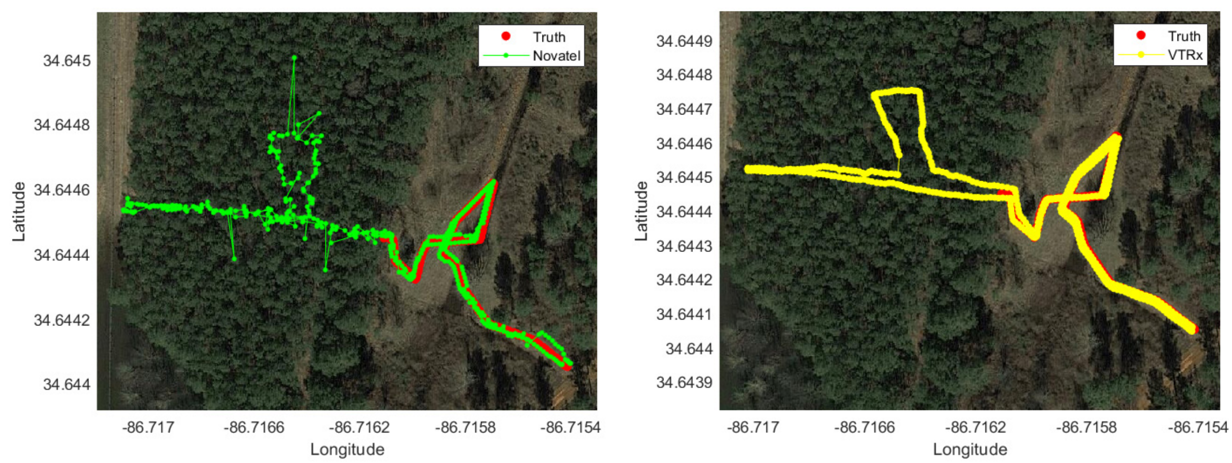

Figure 7-16. Point Map Showing Whole Course

A zoomed-in version of the plot on the area of truth coverage is found in Figure 7-17.

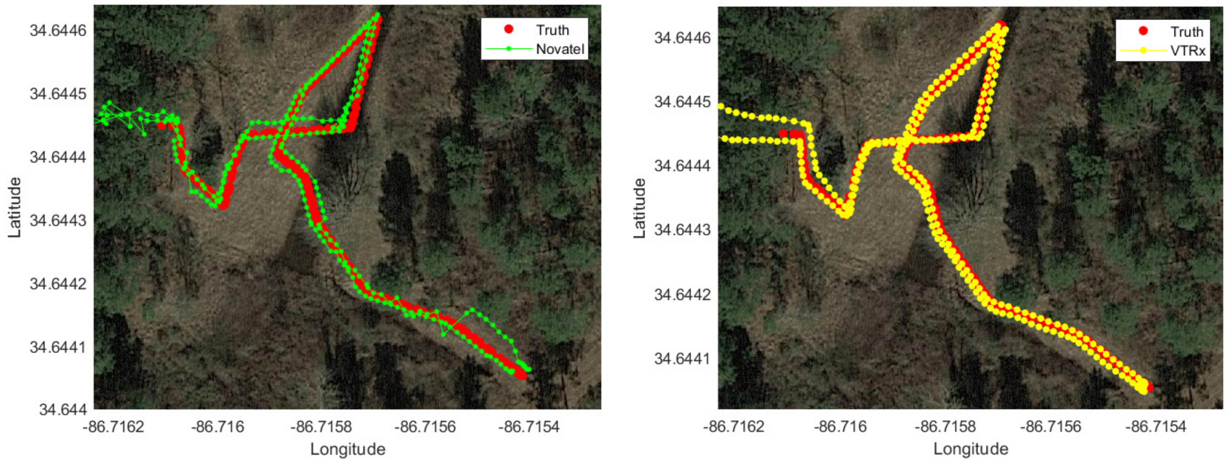

Figure 7-17. Point Map Showing Zoomed Area of Truth Coverage

A total position error plot between the receiver and the truth data is shown in Figure 7-18. The portions not covered by truth data were omitted from this plot.

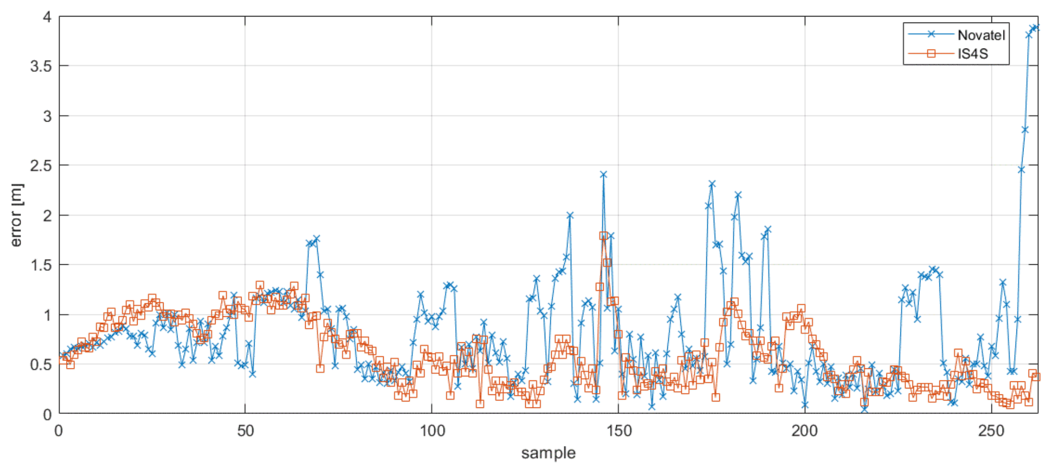

Figure 7-18. Position Error of Test Receivers versus Truth

Table 7-11 shows the statistics of the error between the truth data and the receiver output data for this run. The information below excludes the points for which the truth data was not available.

Table 7-11. Error Statistics for Run

Receiver	Mean [m]	Std Dev [m]
VTRx	0.60	0.34
Novatel	0.86	0.65
Improvement	30%	48%

Table 7-12 shows the percentage of the samples that each receiver had a valid position solution.

Table 7-12. Percentage Fix for Run

Receiver	Percentage Fix
VTRx	100%
Novatel	99%

This data run highlights the similar performance of the two receivers in live sky environment. However, it can also be seen visually in the data that the vector tracking receiver outperformed the Novatel receiver in the dense foliage area.

7.1.2.4 Run: Day 2 – Real-time 4 (11:28 10/25/2018)

In this run, the truth system again covered the open-sky area. The vector tracking receiver tracked 5 satellites throughout the entire course. The Novatel receiver appears to have lost lock as the receiver into the wooded area and never recovered.

An overhead map comparison of this run is shown in Figure 7-19.

Figure 7-19. Point Map Showing Whole Course

A zoomed-in version of the plot on the area of truth coverage is found in Figure 7-20.

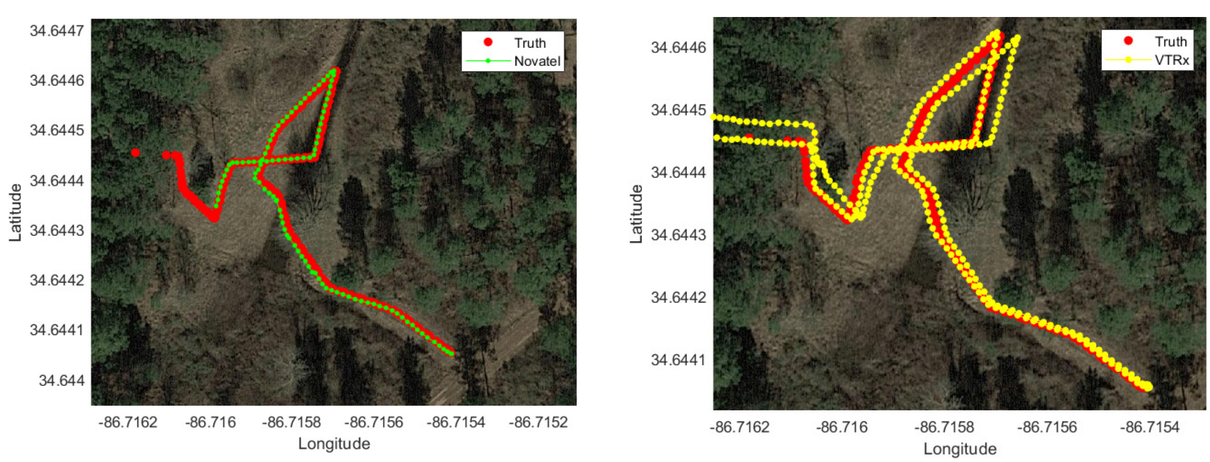

Figure 7-20. Point Map Showing Zoomed Area of Truth Coverage

A total position error plot between the receiver and the truth data is shown in Figure 7-21. The portions not covered by truth data were omitted from this plot.

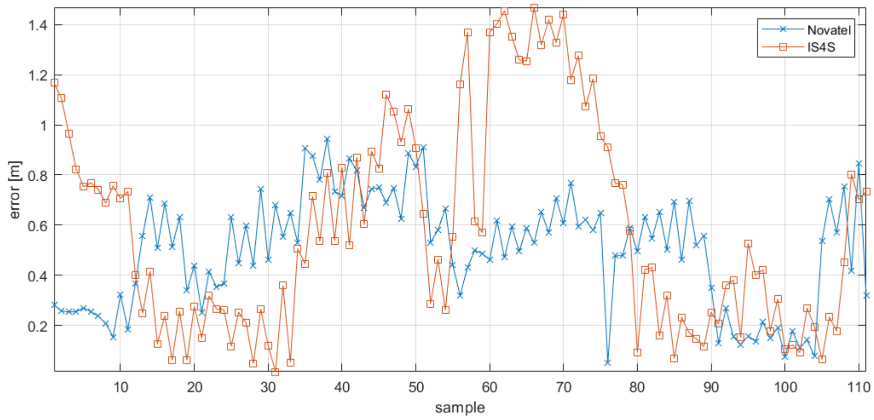

Figure 7-21. Position Error of Test Receivers Versus Truth

Table 7-13 shows the statistics of the error between the truth data and the receiver output data for this run. The information below excludes the points for which the truth data was not available.

Table 7-13. Error Statistics for Run

Receiver	Mean [m]	Std Dev [m]
VTRx	0.59	0.42
Novatel	0.50	0.22
Improvement	-18%	-91%

Table 7-14 shows the percentage of the samples that each receiver had a valid position solution.

Table 7-14. Percentage Fix for Run

Receiver	Percentage Fix
VTRx	100%
Novatel	100% (only 24% of run reported)

This data run highlights the similar performance of the two receivers in live sky environment. However, due to the lack of Novatel data, the comparative analysis is of limited use.

7.1.2.5 Run: Day 2 – Processed Raw Data 2 (11:39 10/25/2018)

In this run, the truth system was active in the open-sky portion of the course. Both receivers reported a position through the course. The data was captured raw and processed by the software-only version of the receiver. The navigator was not tuned in the software-only receiver.

An overhead map comparison of this run is shown in Figure 7-22.

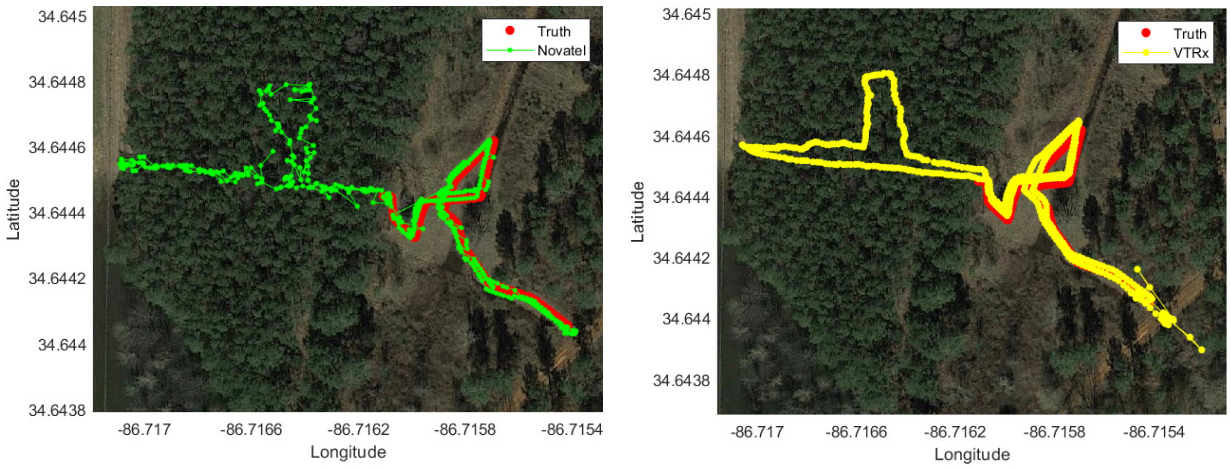

Figure 7-22. Point Map Showing Whole Course

A zoomed-in version of the plot on the area of truth coverage is found in Figure 7-23.

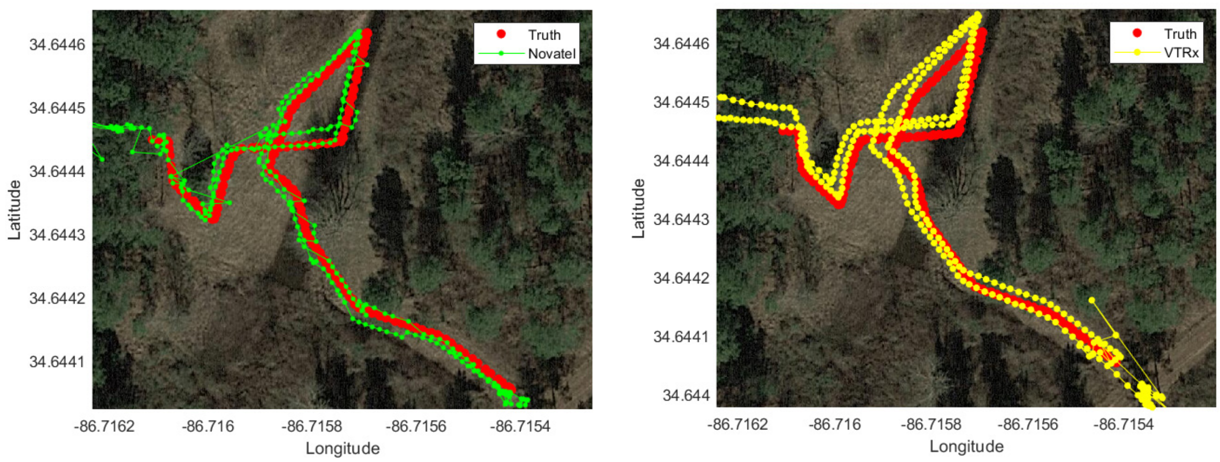

Figure 7-23. Point Map Showing Zoomed Area of Truth Coverage

A total position error plot between the receiver and the truth data is shown in Figure 7-24. The portions not covered by truth data were omitted from this plot.

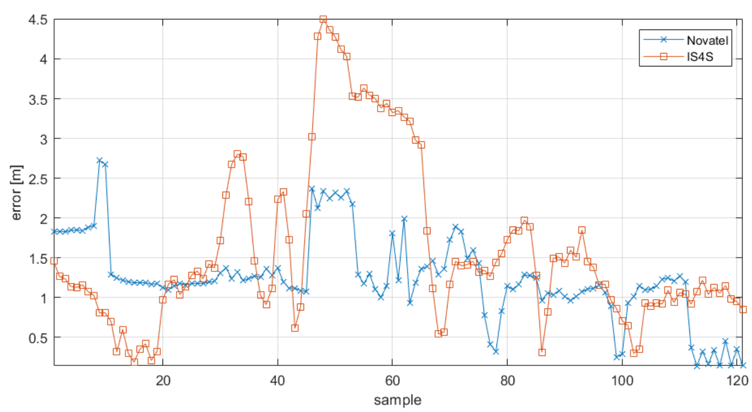

Figure 7-24. Position Error of Test Receivers Versus Truth

Table 7-15 shows the statistics of the error between the truth data and the receiver output data for this run. The information below excludes the points for which the truth data was not available.

Table 7-15. Error Statistics for Run

Receiver	Mean [m]	Std Dev [m]
VTRx	1.60	1.04
Novatel	1.24	0.52
Improvement	-29%	-100%

Table 7-16 shows the percentage of the samples that each receiver had a valid position solution.

Table 7-16. Percentage Fix for Run

Receiver	Percentage Fix
VTRx	100%
Novatel	99.6%

The open-sky performance of the untuned navigator in the software receiver did not perform as well as the Novatel receiver in this capture.

7.1.2.6 Run: Day 2 – Real-time 5 (12:18 10/25/2018)

In this run, the truth system was moved to cover the area inside the area of dense foliage. The truth system was only able to cover a portion of the run due to obstruction. The Novatel data cuts off as the dense foliage section is entered, so this run is of limited use.

An overhead map comparison of this run is shown in Figure 7-25.

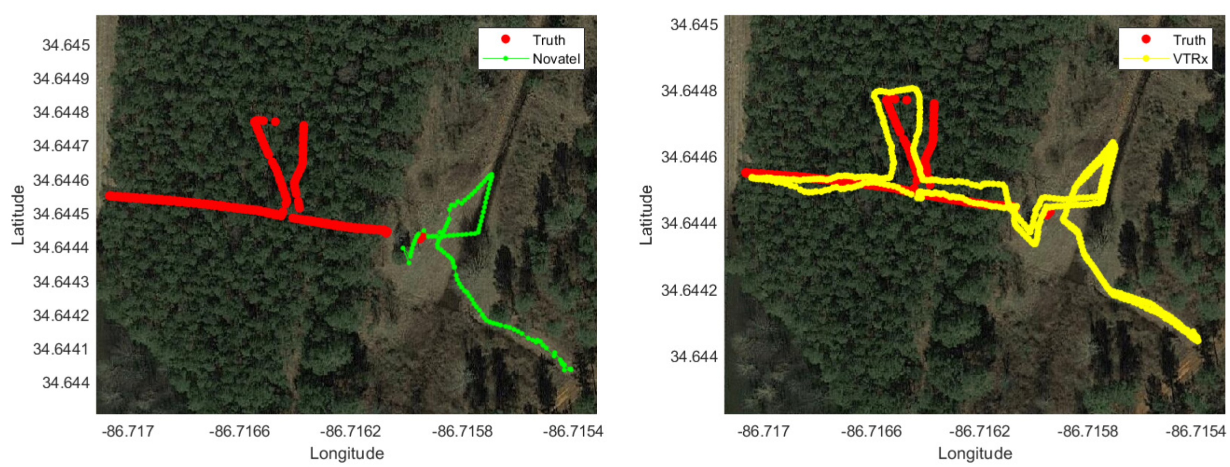

Figure 7-25. Point Map Showing Whole Course

A zoomed-in version of the plot on the area of truth coverage is found in Figure 7-26.

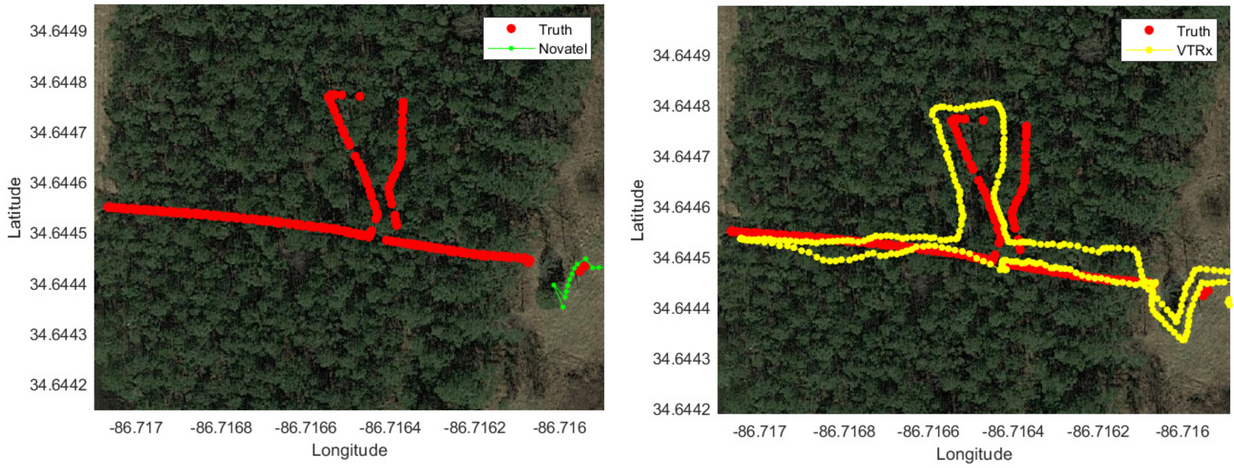

Figure 7-26. Point Map Showing Zoomed Area of Truth Coverage

A total position error plot between the receiver and the truth data is shown in Figure 7-27. The portions not covered by truth data were omitted from this plot. The receiver error was calculated by differencing the receiver position and truth position and calculating the norm.

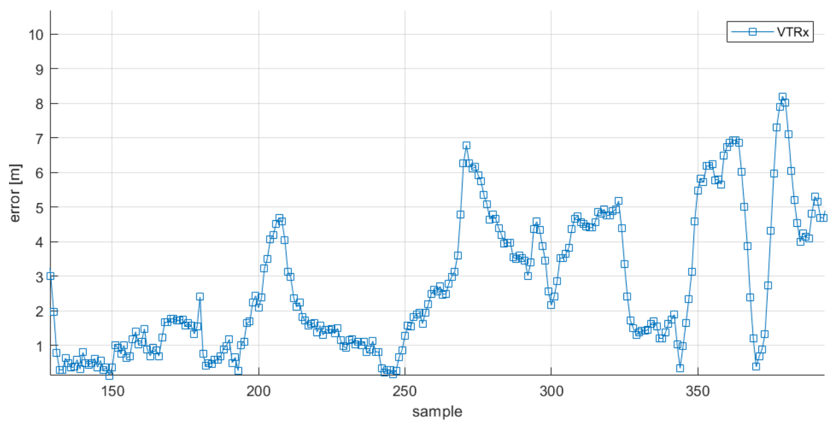

Figure 7-27. Position Error of Test Receivers versus Truth

Table 7-17 shows the statistics of the error between the truth data and the receiver output data for this run. The information below excludes the points for which the truth data was not available. It also excludes the Novatel data, as there was no overlapping truth data.

```
areaWithTruthData = [132:394]
```

Table 7-17. Error Statistics for Run

Receiver	Mean [m]	Std Dev [m]
VTRx	2.72	1.99
Novatel	N/A	N/A

Table 7-18 shows the percentage of the samples that each receiver had a valid position solution.

Table 7-18. Percentage Fix for Run

Receiver	Percentage Fix
VTRx	100%
Novatel	100% (only 23% of run reported)

This data run highlights the similar performance of the two receivers in live sky environment. However, due to the lack of Novatel data, the comparative analysis is of limited use.

7.1.2.7 Run: Day 2 – Real-time 6 (12:30 10/25/2018)

In this run, the truth system was active in the dense foliage portion of the course. Both receivers reported a position through the course.

An overhead map comparison of this run is shown in Figure 7-28.

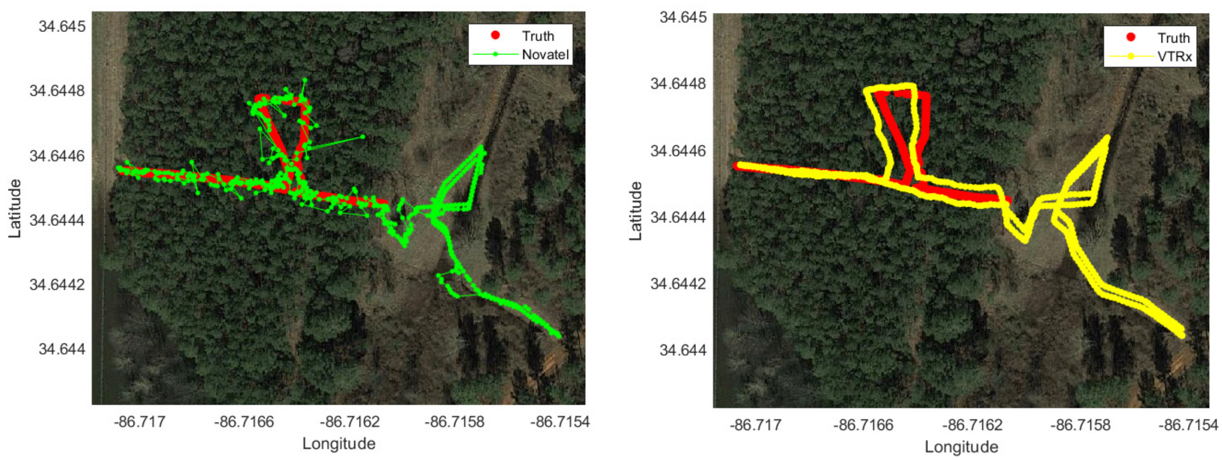

Figure 7-28. Point Map Showing Whole Course

A zoomed-in version of the plot on the area of truth coverage is found in Figure 7-29.

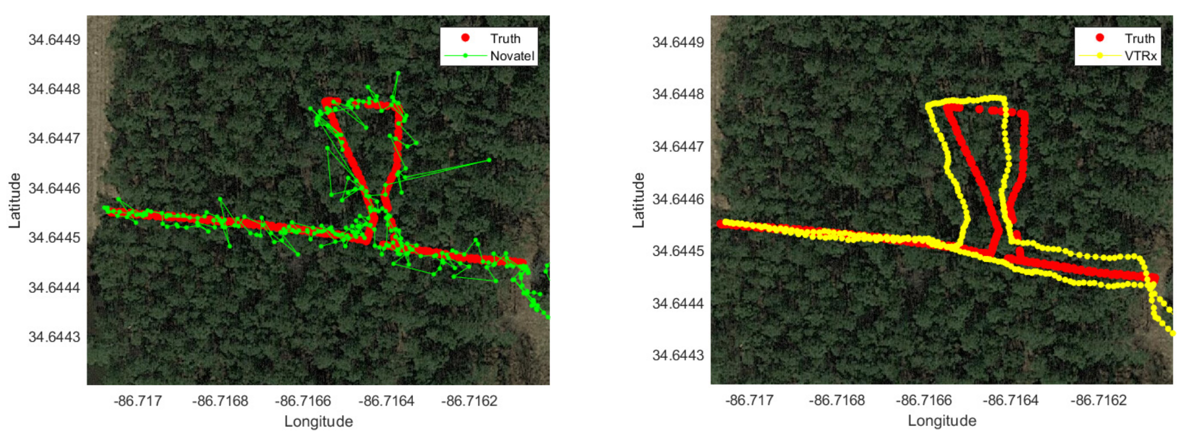

Figure 7-29. Point Map Showing Zoomed Area of Truth Coverage

A total position error plot between the receiver and the truth data is shown in Figure 7-30. The portions not covered by truth data were omitted from this plot.

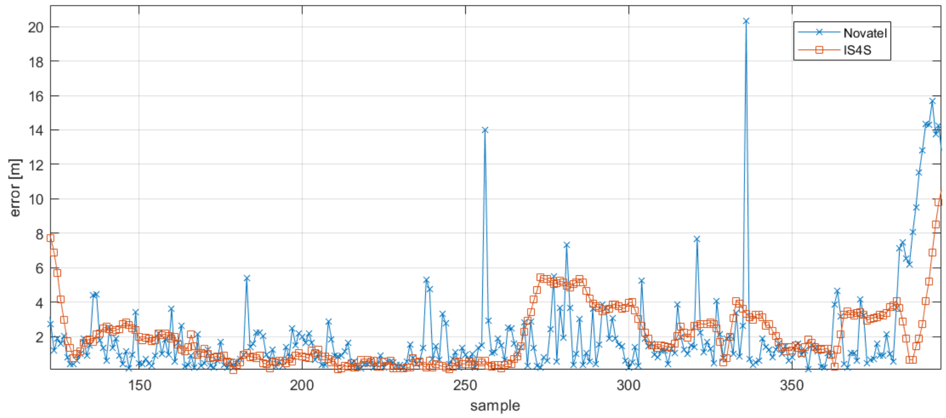

Figure 7-30. Position Error of Test Receivers Versus Truth

Table 7-19 shows the statistics of the error between the truth data and the receiver output data for this run. The information below excludes the points for which the truth data was not available.

Table 7-19. Error Statistics for Run

Receiver	Mean [m]	Std Dev [m]
VTRx	1.84	1.41
Novatel	1.64	2.02
Improvement	-12%	30%

Table 7-20 shows the percentage of the samples that each receiver had a valid position solution.

Table 7-20. Percentage Fix for run

Receiver	Percentage Fix
VTRx	100%
Novatel	99.6%

This data run highlights the improved performance of the vector tracking receiver versus the Novatel in dense foliage environments. The performance would almost certainly have been improved if more satellites were able to be tracked by the receiver. The coupling of IMU data would have also almost certainly improved the position error offset seen in the VT solution.

7.1.2.8 Run: Day 2 – Processed Raw Data 3 (12:45 10/25/2018)

In this run, the truth system was active in the dense foliage portion of the course. Both receivers reported a position through the course. The data was captured raw and processed by the software-only version of the receiver. The navigator was not tuned in the software-only receiver.

An overhead map comparison of this run is shown in Figure 7-31.

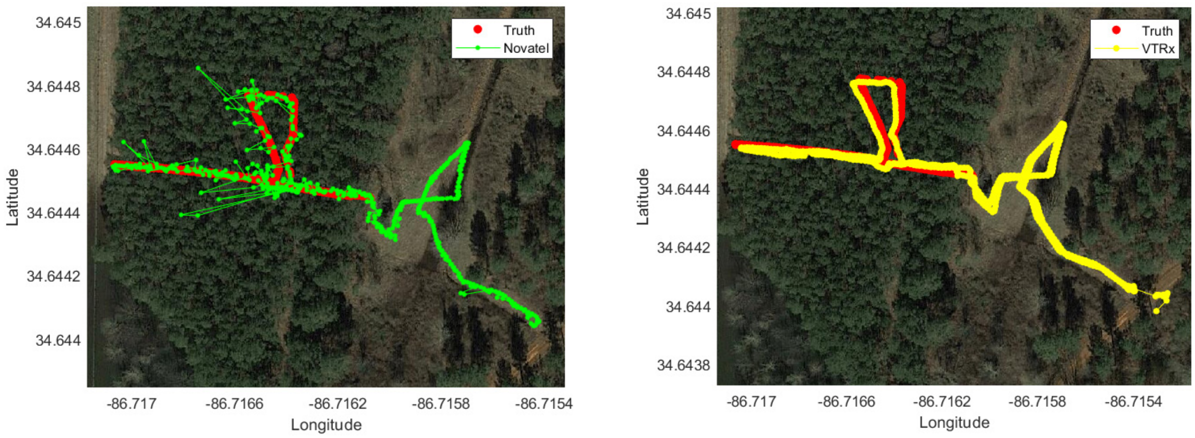

Figure 7-31. Point Map Showing Whole Course

A zoomed-in version of the plot on the area of truth coverage is found in Figure 7-32.

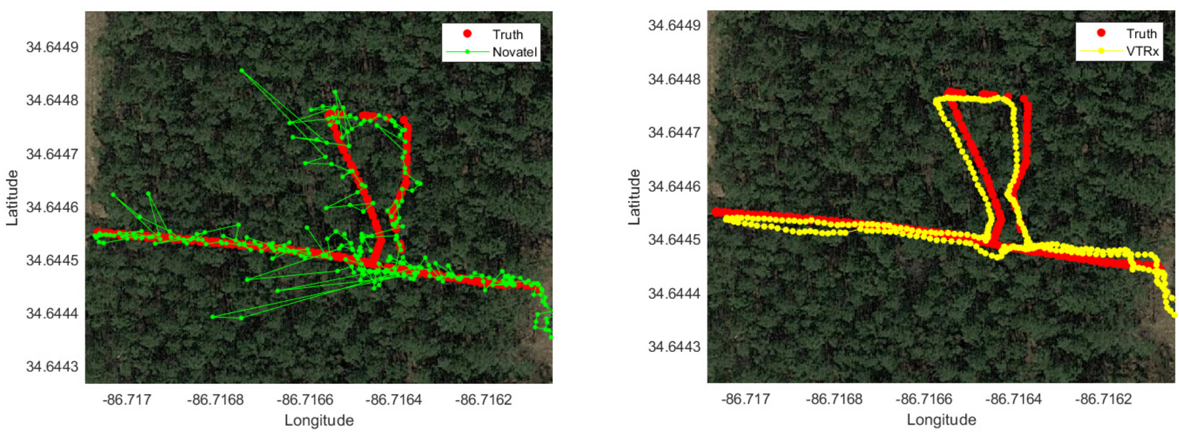

Figure 7-32. Point Map Showing Zoomed Area of Truth Coverage

A total position error plot between the receiver and the truth data is shown in Figure 7-33. The portions not covered by truth data were omitted from this plot.

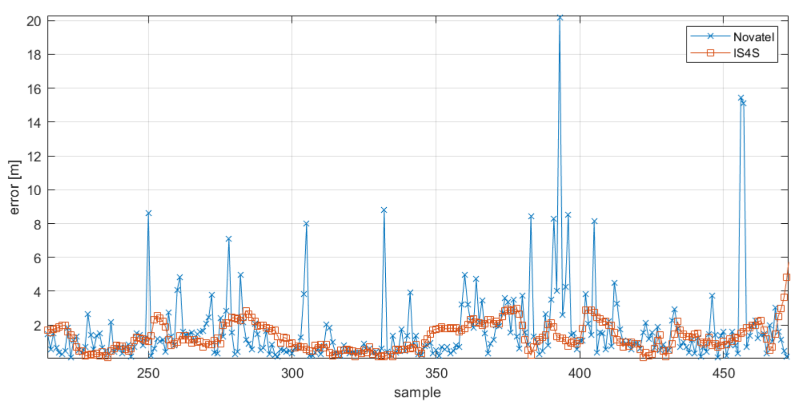

Figure 7-33. Position Error of Test Receivers Versus Truth

Table 7-21 shows the statistics of the error between the truth data and the receiver output data for this run. The information below excludes the points for which the truth data was not available.

Table 7-21. Error statistics for run

Receiver	Mean [m]	Std Dev [m]
VTRx	1.27	0.75
Novatel	1.68	2.32
Improvement	24%	68%

Table 7-22 shows the percentage of the samples that each receiver had a valid position solution.

Table 7-22. Percentage fix for run

Receiver	Percentage Fix
VTRx	100%
Novatel	99.5%

This data run highlights the improved performance of the vector tracking receiver versus the Novatel in dense foliage environments. This run shows the advantage of the tuning of the receiver available in a software defined radio. The performance of the vector tracking receiver outperforms the Novatel by a significant amount which could be improved by IMU integration and filter tuning.

7.1.3 Site 5 – Mixed Course

7.1.3.1 Run: Day 2 – Processed Raw Data 4 (13:53 10/25/2018)

In this run, the truth system data collection was abandoned due to inclement weather. A comparison of the two receiver solutions is shown.

An overhead map comparison of this run is shown in Figure 7-34.

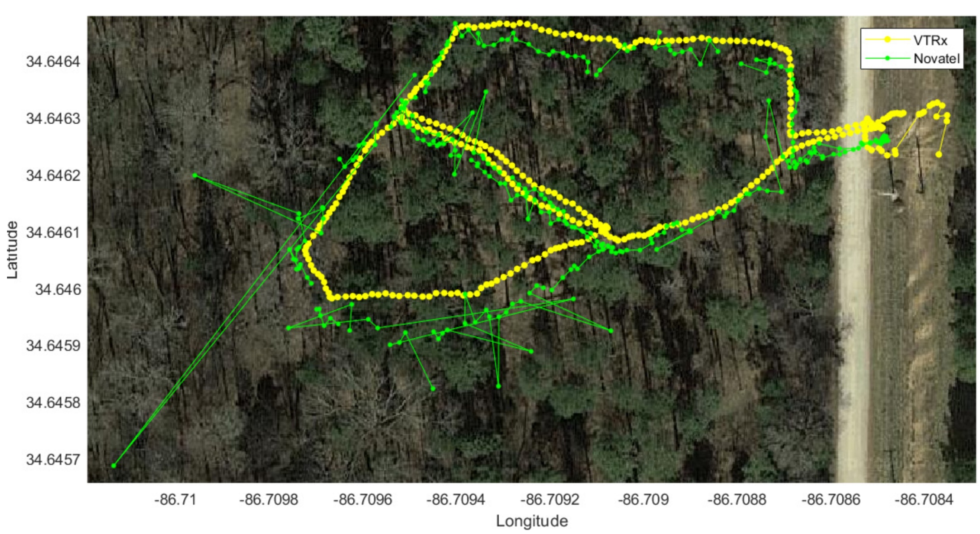

Figure 7-34. Point Map Showing Whole Course

Figure 7-35 shows the total differenced distance in ENU between the two receivers. Since truth data is not available, this metric is an indicator of the vector tracking receiver's tracking performance compared to the Novatel receiver. The figure on the right shows a zoomed in version with the large outliers from the Novatel removed. The low values at the left of each plot shows the long stationary capture.

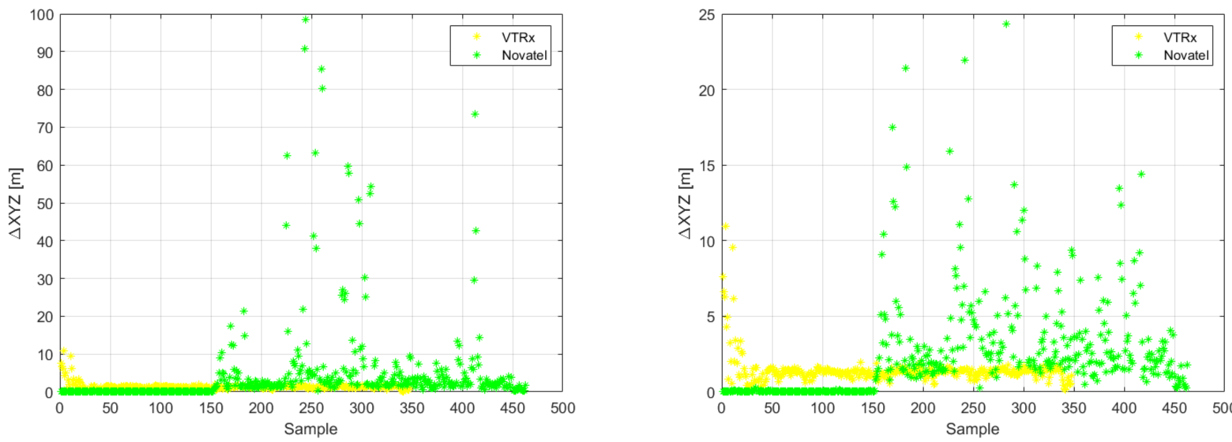

Figure 7-35. Sample-to-sample Position Difference Magnitude

Table 7-23 shows the statistics of the point-to-point variability between each datapoint with and without the outliers (defined as >25m).

Table 7-23. Sample-to-sample Error Statistics for Run

Receiver	Mean | (no outliers) [m]	Std Dev | (no outliers) [m]
VTRx	1.41 (1.41)	1.00 (1.00)
Novatel	4.90 (2.42)	12.31 (3.37)
Improvement	42%	70%

Table 7-24 shows the percentage of the samples that each receiver had a valid position solution.

Table 7-24. Percentage Fix for Run

Receiver	Percentage Fix
VTRx	100%
Novatel	96.1%

This data run highlights the performance of the vector tracking receiver in a dense foliage environment. The large variability in the Novatel data as compared to the vector tracking receiver is considerable.

7.2 REPEATABILITY COMPARISON

A comparison of the data with respect to repeatability is also shown here. From run to run, a consistent navigation solution with persistent availability is preferred. Only one capture was taken at Site 5, so it will be omitted from these results.

7.2.1 Site 13 – Light Foliage

Repeated runs of the Novatel data on Site 13 are overlaid in Figure 7-36.

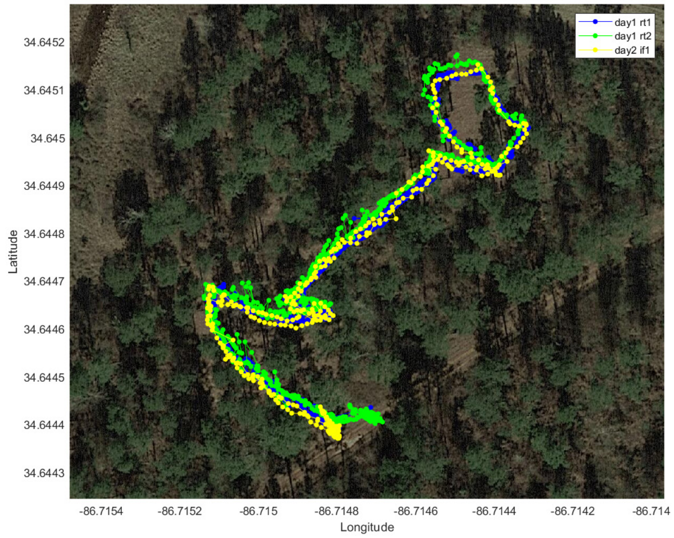

Figure 7-36. Point Map Showing Repeatability of the Novatel Receiver Position Solution at Site 13

Repeated runs of the vector tracking receiver data on Site 13 are overlaid in Figure 7-37.

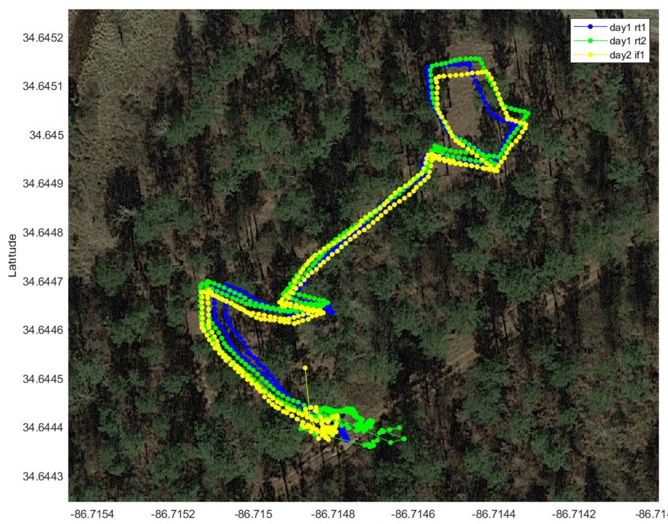

Figure 7-37 Point Map Showing Repeatability of the Vector Tracking Receiver Position Solution at Site 13

The repeatability of the vector tracking receiver can be clearly seen in the runs with light foliage at Site 13. While there is a constant bias in some of the runs on the vector tracking solution, the variability between runs is significantly smaller than that of the Novatel solution in the foliage environments. In the clear sky environments, the Novatel is able to obtain strong GPS measurements and so does not exhibit the same inconsistencies it does in the heavier foliage environments.

7.2.2 Site 9 – Dense Foliage

Repeated runs of the Novatel data on Site 9 are overlaid in Figure 7-38.

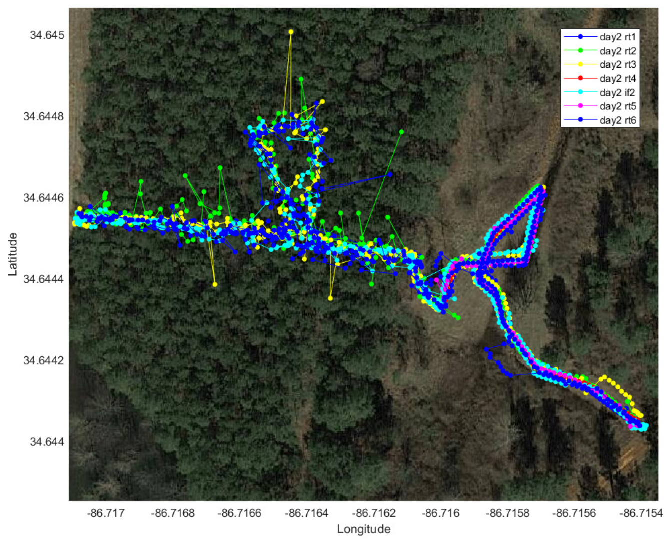

Figure 7-38. Point Map Showing Repeatability of the Novatel Receiver Position Solution at Site 9

Repeated runs of the vector tracking receiver data on Site 13 are overlaid in Figure 7-39.

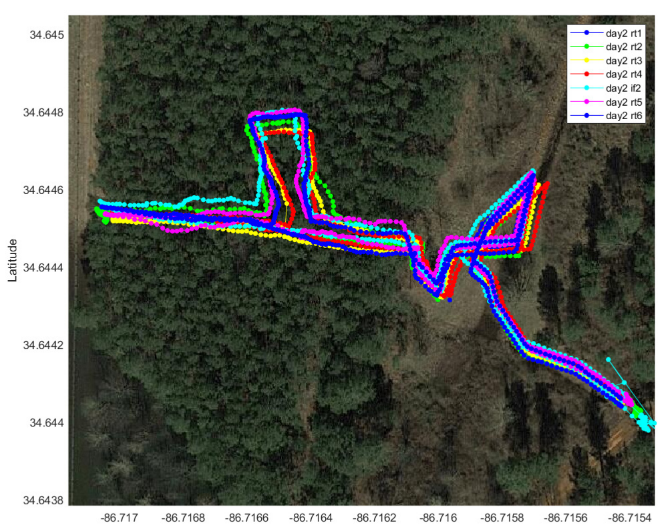

Figure 7-39. Point Map Showing Repeatability of the Vector Tracking Receiver Position Solution at Site 9

The dense foliage captures show the benefit of the vector tracking solution as compared to the Novatel receiver. The Novatel receiver performs very well in the open-sky plots – the repeatability is very high for open sky. However, once the dense foliage area is entered, the Novatel solution variability is significantly higher than the vector tracking solution. The vector solution tracks a minimal number of satellites through this dense area outage. If the number of satellites tracked were to go up, the repeatability performance would improve.

7.3 CHANNEL TRACKING COMPARISON

The performance of the vector tracking receiver and the Novatel receiver can also be compared on a per-channel basis. The channel data for all of these runs is not shown here, but there are two points of significance in comparing the channel-by-channel performance of the receivers.

Figure 7-40 shows the signal-to-noise (C/N_0) level comparison between the two systems. The different systems maintain very similar C/N_0 numbers throughout the course of most of the captures where the same satellites are tracked. This figure shows a run with two separate PRNs, PRN20 and PRN29, that are tracked by each system. The switch to vector tracking in the software defined receiver can be seen by the jump in C/N_0 at the beginning of the capture.

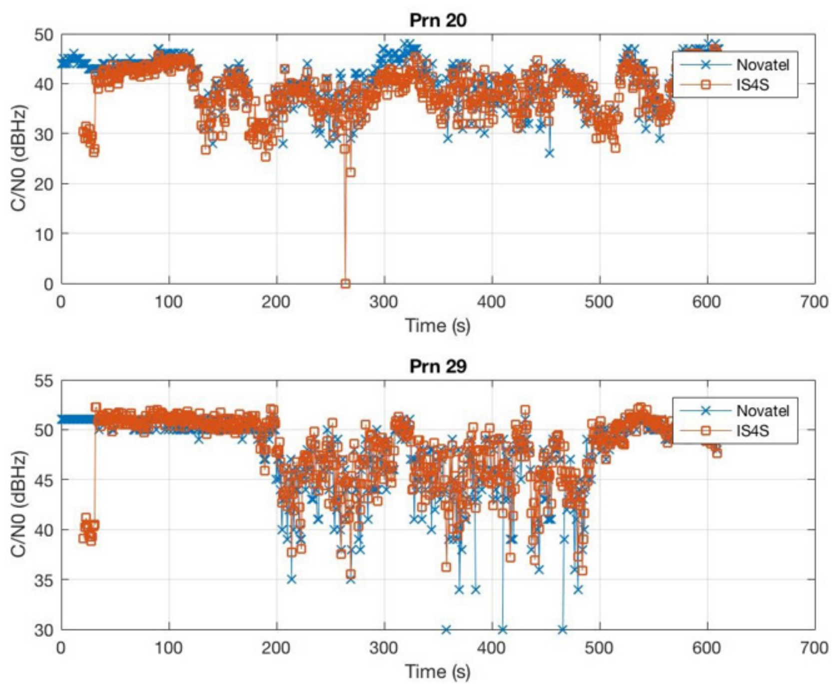

Figure 7-40. C/N_0 Comparison Between Vector Tracking and Novatel Receiver for the same Run Tracking Two of the Same Satellites

The second helpful comparison is the number of locked channels. A typical run is shown in Figure 7-41. The low number of satellites tracked is an issue that can be resolved with firmware upgrades to the SDR platform. This is a shortcoming of the current receiver platform. However, the major point of interest in this figure is the consistency with which all five of the satellites are tracked. If more satellites had been tracked from the beginning, the vector tracking solution would most likely have been able to maintain lock on most of these satellites.

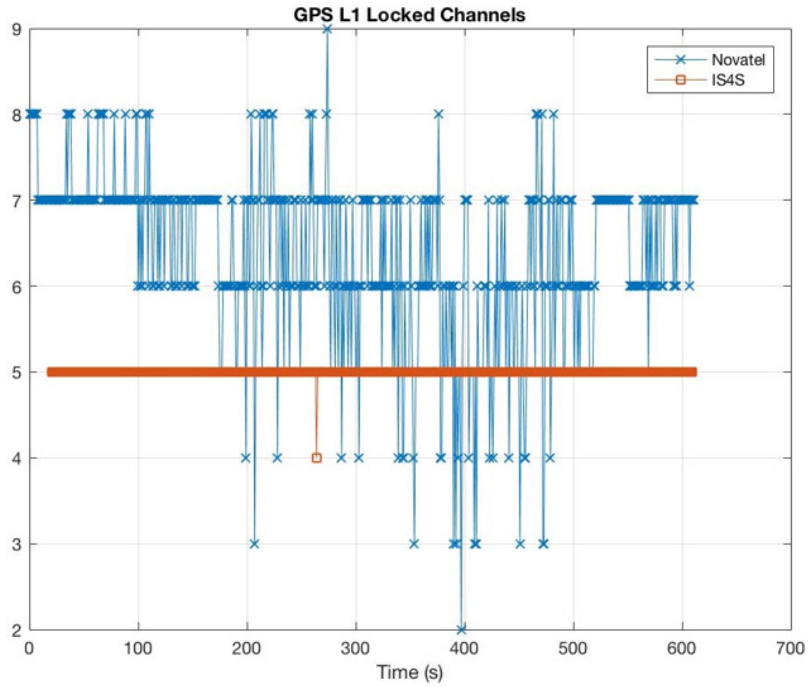

Figure 7-41. Number of Channels Tracked for a Typical Scenario.

A GPS receiver must have at least 4 satellites tracked to produce a navigation solution.

There are several samples where the number of satellites tracked by the Novatel drops below four. This would result in a loss of position lock in the receiver. The denser the foliage or occluded the view of the sky, the more likely this is to happen.

There are some runs that the position bias of the vector tracking receiver is less than optimal. This plot helps to explain that observation, as the dilution of precision in the navigation solution is weaker with less satellites tracked. The scalar tracking solution could have seeded the vector solution with a biased navigation solution, which affects the accuracy of the remainder of the run. With further engineering and firmware upgrades, along with external measurement integration, these shortcomings could be improved.

8.0 COST ASSESSMENT

8.1 COST MODEL

The primary cost associated with the system is the cost of the receiver and other hardware components. In standalone (non-differential) mode the receiver produces real-time outputs and is designed to replace the GPS receiver typically used in surveys. No additional setup or calibration is required beyond what is required for currently used receivers and so survey costs are expected to be unchanged when replacing an existing GPS based setup.

The costs of the system components are given in Table 8-1. A base system requires a VTRx receiver and a GPS antenna for an approximate total cost of $2500. This cost is based on using the dual-frequency Novatel Pinwheel antenna used in the demonstration. Since the VTRx only receives on the L1 band, a lower-cost antenna could be substituted without changing performance. The CSAC and IMU can be optionally added to the system to improve performance, particularly when less than three satellites are visible.

Table 8-1. System Component Costs

Component	Cost
VTRx Receiver	$1,500
CSAC [Optional]	$4,500
HG1930 IMU [Optional]	$7,000-10,000
Novatel Pinwheel Antenna	$1,000

8.2 COST DRIVERS

A primary driver of the cost effectiveness of the system is the amount of GPS challenging terrain (such as heavy foliage areas) that is present on the site. For sites with areas that a traditional GPS receiver cannot reliably track satellites and produce an accurate position, the VTRx provides significant cost savings over other alternatives such as robotic total stations or systems containing high-end IMUs.

8.3 COST BENEFIT

The primary cost benefit of the VTRx system is in the ability to use GPS based survey methods in areas where a standard GPS receiver would not provide acceptable availability. The ability to continue to use GPS deeper into foliage areas provides a significant cost benefit over alternatives such as robotic total stations. The system hardware is less expensive than most robotic total stations or other alternative systems containing high-end IMUs. Additionally, in contrast to a robotic total station, no additional setup is required greatly improving productivity and reducing the per-acre survey cost.

9.0 IMPLEMENTATION ISSUES

The demonstrated system consists primarily of a custom-built prototype that makes use of COTS components to the extent possible. The prototype system was developed exclusively for this effort and is not currently commercially available. Six prototype systems have been built to date. Two receivers developed on this effort are currently located at IS4S and are available as deliverables.

Since the conclusion of this effort, however, IS4S has developed a next generation software receiver (VTRx V2) based on lessons learned in this effort and demand from other DoD customers. While not yet a commercial product, approximately 25 of the receivers have been built and a significant portion of those delivered to customers. The VTRx V2 hardware is shown in Figure 9-1. This system improves on the demonstrated platform in several areas:

- RF front-end replaced by a wide-band front-end capable of receiving signals with bandwidths up to 36 MHz on L1, L2, or L5 (provides capability to receive modern signals such as L2C and L5C).
- Two RF receive chains for multi-band operation.
- Improved enclosure and mechanical designs improve robustness and reduces assembly costs.
- Improved channel manager drastically reduces acquisition time and tracking robustness.

Figure 9-1. VTRx V2 SDR Platform

There are currently no known regulatory issues related to the use of the developed technology.

10.0 REFERENCES

Keyser, B., Hodo, D., Martin, S., Bevly, D., “Implementation Details of Real-Time SoC-Based Vector Tracking Receiver. Proceedings of the 27th International Technical Meeting of the Satellite Division of the Institute of Navigation (ION GNSS+ 2014).

Keyser, B. “Design and Implementation of a SoC-Based Real-Time Vector Tracking GPS Receiver.” Master’s Thesis. Auburn University. May 2015.

Martin, S.M. "Improved GPS Carrier Phase Tracking in Difficult Environments Using A Vector Tracking Approach." Presented, Stanford PNT Symposium. Palo Alto, CA, October 2014.

Martin, S.M. "Improved GPS Carrier Phase Tracking in Difficult Environments Using A Vector Tracking Approach." Presented to Southern California Chapter of the Institute of Navigation. Torrance, CA, December 2014.

Elliott Kaplan and Christopher J. Hegarty. 2017. Understanding GPS/GNSS: Principles and Applications, Third Edition (3rd ed.). Artech House, Inc. USA.

APPENDIX A POINTS OF CONTACT

POINT OF CONTACT Name	ORGANIZATION Name Address	Phone Fax E-mail	Role in Project
David Hodo	IS4S, 4276 US Hwy 29 S, Auburn, AL 36830	(256) 975-2237 david.hodo@is4s.com	PI
Bob Selfridge	USAESCH 4820 University Square Huntsville, AL 35816	(256) 990-1891 Bob.J.Selfridge@usace.army.mil	Demonstration Support, USAESCH PI
David Bevly	Auburn University 2418F Wiggins Hall Auburn, AL 36849	(334) 844-3446	Auburn University PI, GPS Subject Matter Expert